5-2015

SUNITINIB-INDUCED CARDIOTOXICITY EXPOSES MICROVASCULAR AND METABOLIC DERANGEMENTS IN THE FAILING HEART

Meredith R. Rodriguez

SUNITINIB-INDUCED CARDIOTOXICITY EXPOSES MICROVASCULAR AND METABOLIC DERANGEMENTS IN THE FAILING HEART

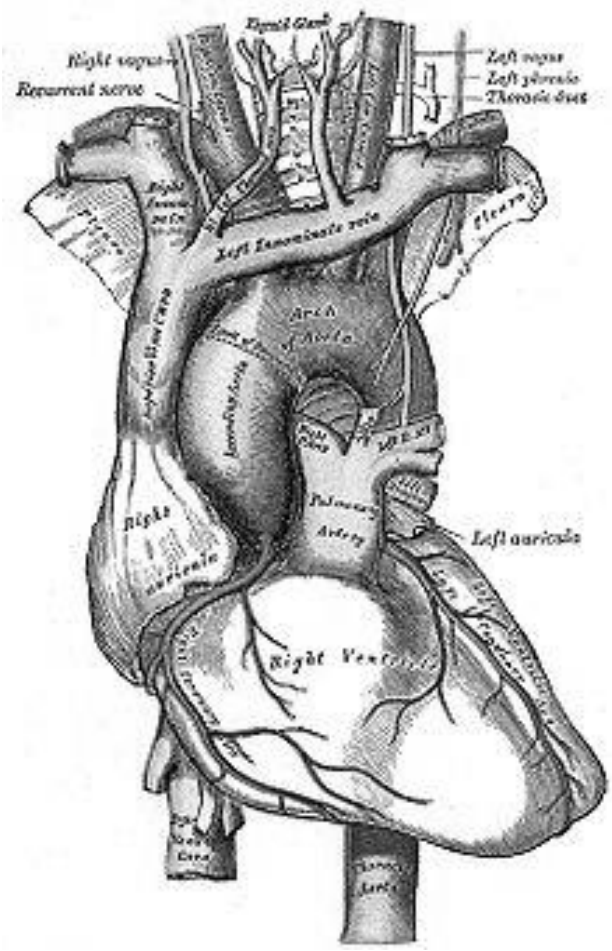

Meredith Rees Rodriguez, BA

Defense Date: April 13, 2015

SUNITINIB-INDUCED CARDIOTOXICITY EXPOSES MICROVASCULAR AND METABOLIC DERANGEMENTS IN THE FAILING HEART

by

Meredith Rees Rodriguez, BA

APPROVED:

Heinrich Taegtmeyer, M.D. D.Phil
Supervisory Professor

Diane Bick, Ph.D.

Mark Entman, M.D.

Hui-Kuan Lin, Ph.D.

David Moore, Ph.D.

APPROVED

Dean, UTHealth Graduate School of
Biomedical Sciences

SUNITINIB-INDUCED CARDIOTOXICITY EXPOSES MICROVASCULAR AND METABOLIC DERANGEMENTS IN THE FAILING HEART

A

THESIS

Presented to the Faculty of

The University of Texas

Health Science Center at Houston

and

The University of Texas

MD Anderson Cancer Center

Graduate School of Biomedical Sciences

in Partial Fulfillment

of the Requirements

for the Degree of

DOCTOR OF PHILOSOPHY

By

Meredith Rees Rodriguez

Houston, Texas

May 2015

DEDICATION

This dissertation is dedicated to my family: my loving husband Robert Rodriguez and the world's most supportive parents, James and Tina Rees. Without your love and support none of this would have been possible.

ACKNOWLDEGEMENTS

One should always be as lucky to find themselves in my position. I have the fortune of being surrounded by more brilliant, caring and supportive people than I could've asked for. I cannot thank you all but this is my humble attempt.

I must begin with expressing my deep gratitude to Dr. Heinrich Taegtmeyer. From taking me in when I washed up on your shores, to pointing out examples of prominent women scientists, to reading—and rereading—my abstracts, applications and manuscripts, to forcing me to ask a question in packed seminar, you have truly prepared me for a successful career. I never doubted that you had my best interest at heart and I will always trust your judgment and your guidance. You are humble, yet brilliant, and the world of cardiac metabolism would be fraught without your magnanimous contributions.

To the members of my committee: Dr. David Moore, Dr. Hui-Kuan Lin, Dr. Diane Bick and Dr. Mark Entman, thank you. Dr. Bick: for your guidance through the first few years of this adventure, from helping me chose rotations to my transition to Dr. Taegtmeyer's lab. Dr. Entman: without your wisdom, your benevolence and your direction, I would be nowhere near the person I am today. I am also indebted to the mentors led me down this path. Dr. Genevieve Sparanga and the entire lab of Dr. Russell Moore: thank you for kindling my passion for research and ensuring that I never gave up. Lastly, but certainly not least, Dr. Aarif Khakoo: who could've seen the twists and turns this road has taken? Thank you for your unyielding support no matter how demanding your new life has become. I hope to one day emulate your unique ability to lead with such dedication and tenacity yet compassion and light heartedness.

To the past and present members of the Taegtmeyer lab: Kedryn Baskin, Romain Harmancey, Truong Lam, Giovanni Davogustto, Janani Subramaniam, Hernan Vasquez,

Anja Karlstaedt, Rebecca Salazar and Patrick Guthrie, thank you for your advice, you support and your friendship. From troubleshooting western blots to Starbucks coffee runs, the lab was a better place to be because I shared it with you.

I would also like to thank Dr. O. Howard Frazier and Dr. Dale Hamilton for their generous support in providing human heart tissue samples.

Finally to my family, thank you. Robert Rodriguez, I love you with all my heart. Thank you for holding me through the tears, the frustration and the laughter. I am blessed to have you by my side and cannot imagine a world without you in it. James, you are too young to understand the pure joy you bring to me each and every day, but your smile is enough to pull me through the hardest of times. To my parents, James and Tina Rees, I will never be able to fully express the deep gratitude I feel for your unquestioning love and support. You have never failed to encourage my dreams and to make sure I knew I always have a soft place to land. I strive to make your proud. You are my inspiration and I love you. Adrienne Rees, my twin and best friend, you are my biggest cheerleader. As we each find our way in this busy, confusing and scary world I never doubt that you will be there when I need you, whether it is a phone call or a trip down to Houston. To Nolan and Briana Rees, thank you for all your support.

To my mentors, my colleagues, my friends and, most importantly, my family I am nothing without your guidance, support and love. For you, I am forever grateful.

ABSTRACT

Cardiac dysfunction is one of the largest obstacles to effective cancer treatment. Not only do a growing number of cancer patients have significant cardiovascular risk factors at the time of diagnosis, but a number of targeted therapies can themselves cause cardiac dysfunction. These newer treatment options are also increasingly effective, placing a growing emphasis on post-cancer quality of life. In some instances, a patient may outlive his or her cancer only to succumb to heart failure in as little as five years. One such targeted therapy is the small molecular receptor tyrosine kinase sunitinib. Sunitinib was developed in the early 2000's as part of a wave of antiangiogenic drugs that target the vascular endothelial growth factor receptors and platelet-derived growth factor receptors. Unfortunately, up to 47% of patients treated with sunitinib develop severe hypertension and approximately 20% develop cardiac dysfunction. The aim of my dissertation is therefore twofold: First, to identify the mechanism of sunitinib-induced cardiotoxicity in order to develop strategies to prevent clinical cardiotoxicity and, secondly, to use this mechanistic insight as a discovery platform to identify new targets for the treatment of human heart failure. My work led to the discovery that coronary microvascular pericytes are a primary target of sunitinib. Furthermore, co-treatment with thalidomide can protect from sunitinib-induced cardiac dysfunction without altering the antitumor effect of the drug. Examination of sunitinib-induced metabolic changes revealed that sunitinib treatment leads to a profound increase in glucose uptake in the heart and induction of the M2 isoform of pyruvate kinase. Collectively, my work suggests that vessel normalization and the Warburg Effect may be novel targets for the treatment of human heart failure.

LAY SUMMARY

When one thinks of the side effects of chemotherapy, hair loss and nausea commonly come to mind. However, a much less recognized—yet grave—side effect of certain chemotherapies is heart failure. This is because newer treatment options have vastly improved survival, making post-cancer quality of life much more relevant. The development of cardiac dysfunction while receiving cancer treatment is exacerbated by the fact that a growing number of patients have significant cardiovascular risk factors—such as obesity, diabetes or smoking—at the time of diagnosis. Nonetheless, a patient may outlive his or her cancer only to succumb to heart failure in as little as five years. Sunitinib is one such chemotherapy. Primarily used to inhibit blood vessel growth in tumors, sunitinib causes a severe increase in blood pressure in up to 47% of patients and causes cardiac dysfunction in another 20% of patients. The aim of my dissertation is therefore twofold: First, to develop strategies to prevent heart failure in patients receiving sunitinib and, secondly, to use what I learn about how sunitinib affects the heart to identify new strategies to treat human heart failure. My work led to the discovery that sunitinib disrupts the stability of blood vessels in the heart. Furthermore, this vascular instability can be prevented by co-treatment with the drug thalidomide. Further work revealed that sunitinib treatment leads to increased uptake of sugar by the heart and alters the way it is broken down into fuel. My results suggest that these changes may lead to a thickening of the walls of the heart and subsequent heart failure. Collectively, my work demonstrates that blood vessel stability and the utilization of sugar may be novel targets for the treatment of human heart failure.

TABLE OF CONTENTS

ABBREVIATIONS

2DG	[U-^{14}C]-2-deoxyglucose
ACC	acetyl-CoA carboxylase
ACE	angiotensin converting enzyme
ACM	adult cardiomyocytes
Alk	activin receptor-like kinase
AMPK	AMP-activation protein kinase
ANF	atrial natriuretic factor
CCTAE	Common Criteria for Adverse Events
CFR	coronary flow reserve
CHF	congestive heart failure
CRBN	cereblon
DMOG	dimethyloxalylglycine
dP/dt_{max}	maximum developed pressure in the left ventricle over time
ECG	electrocardiogram
EDV	end-diastolic volume
EDPVR	end-systolic pressure volume relation
eNOS	endothelial nitric oxide synthase
ESV	end-systolic volume
FDG	2-deoxy-2-[^{18}F]fluoro-D-glucose
FLT3	fms-related tyrosine kinase 3
G6P	glucose 6-phosphate
GAPDH	glyceraldehyde 3-phosphate dehydrogenase
GDR	glucose disposal rate
GIST	gastrointestinal stromal tumors
GLUT1	glucose transporter type 1

GLUT4	glucose transporter type 4
H&E	hematoxylin and eosin
Hif1α	hypoxia-inducible factor 1 alpha
hnRNP	heterogeneous nuclear ribonucleoproteins
INFα	interferon alpha
LC	lumped constant
LDH	lactate dehydrogenase
LVAD	left ventricular assist device
LVEF	left-ventricular ejection fraction
MAP	mean arterial pressure
MHC	myosin heavy chain
mRCC	metastatic renal cell carcinoma
MRI	magnetic resonance imaging
NG2	neural/glial 2
NO	nitric oxide
NRVM	neonatal rat ventricular myocytes
O-GlcNAc	O-Linked β-N-acetylglucosamine
ORR	objective response rate
PAS	Periodic Acid Schiff
PDGFRβ	platelet-derived growth factor receptor beta
PDK	pyruvate dehydrogenase kinase
PKM1	pyruvate kinase muscle type 1
PKM2	pyruvate kinase muscle type 2
PTB	polypyrimidine tract-binding protein
PV	pressure-volume
RSK	ribosomal S6 kinase

RTKIs	receptor tyrosine kinase inhibitors
SEM	standard error of the mean
TAF	tumor angiogenesis factor
TK	thymidine kinase
TNFα	tumor necrosis factor alpha
Top2	topoisomerase II
VEGF	vascular endothelial growth factor
VHL	von Hippel-Lindau
vSMC	vascular smooth muscle cell

LIST OF TABLES

LIST OF FIGURES

Chapter 1
INTRODUCTION

1. Introduction

This dissertation addresses structural, functional and metabolic features of cardiotoxicity of the chemotherapeutic receptor tyrosine kinase inhibitor, sunitinib. Using this compound as a discovery platform for cellular mechanisms of heart failure my work has also resulted in new insights into microvascular stability and metabolic features of the failing human heart.

1.1 Cardiotoxicity of Chemotherapeutic Agents

Cardiotoxicity is a frequent consequence of cancer chemotherapy. However, a suitable definition of the term is lacking. The term cardiotoxicity includes direct effects on the myocardium, myocardial ischemia, arrhythmias, thromboembolisms, inflammation of the myocardium (myocarditis), and pericardium (pericarditis) as well as alterations in hemodynamic parameters such as hypertension, acute coronary syndrome, and coronary vasospasms. These effects can manifest acutely during treatment or occur many years after treatment as a result of undiagnosed or subclinical cardiovascular dysfunction. Although likely driven by vastly different mechanisms, the management of chemotherapy-induced cardiotoxicity is no different from the management of heart failure in general. For instance, there are no established guidelines for the specific management of chemotherapy-induced cardiotoxicity. Physicians rely on the New York Heart Association Functional Classification and on standard modes of treatment (e.g. beta-blockers, ACE inhibitors, and calcium channel blockers) (**Figure 1.1**).

Building on previous work by Michael Schneider on c-myc signaling in the failing heart, Hoshijima and Chien detailed the strong parallels between signaling pathways that drive cancer growth and cardiac hypertrophy (Cheng and Force, 2010; Hoshijima and

Chien, 2002; Mulvagh et al., 1988) Based on this reasoning it should come as no surprise that many chemotherapeutics are also toxic to the heart.

Cardiotoxicity due to cancer chemotherapeutics is not a new phenomenon. The cardiotoxic effects of Adriamycin® (doxorubicin), a general DNA intercalating agent, were described even before the drug gained FDA approval in 1974. However, it was thought that with the development of more targeted therapies, the prevalence of cardiotoxicity would diminish. It was therefore a surprise when significant cardiotoxicities were identified with modern agents. Cardio-Oncology (or Onco-Cardiology depending on the source) has emerged as a new discipline with a focus on patients who develop heart failure while undergoing cancer treatment. The primary reason for this new subspecialty is simple: along with improving survival rates comes an increased focus on post-cancer quality of life. This is accompanied by soaring rates of cardiovascular disease, diabetes and obesity in the general population, significantly increasing the risk of a cancer patient developing cardiovascular dysfunction while on treatment. Outside of major cancer treatment centers, the underlying cardiac dysfunction is not often recognized until much later, owing to the fact that common signs of heart failure: fatigue, dyspnea and even cachexia, are commonly present in the cancer patient. New drugs may also not carry adequate warnings that would aid the oncologist in recognizing symptoms..

Cardiotoxicity is often not wholly predicted by preclinical and clinical trials. This is primarily because patients with existing cardiovascular disease, or those with risk factors such as hypertension or coronary artery disease, are often excluded from early trials. Additionally, routine cardiac monitoring and identification of cardiovascular endpoints are rarely part of the trial protocol. The exception is when there is precedent of cardiotoxicity in

Figure 1.1

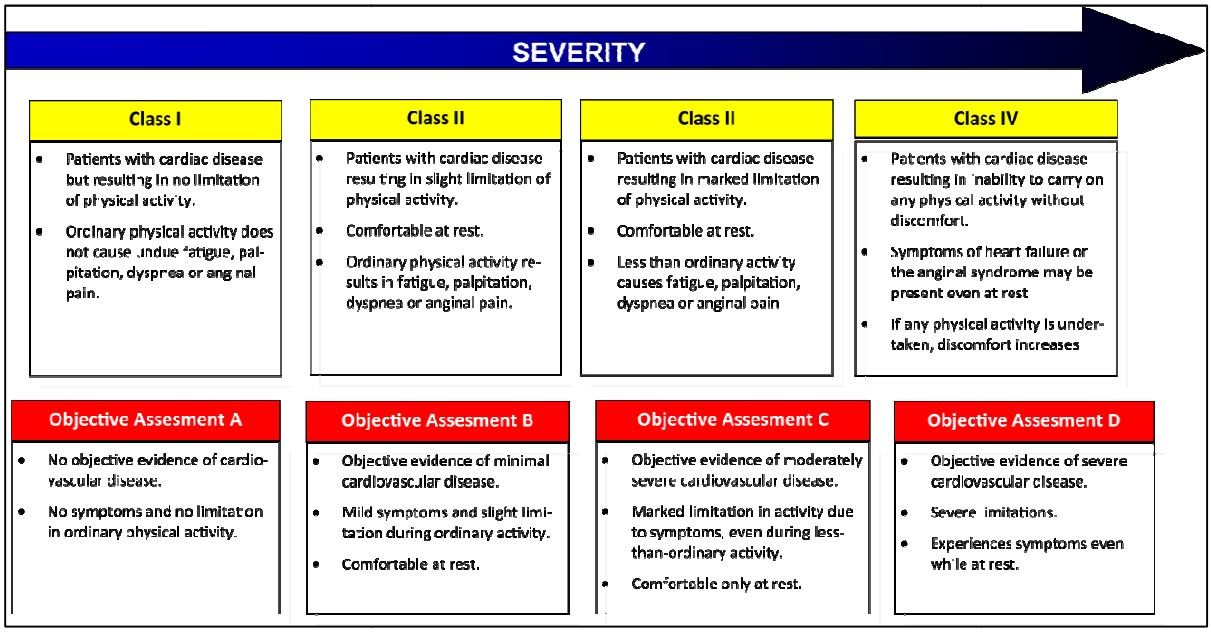

Figure 1.1. New York Heart Association Classification of Heart Failure.

[Source: American Heart Association. “Classes of Heart Failure.” 2014. http://www.heart.org/HEARTORG/Conditions/HeartFailure/AboutHeartFailure/Classes-of-Heart-Failure_UCM_306328_Article.jsp.]

Table 1.1.

Phase	Objective	Goals
Phase I	Safety	• 20-80 healthy volunteers • Determine frequent side effects • Drug metabolism and excretion
Phase II	Effectiveness	• 100's of patients • Determine if the drug works for a certain disease or condition compared to standard treatment/placebo • Safety and side effects continue to be monitored
Phase III	Safety and Effectiveness	• 1000's of patients • Studied in different populations at different doses • Study uses of the drug in combination with other drugs
New Drug Review by FDA	Approval	• Evaluate the quality of the data • Determine labeling and marketing • FDA will inspect facilities where drug will be manufactured
Phase IV	Continued safety	• Monitor post-marketing safety in the larger population • Sponsor is required to submit periodic safety updates to the FDA.

Table 1.1. Classification of Clinical Trials. Clinical trials are stratified based on the goal of the study with drug safety always being the primary concern. [Source: "US Food and Drug Administration Drug Approval Process." Food and Drug Administration website www.fda.gov.]

similar drugs in a class, such as the receptor tyrosine kinase inhibitors. In this case, the FDA may mandate assessment of cardiac function in these patients. Furthermore clinical trials—even large phase III trials (see **Table 1.1** for classification of clinical trials)—are not always sufficiently sized to identify less common toxicities (Hawthorne, 2010). For instance if the rate of cardiotoxicity occurs at 1 in 1000 patients and, on average, a drug is tested in a few thousand patients before approval, there will not be a strong enough correlation to identify the toxicity. Thus significant cardiotoxicity is often not recognized until the drug is available to the larger population (i.e. after marketing of the new drug).

1.2 Classes of Cardiotoxic Agents

Several different types of cancer treatments cause cardiac dysfunction. Therefore, a brief review of these agents and their effects on the heart is in order.

1.2.1 Anthracyclines

The group of anthracyclines continues to account for the majority of chemotherapy-induced cardiotoxicity. Adriamycin® (doxorubicin), a general DNA intercalating agent, induces oxidative damage and cardiomyocyte necrosis in a dose-dependent and cumulative manner. The mechanism of doxorubicin-induced cardiac damage is now relatively well understood and is likely due to the generation of reactive oxygen species and cardiomyocyte apoptosis (Zhou et al., 2001b). Anthracyclines may also target topoisomerase II (Top2)-dependent DNA binding in both the cardiomyocyte nucleus and mitochondria (Zhang et al., 2012). Co-treatment with dexrazoxane, an EDTA-like iron chelator, has proven to be an effective strategy for limiting ROS damage and cardiotoxicity in patients receiving low-dose doxorubicin (Hasinoff et al., 2003; Swain et al., 1997). However, dexrazoxane can interfere with the drug's oncologic efficacy, and therefore since 2011 its use has been limited to breast cancer patients receiving high-dose doxorubicin

(Edvardsen and Sarvari, 2013). Nonetheless, doxorubicin remains a widely used treatment option, particularly for pediatric lymphoma patients.

1.2.2 Her2/neu Inhibitors

Mutations in the ErbB2/Her2 receptor are common drivers of cell growth and proliferation, most notably in ErbB2/Her2-positive breast cancer. Patients treated with trastuzumab (Herceptin®), a monoclonal antibody directed against the ErbB2 receptor, are at significantly higher risk of cardiotoxicity, particularly if previously or co-treated with an anthracycline (Hahn et al., 2014). Her2 receptors are also expressed in the heart. Our lab has found upregulation of the receptor in the failing heart, which is partially reversible with mechanical unloading (Uray et al., 2002). Neuregulin (NRG-1) signaling through the Her2 receptor to ErbB4 regulates an essential pro-survival pathway that mediates the heart's response to pressure overload stress (Sawyer et al., 2002; Zhao et al., 1998). For this reason, angiotensin converting enzyme (ACE) inhibitors are effective in minimizing trastuzumab cardiotoxicity (Mackey et al., 2008). Limited evidence also suggests that moderate exercise can improve cardiac function in these patients (Jones and Alfano, 2013; Scott et al., 2011).

1.2.3 Receptor tyrosine Kinase Inhibitors

Since Judah Folkman's 1971 discovery of TAF (tumor angiogenesis factor), a pro-angiogenic factor isolated from tumor cells, the field of tumor angiogenesis, and the development of antiangiogenic cancer therapies, has rapidly evolved (Folkman, 1971). The first milestone was reached in 2004 when the FDA approved bevacizumab (Avastin®, Genentech), a monoclonal antibody directed against the proagniogenic vascular endothelial growth factor (VEGF). The success of this drug in blocking angiogenesis in several solid tumor types—including metastatic colorectal cancer, and non-small cell lung cancer—led to

the rapid FDA approval of two subsequent small molecule receptor tyrosine kinase inhibitors (RTKIs): sorafenib (Nexavar®, Bayer Pharmaceuticals), in December of 2005, and sunitinib (Sutent®, Pfizer) in January of 2006 (Rock et al., 2007). In addition to targeting the VEGFR, these agents also target the platelet-derived growth factor receptors (PDGFRs). Both of these agents are approved for use in metastatic renal cell carcinoma, among a group of other highly vascularized solid tumors. Two additional small molecule RTKIs have been developed and are now in different stages of clinical trials: axitinib (AG013736, Pfizer) and pazopanib (Votrient®, GlaxoSmithKline).

The principle behind antiangiogenic treatment is to cut off blood supply to the tumor, thereby inducing nutrient deprivation and limiting the potential for cell evasion and metastasis. This is accomplished through three main mechanisms: regression of existing vasculature, normalization of blood vessels and inhibition of the formation of new vessels (Rini, 2007). Angiogenesis is driven primarily by the VEGF receptor, PDGFRβ, fms-related tyrosine kinase 3 (FLT3) and the stem cell factor KIT. While FLT3 and KIT may contribute to blood vessel growth, the antiangiogenic properties of these drugs are conferred primarily through inhibition of the VEGFR on endothelial cells and the PDGFRβ on pericytes (Rini, 2007). While originally touted as the next revolution in cancer treatment, the promise of antiangiogenic drugs has been somewhat disappointing. Some patients do not respond at all whereas others rapidly develop resistance (Rapisarda and Melillo, 2012). Furthermore, the increase in survival has been relatively modest in those who do respond.

1.3 Current Methods of Diagnosis and Treatment

Similar to non-cancer related heart failure, cardiotoxicity is usually first recognized by a significant decrease in left-ventricular ejection fraction or fractional shortening when assessed by echocardiography or cardiac magnetic resonance imaging. Cardiac

arrhythmias may also be present on the electrocardiogram. Elevated circulating levels of cardiac troponins or naturietic peptides are also indicative of cardiac damage and are also used as biomarkers of cardiotoxicity in cancer patients (Cardinale et al., 2004; Dolci et al., 2008). Increasingly, routine cardiac monitoring is included for patients receiving known cardiotoxic agents, especially if there are risk factors or a family history of cardiovascular disease.

When clinically significant cardiotoxicity is identified in a patient, an otherwise effective cytostatic treatment must be stopped and the cardiac dysfunction addressed before the patient either resumes treatment or switches to an alternative treatment. Management of chemotherapy-induced cardiotoxicity is no different from treatment of standard cardiac patients, including the usual combination of ACE inhibitors, beta-blockers and diuretics. Two recent studies found that prophylactic treatment with the ACE inhibitor enalapril or the beta-blocker carvedilol helped mitigate cardiotoxicity associated with anthracycline (doxorubicin) treatment (Lipshultz et al., 2002; Santos et al., 2002). Longer drug infusion times have also been shown to decrease cardiotoxicity but require the use of infusion pumps and indwelling catheters (Ewer et al., 2005). Most patients who receive proper cardiac care will recover cardiac function. However, approximately 8% of patients who develop heart failure do not survive past 10 years (Cheng and Force, 2010).

1.4 Sunitinib

1.4.1 Discovery and Development

Shortly after Dr. Folkman's discovery of TAF, a number of companies developed ATP analogs that could compete with ATP for the catalytic site on most tyrosine kinases. This research led to the develoment of receptor tyrosine kinase inhibitors, including

Gleevec® (imatinib), Tarceva® (erlotinib) and Sutent® (sunitinib), all of which are in current clinical use.

Sunitinib (SU11248) was developed by Schlessinger and Ullrich who formed SUGEN, a biotechnology company which was bought by Pharmacia and subsequently by Pfizer (Faivre et al., 2007). After undergoing multiple iterations of the chemical due to low solubility and high toxicity, SU11248 showed antitumor efficacy in both cell and animal studies. Ensuing phase I trials in patients with acute myeloid leukemia and solid tumors established a dose of 50mg per day on a 4 weeks on, 2 weeks off, cycle schedule. This was primarily to avoid bone marrow and adrenal toxicity (Faivre et al., 2007). Phase I trials also revealed specific efficacy for the treatment of imatinib resistant gastrointestinal stromal tumors (GIST) and metastatic renal cell carcinoma (mRCC). Sunitinib treatment of mRCC in Phase II trials resulted in an objective response rate (ORR) of approximately 42%. This was far superior to the existing therapy for mRCC, interferon alpha (INFα), which had an average ORR of less than 20% (Faivre et al., 2007). Thus sunitinib was first approved for, and is still predominantly used for, the treatment of mRCC. Cardiotoxicity associated with sunitinib treatment was not recognized until later Phase III trials.

Approximately 60% of mRCC tumors have mutations in the tumor suppressor, von Hippel-Lindau (VHL) (Rini et al., 2009). VHL is an E3 ligase that under normoxic conditions binds to hydroxylated proline residues in the alpha subunit of hypoxia inducible factor 1 alpha (Hif1α), thereby targeting it for degradation by the proteasome. When intracellular oxygen levels fall, VHL dissociates from Hif1α, allowing it to dimerize with Hif1β and induce transcription of a multitude of genes, including VEGF and PDGF. Accordingly, VHL mutations in mRCC result in a strong induction of angiogenesis and highly vascularized solid tumors. The most common clinical manifestation of VHL syndrome is angioblastoma.

Over 1500 germline or somatic mutations have been described in VHL disease, which is an autosomal dominant disease occurring in 1/100,000 people.

Sunitinib exhibits strongest affinity for the VEGFR followed closely by the PDGFR, Fms-related tyrosine kinase 3 (FLT3) and KIT (Faivre et al., 2007). Sunitinib, however, is an extremely promiscuous TKI, owing to the high conservation of the ATP binding pocket across the kinome. In an *in vitro* test, sunitinib inhibited nearly 20% of all kinases tested (Rock et al., 2007) and it is estimated that it can inhibit up to 300 different kinases (Force et al., 2007). Nonetheless, there is a tendency to develop resistance when used as a single treatment and there has been a push to combine sunitinib treatment with other treatments (Faivre et al., 2007). This combination therapy may hold promise in limiting sunitinib toxicity as the drug could be used at lower doses.

1.4.2 Clinical Incidence of Cardiotoxicity with Sunitinib.

In accordance with the National Cancer Institute's Common Criteria for Adverse Events (CCTAE) National Cancer (Institute, 2009), clinical trials report the incidence of adverse events in patients receiving a new drug. Adverse events are scored on a scale of 1-5, with 1 being the least severe (see **Table 1.2** for a description of the grading of adverse cardiac events in clinical trials). Diarrhea, nausea, fatigue and vomiting are common with most chemotherapeutics, but it was the high incidences of hypertension and decline in left-ventricular ejection fraction (LVEF) that was most striking with sunitinib, though the reported incidences of both vary widely (see below). This may be for several reasons including the extent of cardiac monitoring and trial exclusion criteria.

Table 1.2 National Cancer Institute's Common Terminology Criteria for Adverse Cardiac Events.

CARDIAC GENERAL						Page 1 of 3
		Grade				
Adverse Event	Short Name	1	2	3	4	5
NAVIGATION NOTE: Angina is graded as Cardiac ischemia/infarction in the CARDIAC GENERAL CATEGORY.						
Cardiac ischemia/infarction	Cardiac ischemia/infarction	Asymptomatic arterial narrowing without ischemia	Asymptomatic and testing suggesting ischemia; stable angina	Symptomatic and testing consistent with ischemia; unstable angina; intervention indicated	Acute myocardial infarction	Death
Cardiac troponin I (cTnI)	cTnI	—	—	Levels consistent with unstable angina as defined by the manufacturer	Levels consistent with myocardial infarction as defined by the manufacturer	Death
Cardiac troponin T (cTnT)	cTnT	0.03 – <0.05 ng/mL	0.05 – <0.1 ng/mL	0.1 – <0.2 ng/mL	0.2 ng/mL	Death
Cardiopulmonary arrest, cause unknown (non-fatal)	Cardiopulmonary arrest	—	—	—	Life-threatening	—
REMARK: Grade 4 (non-fatal) is the only appropriate grade. CTCAE provides three alternatives for reporting Death: 1. A CTCAE term associated with Grade 5. 2. A CTCAE 'Other (Specify, __)' within any CATEGORY. 3. Death not associated with CTCAE term – *Select* in the DEATH CATEGORY.						
NAVIGATION NOTE: Chest pain (non-cardiac and non-pleuritic) is graded as Pain – *Select* in the PAIN CATEGORY.						
NAVIGATION NOTE: CNS ischemia is graded as CNS cerebrovascular ischemia in the NEUROLOGY CATEGORY.						
Hypertension	Hypertension	Asymptomatic, transient (<24 hrs) increase by >20 mmHg (diastolic) or to >150/100 if previously WNL; intervention not indicated	Recurrent or persistent (≥24 hrs) or symptomatic increase by >20 mmHg (diastolic) or to >150/100 if previously WNL; monotherapy may be indicated	Requiring more than one drug or more intensive therapy than previously	Life-threatening consequences (e.g., hypertensive crisis)	Death
		Pediatric: Asymptomatic, transient (<24 hrs) BP increase >ULN; intervention not indicated	Pediatric: Recurrent or persistent (>24 hrs) BP >ULN; monotherapy may be indicated	Pediatric: Same as adult	Pediatric: Same as adult	
REMARK: Use age and gender-appropriate normal values >95th percentile ULN for pediatric patients.						

CARDIAC GENERAL

		Grade				
Adverse Event	Short Name	1	2	3	4	5
Hypotension	Hypotension	Changes, intervention not indicated	Brief (<24 hrs) fluid replacement or other therapy; no physiologic consequences	Sustained (≥24 hrs) therapy, resolves without persisting physiologic consequences	Shock (e.g., acidemia; impairment of vital organ function)	Death
ALSO CONSIDER: Syncope (fainting).						
Left ventricular diastolic dysfunction	Left ventricular diastolic dysfunction	Asymptomatic diagnostic finding; intervention not indicated	Asymptomatic, intervention indicated	Symptomatic CHF responsive to intervention	Refractory CHF, poorly controlled; intervention such as ventricular assist device or heart transplant indicated	Death
Left ventricular systolic dysfunction	Left ventricular systolic dysfunction	Asymptomatic, resting ejection fraction (EF) <60 – 50%; shortening fraction (SF) <30 – 24%	Asymptomatic, resting EF <50 – 40%; SF <24 – 15%	Symptomatic CHF responsive to intervention: EF <40 – 20% SF <15%	Refractory CHF or poorly controlled; EF <20%; intervention such as ventricular assist device, ventricular reduction surgery, or heart transplant indicated	Death
NAVIGATION NOTE. Myocardial infarction is graded as Cardiac ischemia/infarction in the CARDIAC GENERAL CATEGORY.						
Myocarditis	Myocarditis	—	—	CHF responsive to intervention	Severe or refractory CHF	Death
Pericardial effusion (non-malignant)	Pericardial effusion	Asymptomatic effusion	—	Effusion with physiologic consequences	Life-threatening consequences (e.g., tamponade); emergency intervention indicated	Death
Pericarditis	Pericarditis	Asymptomatic, ECG or physical exam (rub) changes consistent with pericarditis	Symptomatic pericarditis (e.g., chest pain)	Pericarditis with physiologic consequences (e.g., pericardial constriction)	Life-threatening consequences; emergency intervention indicated	Death
NAVIGATION NOTE: Pleuritic pain is graded as Pain – *Select* in the PAIN CATEGORY.						
Pulmonary hypertension	Pulmonary hypertension	Asymptomatic without therapy	Asymptomatic, therapy indicated	Symptomatic hypertension, responsive to therapy	Symptomatic hypertension, poorly controlled	Death
Restrictive cardiomyopathy	Restrictive cardiomyopathy	Asymptomatic, therapy not indicated	Asymptomatic, therapy indicated	Symptomatic CHF responsive to intervention	Refractory CHF, poorly controlled; intervention such as ventricular assist device, or heart transplant indicated	Death

CARDIAC GENERAL						Page 3 of 3
		Grade				
Adverse Event	Short Name	1	2	3	4	5
Right ventricular dysfunction (cor pulmonale)	Right ventricular dysfunction	Asymptomatic without therapy	Asymptomatic, therapy indicated	Symptomatic cor pulmonale, responsive to intervention	Symptomatic cor pulmonale poorly controlled; intervention such as ventricular assist device, or heart transplant ind cated	Death
Valvular hear: disease	Valvular heart disease	Asymptomatic valvular thickening with or without mild valvular regurgitation or stenosis; treatment other than endocarditis prophylaxis not indicatec	Asymptomatic; moderate regurgitation or stenosis by imaging	Symptomatic; severe regurgitation or stenosis; symptoms controlled with medical therapy	Life-threatening; disabling; intervention (e.g., valve replacement, valvuloplasty) indicated	Death
Cardiac General – Other (Specify, __)	Cardiac General – Other (Specify)	Mild	Moderate	Severe	Life-threatening; disabling	Death

Table 1.2. National Cancer Institute's Common Terminology Criteria for Adverse Cardiac Events. [Source: National Cancer Institute (2009). Common Terminology Criteria for Adverse Events V4.0 H.a.H. Services, ed. (Institute, 2009)]

In preclinical monkey studies, there was evidence of increased in arterial blood pressure and QT intervals at high doses of sunitinib. However, the first indication of significant hypertension with sunitinib was reported in a 2006 randomized, double blind Phase III trial for sunitinib as a second-line treatment of imatinib-resistant GIST (Demetri et al., 2006; Faivre et al., 2007). Of the 202 patients that received sunitinib, 18 patients (8.9%) developed hypertension with 3 patients (6%) developing grade 3, which is defined as an increase of greater than 20 mmHg (diastolic) or to greater than 150/100 mmHg and requiring more than one antihypertensive medication. The major Phase III study that supported the FDA approval of sunitinib as a second line treatment for GIST, reported hypertension in 31 patients (15%) with 9 patients (4%) developing grade 3/4 (Rock et al., 2007). Most relevant for my experimental work was a decline in LVEF to >50% in 11% of patients treated with sunitinib versus 3% in the placebo group. Closely following this study, a randomized phase III study of sunitinib versus interferon alpha as a first line treatment for mRCC reported that 24 patients (8%) developed hypertension and 10 patients (3%) developed a decline in LVEF of at least 10% (Motzer et al., 2007).

With a longer follow-up, Telli et al found a decline in LVEF to below normal levels occurred in 21%, with 4% of patients experiencing a drop in LVEF of greater than 20% (Telli et al., 2008). This was important because it suggested that a significant portion of patients receiving sunitinib experience subclinical cardiotoxicity. In an effort to clarify the incidence of hypertension with sunitinib, Zhu and colleagues conducted a meta-analysis of 4,999 mRCC patients from 13 different trials and reported the incidence of hypertension to be 21.6% with 6.8% of patients developing high grade (3 or 4) hypertension (Zhu et al., 2009). Similarly, a retrospective, multicenter analysis of 175 patients with mRCC—with a focus on adverse cardiac events—found that 17 patients (18.9%) develop some degree of cardiac abnormality with 12 patients (6.9%) developing grade 3 or higher left ventricular dysfunction and

congestive heart failure (Di Lorenzo et al., 2009). Noting the high incidence of cardiotoxicity in their own clinic, Telli and colleagues at Stanford University performed a retrospective study of 48 patients who had received sunitinib between July 1, 2004 and July 1, 2007 in their clinic (Telli et al., 2008). Seven patients (15%) developed symptomatic grade 3/4 heart failure and 3 patients had persistent cardiovascular dysfunction despite discontinuation of sunitinib and commencement of heart failure treatment. The Telli study is unique in that these patients were treated off-protocol, meaning that no patient was excluded because of hypertension, coronary artery disease or previous treatment with an anthracycline. Therefore Telli's patient population is more representative of the general population. Collectively, the incidence of hypertension with sunitinib is approximately 20% and the incidence of LVEF decline is between 7% and 15%.

The most quoted study of sunitinib cardiotoxicity describes a much higher incidence of cardiotoxicity. Chu et al performed a retrospective analysis of a Phase I/II trial of 75 patients with GIST treated with sunitinib (Chu et al., 2007). Six patients (8%) developed congestive heart failure, while 10 patients (28%) and 7 patients (19%) experienced EF declines to >10% and >15%, respectively. The authors also report that 35 patients (47%) had blood pressures of greater than 150/100 mmHg. In addition to vastly higher incidences of cardiovascular toxicity compared to much of the literature, this study is notable because it was the first attempt to evaluate the mechanism of sunitinib cardiotoxicity.

1.4.3 Proposed Mechanisms of Cardiotoxicity

While the clinical incidence of sunitinib cardiotoxicity has been extensively documented, studies investigating the molecular mechanism tend to be descriptive, primarily noting cardiomyocyte hypertrophy, cellular ATP depletion and apoptosis (Chu et al., 2007; Cohen et al., 2011; French et al., 2010; Kerkela et al., 2009; Korashy et al., 2014; Will et al.,

2008). In these studies, the mechanism is often broadly attributed to the promiscuity of the kinase and the inhibition of a wide range of kinases. In a study using *in vitro* competition binding assay, which screened 38 different compounds against 317 different kinases (~55% of the predicted human kinome), sunitinib inhibited 57% of all kinases tested (Hasinoff et al., 2008; Karaman et al., 2008) (**Figure 1.2**). This was second only to staurosporine, which is well known as a non-selective inhibitor. A similar screen found that sunitinib inhibited up to 147 of the 242 kinases tested (Kumar et al., 2009). Beyond its primary targets (VEGFR, PDGFR, cKIT, FLT3) sunitinib potentially inhibits the metabolic energy regulator, AMP-activated protein kinase (AMPK) and ribosomal S6 kinase (RSK) (Kerkela et al., 2009; Laderoute et al., 2010). Consequentially, most of the investigations into the mechanism of sunitinib cardiotoxicity have centered on these two kinases.

In their pioneering investigation of the molecular mechanism of sunitinib cardiotoxicity, Chu and colleagues obtained endomyocardial biopsies from two patients that had developed left ventricular dysfunction and congestive heart failure while on sunitinib (Chu et al., 2007). Not only was there evidence of cardiomyocyte hypertrophy, but there was also aberrantly shaped and swollen mitochondria with effaced cristae and membrane "whorls" (**Figure 1.3**), though it has been suggested this is a freezing artifact (Dr. Michael Ewer, MD Anderson Cancer Center, personal communication). The same group demonstrated aberrantly shaped mitochondria in mice treated with sunitinib at 40mg/kg for 21 days. Nonetheless, neonatal rat ventricular myocytes treated with sunitinib at clinically relevant concentrations (1uM) displayed increased apoptosis, as evidenced by cytochrome c release and caspase 9 activation (Chu et al., 2007). As a follow-up to this paper, the same group treated mice for 5 weeks at a dose of 25mg/kg (Kerkela et al., 2009). Histological assessment of cardiomyocyte size revealed cardiomyocyte hypertrophy despite no difference in left ventricular mass. This, the

Figure 1.2.

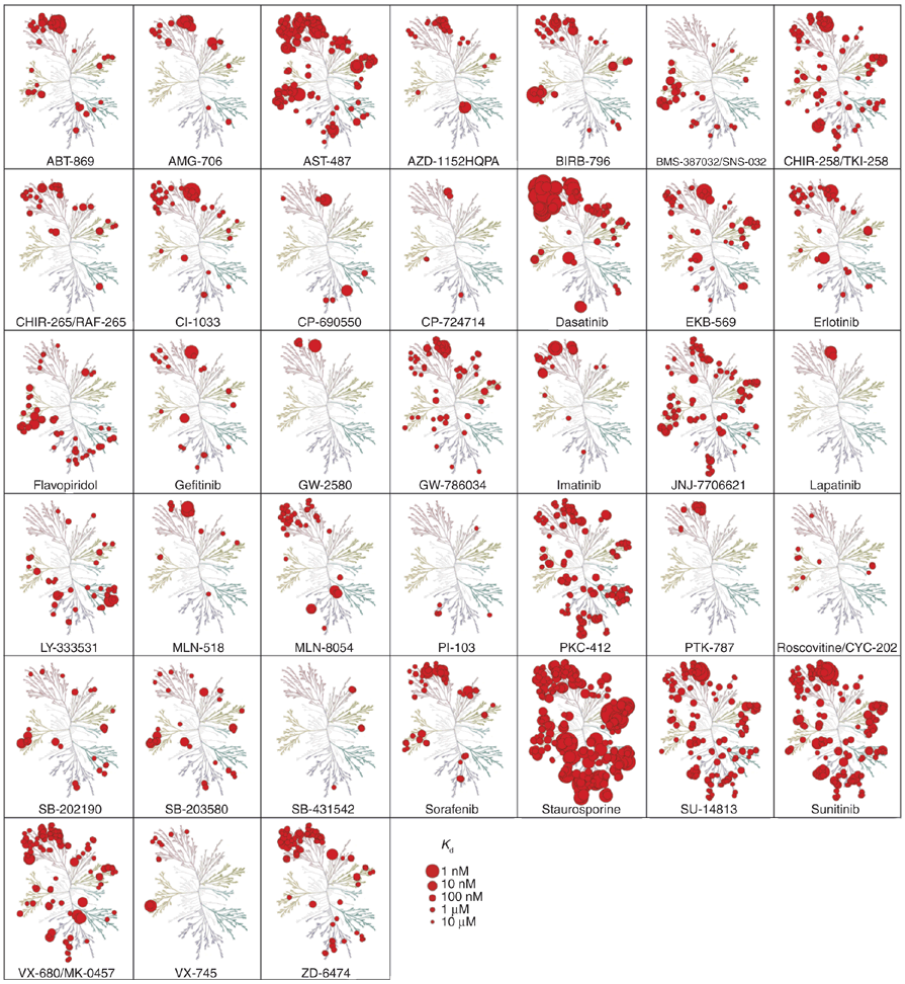

Figure 1.2. Selectivity profiles of receptor tyrosine kinase inhibitors.

The sizes of the red circle represent the affinity of binding for the inhibitor to a given kinase. The smallest circle represents a Kd of 10 µM and 1 nM for the largest circle. The tyrosine kinases are depicted in the upper left of the graph. Sunitinib is the most non-specific kinase inhibitor behind staurosporine. [Source: Karaman, M.W., Herrgard, S., Treiber, D.K., Gallant, P., Atteridge, C.E., Campbell, B.T., Chan, K.W., Ciceri, P., Davis, M.I., and Edeen, P.T. (2008). A Quantitative Analysis of Kinase Inhibitor Selectivity. Nature biotechnology 26, 127-132. (Karaman et al., 2008). Used with permission from the journal, license number 3583190938523.]

Figure 1.3

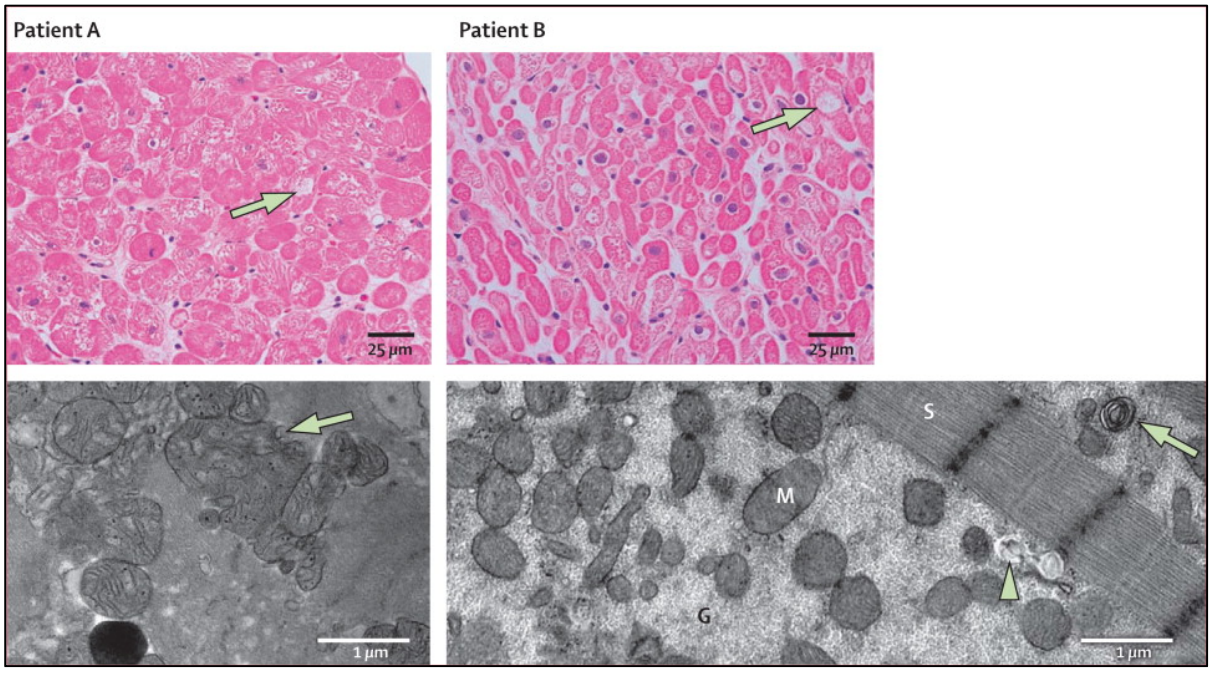

Figure 1.3. Sunitinib-induced mitochondrial structural abnormalities.

Endomyocardial biopsies from two patients who developed heart failure while on sunitinib demonstrating aberrantly shaped and swollen mitochondria with effaced cristae and membrane "whorls." [Source: Figure 5 from Chu, T.F., Rupnick, M.A., Kerkela, R., Dallabrida, S.M., Zurakowski, D., Nguyen, L., Woulfe, K., Pravda, E., Cassiola, F., and Desai, J. (2007). Cardiotoxicity Associated with Tyrosine Kinase Inhibitor Sunitinib. The Lancet 370, 2011-2019. (Chu et al., 2007) Used with permission from the journal, license number 3583200430074.]

authors concluded, was consistent with myocyte loss, and went on to show evidence of apoptosis in NRVMs. The authors also observed a loss of mitochondrial membrane potential and depletion of cellular ATP content. However, mitochondrial respiration was not measured. ATP content does not reflect the rate of ATP turnover (Taegtmeyer et al., 1985). Consistent with the theory that sunitinib inhibits AMPK, the decline in cellular ATP levels did not result in a corresponding activation of AMPK, as measured by phosphorylation of its downstream target acetyl-CoA carboxylase (ACC). Furthermore, restoration of AMPK signaling with adenoviral transfection of constitutively active AMPK reduced sunitinib-induced cell death.

Nonetheless, inhibition of AMPK as the cause of sunitinib cardiotoxicity remains a debated issue. Activation of AMPK using the biguanide metformin did not protect from sunitinib-induced cell death in NRVMs (Hasinoff et al., 2008). The same authors demonstrated that ROS-mediated cell death was also not likely the cause of cardiotoxicity, because dexrazoxane also did not prevent sunitinib-induced cell death. Pretreatment of human induced pluripotent stem-cell derived cardiomyocytes with metformin or AICAR, a similar AMPK activator, also did not protect from sunitinib-induced cell death (Cohen et al., 2011). As an alternative cause of sunitinib-induced energy depletion, others have tested whether sunitinib affects mitochondrial ATP generation. Of four small-molecule receptor tyrosine kinase inhibitors tested (imatinib, dasatinib, sunitinib and sorafenib), only sorafenib significantly affected respiration of isolated mitochondria from H9C2 cardiomyocytes (Will et al., 2008). In particular, sunitinib lacked any direct mitochondrial effects. Still, others have observed the appearance of autophagic vesicles and increased autophagic flux both in vivo and in vitro (Knapton et al., 2013; Zhao et al., 2010). Collectively, these studies support the notion that sunitinib treatment results in cardiac energy depletion, yet the exact mechanism

remains to be determined. My work suggests that hypoxia plays role and is discussed in detail in Chapter 4.

1.5 Cardiotoxicity as a Discovery Platform for Cellular Mechanisms of Heart Failure.

Most of clinical cardiotoxicity research is centered on the development of biomarkers for earlier identification of cardiac dysfunction as well as advancing methods of cardiac imaging (strain-gauge echocardiography, 3D echocardiography). There is also a broad push for increased cardiac monitoring and longer follow-up times in patients receiving known cardiotoxic drugs. Because of the delayed cardiotoxic effects of certain chemotherapeutic agents (Hahn et al., 2014), there has also been a call for the establishment of patient registries to allow for easier identification of cardiotoxic therapies post-FDA approval (Cheng and Force, 2010). Targeted delivery of therapies directly to the cancer cells through new technologies such as nanoparticles or dual-specific antibodies may also decrease cardiotoxicity in the future. As discussed above, comparatively little research has investigated the molecular mechanisms of cardiotoxicity, with the exception of doxorubicin. Ideally, once the mechanism by which a treatment causes cardiac dysfunction is known, adjunct therapies can be developed to protect the heart while still killing the cancer.

To this end, my first mentor Dr. Aarif Khakoo (now of AMGEN in South San Francisco, CA) developed the concept of “cardiotoxicity as a discovery platform” (**Figure 1.4**). His idea was that once significant cardiotoxicity is associated with a particular new therapy—such as sunitinib—the drug can be taken into animal studies for target identification and mechanistic insight. This mechanistic insight can be used to identify novel targets for the treatment of non-chemotherapy related human heart failure. I propose to extend the concept of “cardiotoxicity as a discovery platform” to a discovery platform for the

identification of cellular mechanisms and metabolic derangements in heart failure. Until the work of my previous lab, PDGFRβ signaling and the presence of pericytes in the coronary microvasculature was thought to be unimportant in the adult heart. As it will be demonstrated in Chapter 3, PDGFRβ signaling within the pericyte is essential for the ability of the heart to respond to stress. Increasing pericyte coverage in the failing heart may be a novel treatment strategy for heart failure. Furthermore, as it will be demonstrated in Chapter 4, my experiments in rodents have exposed a major metabolic signaling pathway in failing human hearts which is akin to the Warburg Effect in cancer.

Figure 1.4.

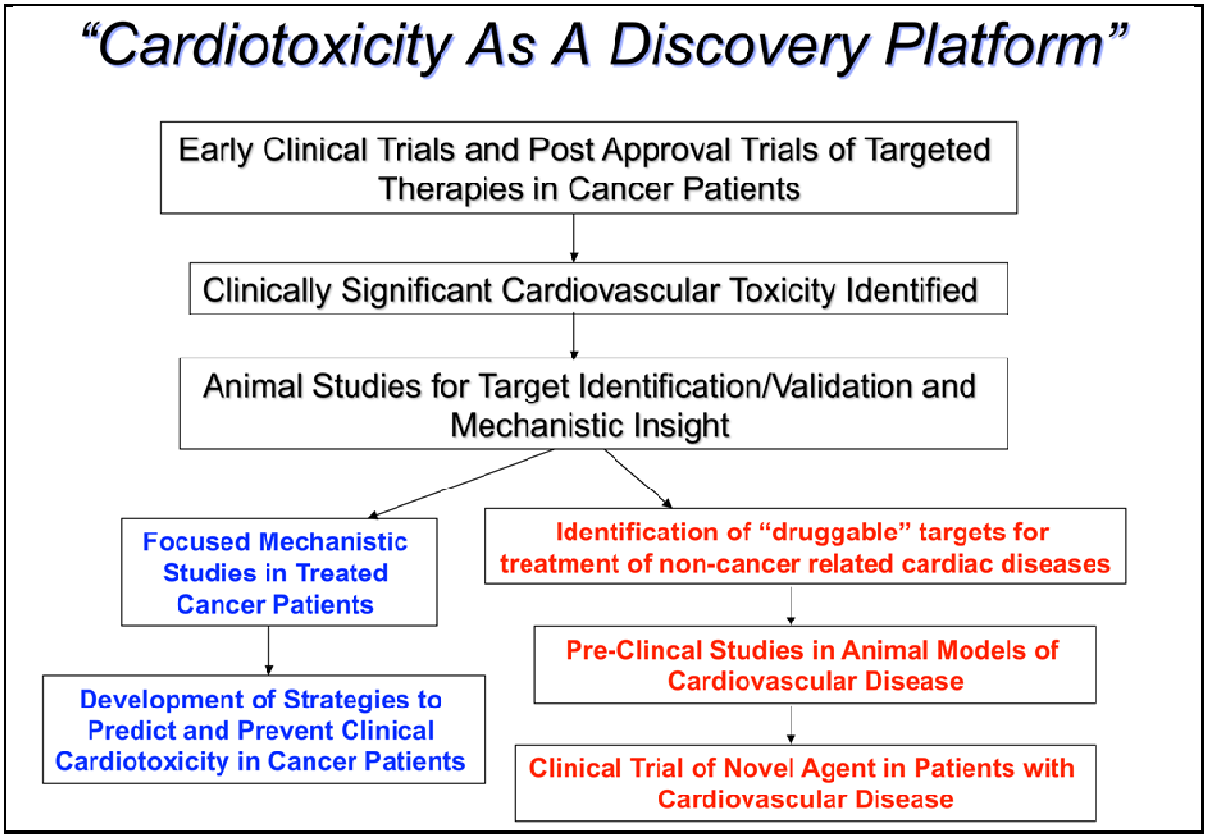

Figure 1.4. Cardiotoxicity as a Discovery Platform. After significant cardiovascular toxicities are identified in early clinical trials or post-approval trails, the drug can be studies in a mouse model for target identification and mechanistic insight. The findings can be used in one of two ways. The first is to identify strategies to prevent and predict cardiotoxicity in the cancer patient. The second is to identify possible novel targets for the treatment of non-chemotherapy related human heart failure. [Source: Khakoo, A. "Cardiotoxicity as a Discovery Platform." Personal communication.]

Chapter 2

MATERIALS and METHODS

2.1 Materials

2.1.1 Animals

Animals were cared for according to the National Institutes of Health guidelines. All protocols were approved by The University of Texas MD Anderson Cancer Center Institutional Animal Care and Use Committee or the Animal Welfare Committee of The University of Texas Health Science Center at Houston. The hyperinsulinemic euglycemic clamp procedures were approved by the Institutional Animal Care and Use Committee of Baylor College of Medicine (Houston, TX). All mice were of C57BL/6J background and obtained from Jackson Labs with the exception of immunodeficient nude mice used for the *in vivo* tumor xenograft experiments.

In vivo tumor xenograft experiments. Immunodeficient nude mice (NU/J) were obtained from Jackson Laboratories. A sunitinib-sensitive, human-derived renal cell carcinoma cell line (786-0) was obtained from Dr. Eric Jonasch at the MD Anderson Cancer Center. Cells (107) were suspended in 150 ml of PBS, mixed with an equal volume of Matrigel (BD Biosciences), and injected subcutaneously into the left flank. Mice were euthanized when tumor volume exceeded 1500 mm^3.

2.1.2 Human Heart Muscle Samples

Tissue Samples from failing hearts: Failing heart muscle samples were obtained from patients referred to the Texas Heart Institute with advanced heart failure and implanted with a left ventricular assist device (LVAD). Tissue from the left ventricular apex was obtained during LVAD implantation and again at the time of device removal by Dr. O. Howard Frazier at the Texas Heart Institute (Houston, TX). Tissue samples were immediately freeze clamped between two aluminum blocks precooled in liquid nitrogen as previously described by Wollenberger et al. (Wollenberger et al., 1960). Human subjects

gave informed consent and the study protocol was approved by the Committee for the Protection of Human Subjects of CHI St. Luke's Health in Houston, Texas, and by The University of Texas Medical School at Houston.

Non-failing Heart Samples: Non-failing heart samples were obtained from the apex of the left ventricle of patients undergoing heart-lung transplantation due to pulmonary hypertension and right-ventricular failure. Left-ventricular function was normal, as assessed by echocardiography. A full characterization of these patients and method of tissue harvesting has been published (Cordero-Reyes et al., 2014). This study was approved by the Houston Methodist Hospital's Institutional Review Board.

2.1.3 Reagents

Sunitinib malate obtained from Pfizer for the pericyte experiments and purchased from LC Laboratories (St. Louis, MO) for the metabolic experiments Dimethyloxalylglycine (DMOG) was obtained from Tocris Bioscience (Bristol, United Kingdom). Cobalt chloride and all other laboratory reagents were obtained from Sigma Aldrich (St. Louis, MO). Please refer to **Table 2.1** for a list of antibodies used in western immunoblotting.

2.2 Methods

2.2.1 Assessment of Cardiac Function

2.2.1.1 Cardiac Magnetic Resonance Imaging

Magnetic resonance imaging (MRI) allows for the acquisition of precise, high-resolution images of the heart. A strong magnetic field aligns the protons (mainly water molecules) within a specimen in a single direction. Pulses of radio frequency

electromagnetic fields are applied to alter the alignment of the protons relative to the magnetic field. The contrast between the heart wall and the ventricle is determined by the rate at which the excited atoms return to equilibrium. Next, a Fourier transformation converts this signal into an image. MRI is optimized for cardiac imaging by gating the image sequences to the electrocardiogram. This allowed for synchronization of the pulses with the beating heart, and enabled visualization of cardiac motion and accurate assessment of cardiac output (Epstein, 2007).

With the assistance of Dr. James Bankson and the Small Animal Imaging Facility at M.D. Anderson Cancer Center, a protocol was developed to image mice on a Bruker 7.05-T MR scanner (Bruker Biospin MRI, Billerica, MA). Mice were lightly anesthetized (1-2% inhaled isoflurane) and the flow was adjusted to maintain the heart rate between 350-500 beats per minute and the rate of respiration at 30-40 breaths per minute. Mice were kept warm (37^{o}C) by a circulating water-filled imaging platform. Sagittal and coronal images were first obtained to orient correctly to the left ventricle and apex of the heart. Next, six (~1mm thick) short-axis images were obtained every 6 milliseconds with 3 milliseconds between pulses moving from the apex to the base of the heart. The left ventricular chamber size was determined in both systole and diastole for each of the six images by tracing the contour of the left ventricular and using the modified Simpson's rule for volume determination (Folland et al., 1979). Left ventricular ejection fraction, a measure of systolic function, was defined as LVEF = ((EDV – ESV)/EDV)*100 and averaged across the six sections.

2.2.1.2 Coronary Flow Reserve

Doppler ultrasound is an proven non-invasive method for determining blood flow in the heart and major vessels in the mouse (Hartley et al., 2011; Hartley et al., 2008). Blood

flow velocity is determined as the difference in wave frequency between and emitted signal and the returning echoes from moving red blood cells. The Doppler signal is the summation of Doppler shifted echoes from different red blood cells moving at different velocities. Doppler shift frequency (Δf) is related to blood flow velocity (V) by the following equation:

$$\Delta f = 2f_o (V / c) \cos\theta$$

Where f_o is the ultrasonic frequency (20 MHz for use in mice), c is the speed of sound in blood (~1,540 m/s), and θ is the angle between the sound beam and the direction of flow. When the sound beam is parallel to the direction of flow (θ is zero), the conversion factor relating velocity to the Doppler shift is 3.75 (cm/s)/kHz at 20 MHz (Hartley et al., 2011).

Blood flow velocity through the left descending coronary artery was measured using a 2mm diameter 20-Mhz ultrasound probe connected to a signal processing unit (MouseDoppler, Indus Instruments, Webster, TX). The animal was lightly anesthetized and placed in the supine position on a warmed (37^{o}C) procedure board containing ECG electrodes. The ultrasound tip was stabilized and maneuvered using a micromanipulator (model MM3-3, World Precision Instruments, Sarasota, FL) until the characteristic LAD Doppler signal was obtained. Coronary flow velocities were determined at baseline (1% isoflurane) and after application of a hyperemic stimulus (2.5% isoflurane). The vasodilatory properties of isoflurane are well described and provide an advantage over adenosine in that isoflurane has a smaller effect on heart rate (Hartley et al., 2011). The ratio of peak flow velocities at baseline and 2.5% isoflurane is reported as the coronary flow reserve.

2.2.1.3 Mean Arterial Pressure

Mouse blood pressure was measured non-invasively with a specialized tail pressure transducer and occlusion cuff (CODA, Kent Scientific, Torrington, CT). This specialized cuff directly measures blood volume in the tail (Feng et al., 2008). Non-anesthetized mice were placed into nose cone holders and the sensor and occlusion cuff were slid onto the tail. This was repeated on three consecutive days before the start of the experiment to allow for acclimatization. During a given session, 10 acclimatization cycles were taken followed by 20 measurement cycles for each mouse. The system measured a total of 6 blood pressure parameters simultaneously: systolic blood pressure, diastolic blood pressure, mean arterial blood pressure, heart pulse rate, tail blood volume and tail blood flow (Malkoff, 2005).

2.2.1.4 Cardiac Contractile Reserve (dP/dt_{max})

The ventricular pressure-volume (PV) loop relates changes in ventricular volume to pressure throughout the cardiac cycle (Lilly and School, 1998). A PV loop begins at the beginning of the cardiac cycle, point a, at the lower left of the loop (**Figure 2.1**). The point represents the opening of the mitral valve and the beginning of ventricular filling in diastole. A small rise in pressure is seen when travelling from point a to point b and the ventricle stretches in accordance with the properties of passive elastic compliance. Point b is reached when this pressure exceeds a, causing the mitral valve to close and isometric left ventricular contraction commences. This isometric contraction occurs as the volume remains constant as the pressure rises. When the pressure in the left ventricle surpasses the diastolic pressure in the aorta, the aortic valve opens and the ventricle begins to empty (point c). The pressure continues to increase until the ventricle relaxes. The curve from point c to d represents the afterload, the pressure against which the left ventricle ejects. As the left ventricle beings to relax (point d) the pressure in the left ventricle falls and no more blood is

ejected from the heart. Isovolumetric relaxation will continue until the pressure in the left ventricle drops below the pressure in the left atrium when the mitral valve opens and the loop begins again at point a. Changes in cardiac contractility are represented by the slope of the end-systolic pressure volume relation (EDPVR) curve. When cardiac contractility is increased, such as by the infusion an inotropic agent such as of dobutamine (see **Figure 2.1**), this curve shifts upward and to the left (from 1 to 2). As a result, the stroke volume increases and the end systolic volume decreases. When there is a defect in cardiac contractility, such as I have observed in sunitinib-treated mice, this curve does not shift as far, resulting in a decreased slope (Lilly and School, 1998). These experiments were expertly performed by Vishnu Chintalgattu with assistance from me.

For the measurement of cardiac contractility, maximum pressure in the left ventricle over time was measured by inserting a pressure sensitive catheter (1 French, Millar Instruments, Houston, TX) into the left ventricle. Mice were deeply anesthetized with isoflurane and fixed to a heated (37^{o}C) procedure board containing ECG electrodes. Mice were intubated, ventilated and a cervical incision exposed the trachea and carotid arteries. The catheter was inserted into the left carotid artery and advanced into the left ventricle. After stabilization of the heart rate and left ventricular pressures, pressure-volume loops were generated using the Millar Pressure-Volume Loop System (Millar Inc. Houston TX). PV loops were generated at baseline and with increasing concentrations of dobutamine (1, 3 and 5 mg/kg per minutes) administered through the tail vein using a syringe infusion pump.

Figure 2.1.

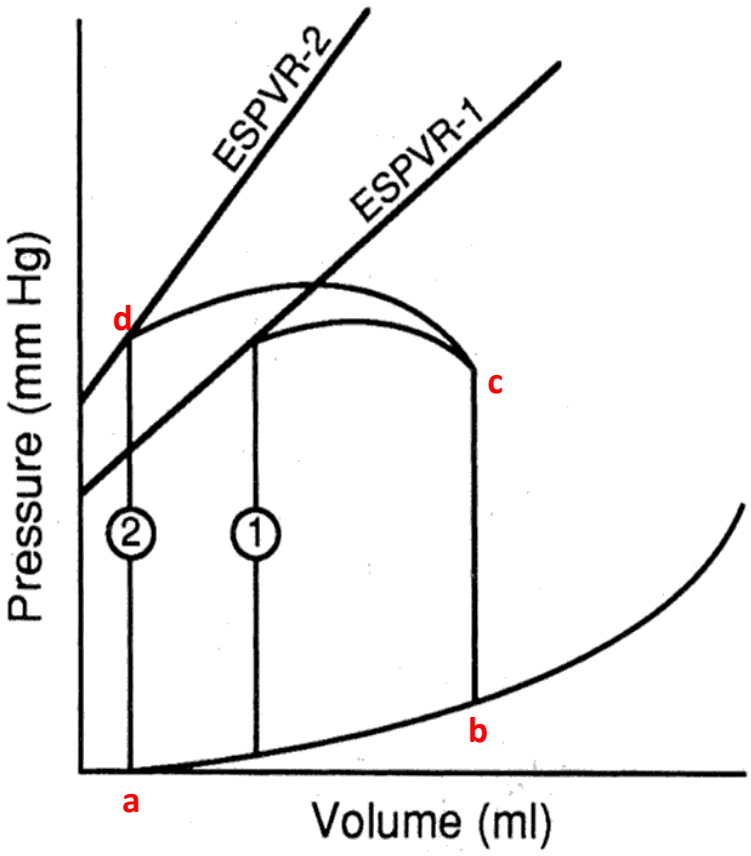

Figure 2.1. Left-ventricular Pressure-Volume Loop. A plot of the ventricular pressure as a function of volume, over the course of the cardiac cycle. See text for a full description of the cycle. ESPVR, end-systolic pressure-volume relation. [Source: Lilly, L.S., and School, H.M. (1998). Pathophysiology of Heart Disease: A Collaborative Project of Medical Students and Faculty. (Williams & Wilkins). (Lilly and School, 1998)].

2.2.1.5. Wire Myography of Isolated Aortic Rings

Vascular reactivity of isolated aortic rings from mice treated with sunitinib or vehicle was performed in a blinded fashion by the lab of Dr. Nathan Bryan at The University of Texas Institute of Molecular Medicine as previously described (Erez et al., 2011).

2.2.2 Hyperinsulinemic Euglycemic Clamp*

**This procedure was performed by Dr. Pradip Saha of the Mouse Metabolism Core at Baylor College of Medicine.*

The hyperinsulinemic euglycemic clamp procedure was first developed by DeFronzo and colleagues in 1979 and has since become the gold standard for assessing whole-body glucose homeostasis and insulin sensitivity in both the lab and the clinic (Defronzo et al., 1979). During this procedure, relatively high blood insulin levels are maintained in order to suppress hepatic gluconeogenesis such that a steady-state condition is reached where the infusion of exogenous glucose is equivalent to the rate of whole-body glucose disposal (GDR) (Tam et al., 2012). The GDR is directly correlated with insulin sensitivity such that a high GDR indicates increased insulin sensitivity.

Five days before the procedure, mice were anesthetized using Nembutal (1ul/g body weight)/ avertine (15ul/g of body weight) and a micro catheter was implanted into the jugular vein until its tip reached to the right atrium; the catheter was tied with silk sutures at the venotomy site. The other end of the catheter was tunneled subcutaneously around the side of the neck to the top of the skull where it was exteriorized through skin filled with sterile EDTA (0.45%) solution and closed the open end of the catheter using a hot metallic surface. On the day of the procedure fasted (overnight), conscious mice were infused with insulin at

a constant rate for 5 hours. Blood samples were collected from tail vein before infusion and at every hour during infusion. Mice first received a primed (10uCi) and then constant rate intravenous infusion (0.1uCi/min) of HPLC purified [3-^{3}H] glucose for 5 hours using a syringe infusion pump. After 60 minutes, mice were infused with 25-50% unlabeled glucose with another infusion pump at a rate adjusted to maintain the blood glucose level at 100-140 mg/dl. For tissue specific uptake, a 2-deoxy-D-[^{14}C] glucose (2DG) (10uCi) bolus was injected 45min before the end of the clamp procedure and a blood sample was collected at the administration of 2DG. 2DG is taken up by the cell and rapidly phosphorylated by hexokinase but not metabolized further. At the end of the procedure mice were sacrificed and tissues were evaluated for radiolabeled 2DG content by liquid scintillation counting.

Liquid scintillation counting is the standard method to determine the radioactivity of a sample. The energy emitted from low-energy radioisotopes is converted to light by the liquid scintillation cocktail. This cocktail contains two main components, an organic solvent and a scintillator(s) or fluor. The energy released from the radioactive decay excites the scintillator which a light pulse. This light pulse is then captured by the scintillation counter's photomultiplier tube and counted (Bray, 1960).

2.2.3 Isolated Cells

2.2.2.1 *In* Vitro Cell Proliferation (MTT) Assay

Human placental pericytes (PromoCell, Heidelberg, Germany), human umbilical vein endothelial cells (Genlantis, San Diego, CA) and human cardiac fibroblasts (Cell Systems Corporation, Kirkland, WA) were serum starved for 6 hours followed by treatment with sunitinib for 24 hours. Cell proliferation was measured using an MTT assay kit (Vybrant MTT, Life Technologies, Grand Island, NY). A MTT assay is a colorimetric assay that

measures cell proliferation by measuring the reduction of the yellow MTT dye (3-(4,5-dimethylthiazol-2-yl)-2,5-diphenyltetrazolium bromide) to its insoluble state, which has a purple color. This reduction requires NADH and therefore only occurs in viable, metabolically active cells (Fotakis and Timbrell, 2006).

2.2.3.2 Neonatal Rat Ventricular Myocytes (NRVMs)

The protocol for the isolation of neonatal rat ventricular myocytes was adapted from a method used by Dr. Diane Bick's lab at The University of Texas Health Science Center at Houston, Department of Pathology (Lash and Jones, 2013). All procedures were carried out in a biological safety hood. Neonatal Sprague-Dawley rats (1-2 day old) were briefly washed in 70% ethanol and decapitated. The heads were immediately dropped in liquid nitrogen. The chest cavity was opened, the heart removed and placed in 1X ADS buffer (NaCl [6.8g], KCl [0.4g], glucose [1.0g], NaH_2PO_4 [1.5g] $MgSO_4$ [0.1g] HEPES [4.76g] and pH adjusted to 7.38 with HCl/NaOH in 1L total volume of double distilled water [ddH_2O]) until all hearts (60 total) were collected. Hearts were rinsed once with 1X ADS buffer, halved and transferred to 25mm^2 tissue culture flask (15 hearts/flask) containing 9ml of enzyme buffer (1X ADS containing pancreatin [0.6mg/mL] and collagenase type II [73U/mL). Flasks were incubated for 20 minutes at 37^oC in a shaking water bath a total of five times. The supernatant from the first step was discarded. The others were collected, centrifuged for 5 minutes at 300g and the pellet resuspended in 2-3 newborn calf serum. All fractions were kept in the 37^oC incubator until the digestion was complete (no visible chunks of heart remaining).

The pooled pellets were centrifuged for 5 minutes at 300*g* and resuspended in 4mL of Percoll gradient (1.082 g/mL). Percoll gradient tubes were prepared in 15ml Falcon tubes using a 15 gauge feeding needle. Gradients were added slowly in order of increasing density (1.05 g/mL, 1.062 g/mL, and 1.082 g/mL). Percoll gradients were centrifuged for 20

minutes at 300g is a swing bucket rotor a room temperature. The cardiomyocytes remained in the 1.802 g/mL layer and were collected and washed 2X with 1x ADS. After the final wash, cardiomyocytes were re-suspended in complete media (DMEM [500mL}, BCS [50mL], and penicillin/streptomycin [10mL of 100U/mL]). Cardiomyocytes plated at a density of 2 million cells per 60mm dish (protein) or 0.75 million cells per well in a 6-well plate (RNA). The cell culture medium was replaced the next morning and then daily for the remainder of the experiment. NRMVs spontaneously contract for up to 7 days in culture.

2.2.3.3 Adult Mouse Cardiomyocytes

The procedure for the isolation of adult cardiomyocytes (AMCs) was adopted from the lab of Paul Simpson (O'connell et al., 2007). The isolation was performed under semi-sterile conditions; all buffers and equipment were filtered and autoclaved, respectively, however hearts were removed and digested outside of the tissue culture hood.

Mice (6-10 weeks old) were deeply anesthetized with chloral hydrate (60mg/kg) via intraperitoneal injection. To avoid clotting in the cardiac vessels, heparin (0.2mL of 1000U/mL) was injected intraperitoneally. The mouse was deemed fully anesthetized when he did not respond to reflex tests (toe or tail pinch). A thoracotomy was performed and the beating heart removed by clipping the aorta and pulmonary veins. The heart was immediately dropped into ice-cold perfusion buffer (NaCl [120.4mM, KCl [14.7mM], KH_2PO_4 [0.6mM], $NaHPO_4$ [0.6mM], $MgSO_4$-$7H_2O$ [1.2mM], Na-HEPES [10mM], $NaHCO_3$ [4.6mM], taurine [30mM], BDM [10mM], and glucose [5.5mM] in cell culture grade water and pH adjusted to 7.0 with HCl). Excess tissue (e.g. thymus) was removed and the aorta teased from the surrounding connective tissue. The aorta was cannulated using a 22-gauge pediatric catheter cover on a 1mL syringe containing perfusion buffer. The aorta was

temporarily fixed onto the cannula using a microclip and the syringe was depressed to ensure the heart inflated and there were no leaks from the aorta. The cannula was placed on a primed, water-jacketed Langendorff-style apparatus containing warmed (37°C) perfusion buffer and tied with silk suture. The heart was perfused in retrograde at 4 mL/minute for 4 minutes to flush and excess blood from the heart. Next, the buffer was switched to perfusion buffer containing collagenase type II (Lot 305, Worthington Biochemical, Lakewood, NJ) and $CaCl_2$ [40 μM]. Once the heart became pale and soft (16-20 minutes) it was cut from the cannula and immediately placed in a $60mm^2$ dish containing 2.5mL of stopping buffer (perfusion buffer containing 10% bovine calf serum and 100mM $CaCl_2$).

The heart was teased apart with forceps and pipetted up and down a few times with a transfer pipette. The suspension was passed through a cell strainer (100μM), transferred to a 15mL Falcon tube and centrifuged at room temperature for 3 minutes at 20*g*. The supernatant was discarded and the pellet resuspended in stopping buffer containing 100μM $CaCl_2$. The cells were incubated at room temperature for 2 minutes and next spun again at 20*g* for 3 minutes. This was repeated with stopping buffer containing 400μM $CaCl_2$ and 900μM $CaCl_2$ to gradually restore cellular calcium levels to near physiologic concentrations. After the final spin, cells were resuspended in plating medium (MEM [Eagle's with Hank's Buffered salts] containing 10% bovine calf serum, BDM [10mM], penicillin [100U/mL] and ATP [2mM]). Cell density was determined by counting the number of rod-shaped cardiomyocytes. The quality of the isolation was determined by the percentage of rod-shaped, compared to round-shaped cells under an inverted light microscope. At percentage of least 50% was considered acceptable for further experimental use. Cardiomyocytes were incubated for one hour at 37°C in 2% CO_2. Plating medium was then changed to culture medium (MEM [Eagles with Hank's buffered salts], BSA [1mg/mL], penicillin [100U/mL, ITS

[insulin (5ug/mL, transferring (5ug/mL) and selenium (5ng/mL)] and BDM [10mM]). Experimental procedures began 2 hours after plating.

2.2.4 Tissue Collection and Preservation

2.2.4.1 Protein Isolation and Quantification

Previously collected tissue was removed from a -80°C freezer and immediately placed in liquid nitrogen. Approximately 50mg of tissue was homogenized using a 2mL Dounce homogenizer in 1mL of protein lysis buffer (KCl [20mM], HEPES [30mM], EGTA [2.5mM], EDTA [2.5mM], β-glycerophosphate [40mM], NaF [40mM], $Na_4P_2O_7$ [4mM], glycerol (10%), Nondiet-40 [0.25%], protease inhibitor [cOmplete Mini tablets, Roche], phosphatase inhibitor cocktail 2 and 3 [100µl each/10mL, Sigma]). Samples were centrifuged at 14,000x*g* for 10 minutes at 4°C and the supernatant collected in a new tube on ice. For cells, each plate was washed 2x with PBS and 1mL (60mm2 dish) or 100ul/well (6-well plate) of protein lysis buffer (NaCl [150mM], HEPES [5mM, pH 7.4], EDTA [0.1mM, pH 8.0], MgCl2 [0.1mM], DTT [0.1mM], Triton X-100 [1%], protease inhibitor [cOmplete Mini tablets, Roche], phosphatase inhibitor cocktail 2 and 3 [100µl each/10mL, Sigma]) was used to scrape the cells from the well. Cells were sonicated and then centrifuged at 14,000x*g* for 10 minutes at 4°C.

Protein concentration was quantified using a bicinchoninic acid (BCA) colorimetric assay (Pierce, Rockford, IL) (Smith et al., 1985). Proteins in an alkaline (biuret reaction) solution reduce Cu^{2+} to Cu^{+}. Two molecules of bicinchoninic acid then chelate with each Cu^{+} ion to form a purple reaction product that is observed at 562nm. The amount of reduced Cu+ is proportional to the amount of protein in the sample. This reaction does not have a true end point, the color continues to develop, but the reaction is sufficiently slow to allow for

accurate assessment of protein concentration. Protein concentration was calculated based on a set of BSA standards (12.5-2000 µg/µl). Protein samples were diluted (1:5-1:20) and 5µl of diluted sample was plated in triplicate in a 96-well plate. The plate was left at room temperature for 30 minutes before being read on a plate reader.

2.2.4.2 Nuclear Fractionation

Nuclear fractionation was performed on fresh tissue on the day of sacrifice following a protocol described by Luo et al (Luo et al., 2011). Fresh tissue or cells were homogenized with a Dounce homogenizer in hypotonic buffer (HEPES/KOH [10mM, pH 7.5], KCl [10mM], MgCl2 [1.5 mM], K_2EDTA [1 mM], EGTA [1 mM], Igepal [0.1%], DTT [1 mM], and protease inhibitor [cOmplete Mini tablets, Roche], phosphatase inhibitor cocktail 2 and 3 [100µl each/10mL, Sigma]) and left on ice for 30 minutes. Intact cells were removed by centrifugation at 53 g for 10 min. The supernatant was then centrifuged at 800x*g* for 10 min. The supernatant was kept as the cytosolic fraction. The nuclear pellet was washed twice with hypotonic buffer and lysed in isotonic buffer (hypotonic buffer plus 250 mM sucrose) by sonication. Protein concentrations were assessed as described above.

2.2.5 Histology and Immunohistochemistry

For histological and immunological examination, hearts were removed from the mice, rinsed in ice-cold PBS, cut on the transverse short axis near the apex of the heart. The remaining heart was quickly frozen in liquid nitrogen. For paraffin-embedded sections, the remaining tissue was placed in 4% paraformaldehyde or optimal cutting temperature medium (OCT) and taken to the Histology Research Lab in the UT Department of Pathology

and Laboratory Medicine for processing, embedding and sectioning. Both paraffin-embedded and frozen tissues were sectioned at 5 microns thick slices.

2.2.5.1 Hematoxylin and Eosin (H&E) Staining

H&E staining is the most widely used stain for basic observation of tissue morphology. Hematin, the oxidation product of hematoxylin, stains nucleic acids and other basophilic features blue through when oxidized *in situ* with a strong oxidant such as sodium iodate (Cardiff et al., 2014). Hematin binds to lysine residues of nuclear histones through a metallic ion, usually aluminum. The tissue is oversaturated with the dye to ensure binding and the undesirable background staining is then removed by leaching in an alcohol acid solution. The blue is then differentiated when returned to an alkaline solution. Next, the tissue is stained with eosin which, through a complex and poorly understood mechanism, dyes acidic features pink.

Paraffin-embedded tissue sections were rehydrated through alcohol gradients to distilled water. Sections were then placed in Lillie Mayer's alum hematoxylin (Sigma Aldrich, St. Louis, MO) for 4 minutes, rinsed in running tap water and differentiated in 0.3% acid alcohol (350mL ethanol, 125mL ddH_2O and 1.5mL concentrated hydrochloric acid) until the background was almost colorless. Sections were rinsed in running tap water and then Scott's tap water substitute (2g sodium bicarbonate, 20g magnesium sulfate in 1L ddH_2O) to differentiate the blue. Next, sections were stained in Eosin-Y (Richard-Allan Scientific) for 2 minutes, dehydrated, cleared in xylene and mounted. Five random fields from the endocardial and epicardial areas of the left ventricle were imaged at 400x using an inverted light microscope (Motic AE2000) connected to a 3.0 megapixel camera (Moticam 3). For measurement of cardiomyocyte cross-sectional area, round cells (40-60 per heart)

displaying clear membrane staining and visible nuclei were traced and area calculated using ImageJ software (Abràmoff et al., 2004).

2.2.5.2. Masson Trichrome Staining

Masson's trichrome staining is a three color staining protocol whose primary use in cardiology is to determine the extent of collagen deposition in the heart. Paraffin-embedded sections were stained using a commercially available kit (Accustain Trichrome Stains, Sigma Aldrich, St. Louis, MO). Slides were rehydrated in water and left in Bouin's solution (Sigma Aldrich, St Louis, MO) at room temperature overnight to achieve intense coloration of the tissue. Slides were rinsed in running tap water until the yellow color was removed. The nuclei were then stained in working Weigert's Iron Hematoxylin solution (Sigma Aldrich, St. Louis, MO) for 5 minutes and rinsed in running tap water followed by ddH_2O. Next, slides were placed in Biebrich Scarlet-Acid Fuchsin for 5 minutes to stain the cytoplasm and muscle fibers red. After rinsing in ddH_2O, slides were placed in fresh Phosphomolybdic/Phosphotungstic acid for 5-10 minutes to prepare the sections for uptake of the Aniline blue stain. Collagen was stained blue in a Aniline blue solution and differentiated in 1% acetic acid. Slides were rinsed, dehydrated through alcohol, cleared in xylene and mounted.

2.2.5.3 Periodic Acid Schiff (PAS) Staining

PAS staining is used to detect glycogen in the heart. Paraffin-embedded tissues were rehydrated to water and incubated in periodic acid (0.5%) for 5 minutes. Periodic acid is used to oxidize the carbohydrates containing 1-2 glycols, forming aldehyde groups. The

slides were then rinsed and placed in Schiff's reagent (Sigma Aldrich, St. Louis, MO) for 15 minutes. The aldehyde groups react with Schiff's reagent to form a deep pink color. Slides were rinsed in lukewarm tap water and counterstained with Mayer's hematoxylin. Slides were dehydrated, cleared and mounted. Finished slides were imaged as described above.

2.2.5.4 Scanning electron microscopy

Scanning electron microscopy was performed in a blinded fashion by Dr. Kenneth Dunner Jr. in the lab of Dr. Robert Langley at MD Anderson Cancer Center. Briefly, hearts were fixed in 2% glutaraldehyde in a 0.1M phosphate buffer (pH 7.4) for 24 hours at 4°C and then transported to Dr. Langley's lab for imaging. Imaging was performed as previously described (Higuchi et al., 2000). Images were psuedocolored in Adobe Photoshop. Grayscale images were colored with the "hue/saturation" function and the "history brush."

2.2.5.5. Immunofluorescence and confocal microscopy

Immunofluorescence and confocal imaging of cardiac sections for the assessment of microvascular pericyte coverage was performed by Vishnu Chintalgattu. Hearts were fixed in 10% formalin overnight and then embedded in optimum cutting temperature (OCT) medium. Frozen sections were incubated overnight at 4°C with anti-NG2 (1:200, Chemicon International) or anti-CD31 (1:200 Phamingen) and then incubated at room temperature with a fluorescently labeled secondary antibody followed by DAPI. Sections were imaged with an LSM 510 META inverted confocal microscope (Zeiss Instruments). ImageJ was used to quantify the NG2 and CD31 coverage area for each image.

2.2.5.6. Vessel tortuosity

Vessel tortuosity measurements were performed by James Culver, a graduate student in the lab of Mary Dickinson at Baylor College of Medicine, who was blinded to the treatment groups. Isolated hearts were infused with a 70kDa tetramethylrhodamine-labeled dextran (Invitrogen, Waltham, MA) and placed in a 1% agarose gel mold poured into a glass bottomed tissue culture dish (MatTek, Ashland, MA). Confocal Z-stacks were acquired beginning at the apex of the heart. Images were reconstructed and analyzed with Imaris (Bitplane, Oxford Instruments) with custom extensions written by James Culver in MATLAB. Vessel tortuosity was calculated for each branch (tortuosity, T, is defined as T = L/D, where L is the total arc length along a vessel trace, and D is the total displacement between the beginning and end of the branch).

2.2.6 SDS-PAGE and Western Blotting

Polyacrylamide gel electrophoresis (PAGE) is used to separate proteins by mass and charge. With the addition of the denaturant sodium dodecyl sulfate (SDS), all proteins become negatively charged and are separated solely by mass as they migrate through a polyacrylamide gel from a negative to positively charged electrode. Gels were poured in two steps, a lower resolving gel and an upper stacking gel. The separation of the proteins is dependent of the percentage of acrylamide in the gel. A 10% resolving gel was used for most proteins. In rare instances, an 8% resolving gel was used for large proteins (>100 kDa). For a 10% resolving gel 8mL of lower buffer (8mL lower buffer stock [36.3g Tris-base, 0.8g SDS, in 200mL of ddH_2O, pH adjusted to 8.8], 10.5 mL acrylamide/bis [30%]. 13.4mL ddH_2O, 300µl ammonium persulfate and 30µl TEMED) was poured between two 1.5mm

Table 2.1

Antibody	Molecular Weight (kDa)	Manufacturer Catalog #	1° Dilution	2° Type (1:5000 dilution unless noted)
GAPDH	37	Fitzgerald 10R-G109A	1:50,000	Mouse 1:10,000
β-tubulin	55	Santa Cruz 5274	1:1000	Mouse
p-PDGFRβ	190	Santa Cruz 12909-R	1:250	Rabbit
PDGFRβ	190	Cell Signaling 3169	1:1000	Rabbit
NG2	270-300	Millipore AB5320	1:500	Rabbit
O-GlcNAc (CTD110.6)	37-250	Cell Signaling 9875	1:1000	Rabbit
PKM1	60	Sigma-Aldrich SAB 42000094	1:10,000	Rabbit
PKM2	60	Cell Signaling 4053	1:500	Rabbit
Hif1α	120	Novus NB100-105	1:500	Mouse
c-myc	57-65	Cell Signaling 8492	1:1000	Rabbit
Histone H1	34	Santa Cruz 10806	1:1000	Rabbit
Histone H3	18	Santa Cruz 8654	1:1000	Goat

Table 2.1 Antibodies used for western blotting. The address of the manufacturers are as follows: Santa Cruz Biotechnology (http://www.scbt.com/) ; Cell Signaling Technology (http://www.cellsignal.com); Fitzgerald (http://www.fitzgerald-fii.com/); Millipore (www.emdmillipore.com/antibodies); Novus Biologicals (www.novusbio.com).

glass plates and allowed to solidify. A layer of isopropanol was floated on top to ensure even transition from resolving to stacking gels. Once the gel was solidified, the isopropanol was poured off and the stacking gel was added (2.5mL buffer stock [6g Tris-HCl, 0.4g SDS, in 100mL of ddH2O, pH adjusted to 6.8], 1.5mL acrylamide/bis [30%], 6mL ddH_2O, 90µl ammonium persulfate and 9µl TEMED). A comb was inserted and the gel was left to solidify a room temperature.

Protein samples (8-20µg in 5X loading buffer [For 30mL, 3.48g DTT, 9mL glycerol, 6mL SDS (20%), 7.5mL 1M Tris-HCl (pH 6.0), 2mL bromophenol blue) were boiled to 10 minutes at 70^{o}C and cooled to room temperature before loading into gels. Gels were run at 50mV in running buffer (6g Tris-base, 28.8g glycine, 1g SDS in 1L) until the protein traveled through the stacking gel and then turned up to 100mV for the remainder of the run.

Separated proteins were transferred to a PVDF (PolyVinyliDene Fluoride) membrane using a wet transfer method. PVDF membranes were pre-soaked in methanol (PVDF is highly hydrophobic, which makes it ideal for protein binding) and then soaked along with sponges and filter paper in cold transfer buffer (100ml of 10x stock [144g Tris-base, 30g glycine, 0.5g SDS in ddH2O [1L], 200mL methanol and 700mL ddH_2O) until use. After completion of the run, gels were soaked in transfer buffer for 10 minutes. A “sandwich” was then prepared from the bottom (cathode side) to the top (anode side) with a sponge, filter paper, gel, PVDF membrane, filter paper and sponge. The transfer was run in the cold room (4^{o}C) for either two hours at 110mV or overnight at 40mV.

Following the transfer, membranes were stained with Ponceau to ensure proper transfer and then blocked for one hour at room temperature in 5% milk. Membranes were incubated overnight in primary antibody (**Table 2.1**) with gentle rocking. Following 3, 10 minute washes in 0.4% Tween-TBS (Tris-Buffered Saline) membranes were incubated with

a HRP (horseradish peroxidase) conjugated secondary antibody in 5% milk for one hour at room temperature. Membranes were washed 3 x 10 minutes and then developed using Western Blotting Luminol reagent (Denville Scientific, South Plainfield, NJ). After developing, membranes were stripped and re-probed up to three times with stripping buffer (6mL Tris-HCl [1M, pH 6.8], 19.2mL SDS [10%], 0.675mL β-mercaptoethanol, and 70mL ddH_20).

Protein levels were quantified using densitometry. Films were scanned in black and white for consistent analysis and images were analyzed using the gel analysis tools in the ImageJ software (Abràmoff et al., 2004).

2.2.7 Analysis of Gene Expression

2.2.7.1 Total RNA Isolation and Quantification

Total RNA was isolated using TRIzol Reagent (Life Technologies, Carlsbad, CA) following the manufacturer's protocol with slight modifications. Human RNA was isolated using a kit per the manufacturer's instructions (RNeasy Fibrous Tissue kit, Qiagen, USA). No more than 20mg of tissue or cells were homogenized in 1mL of TRIzol with a Dounce homogenizer. RNA was then extracted by adding 0.2mL of chloroform to the tube and shaken vigorously for 2-3 minutes at room temperature. Samples were centrifuged at 12,000x*g* for 15 minutes at 4^{o}C. The aqueous phase was carefully removed to a new tube. For RNA extraction of adult cardiomyocytes, RNase-free glycogen (5µg) was added to the tube to aid in RNA precipitation. 0.5mL of isopropanol was added to the new tubes and samples were placed at -20^{o}C overnight to allow for RNA precipitation. The next day, samples were centrifuged for 10 minutes at 12,000x*g.* The pellet was washed one time with

1mL of 75% ethanol and allowed for air dry for 10 minutes. Pellets were resuspended in RNase-free H_2O (20-50µl) and incubated at 60^oC for 10 minutes.

Total RNA was quantified using a NanoDrop 1000 spectrophotometer (Thermo Scientific, Wilmington, DE). RNA quantity was determined using the Beer-Lambert Law, A=ECL (where A=absorbance, E=molar extinction coefficient [0.027 µg/mL/cm for single stranded RNA], C=concentration and L=light path) (Sambrook and Russell, 2001). The purity of the RNA was determined by the $A_{260/280}$ ratio with a ratio of >1.8 accepted as pure RNA.

RNA was reverse transcribed into cDNA in a separate reaction. 2ug of total RNA in a total of 12.5ul was added a nuclease-free tube followed by 7.5ul of reaction mix (0.5µl random hexamer primers [100pmol], 4µl 5x reaction buffer [Thermo Scientific], 2µl dNTPs [10mM], and 1µl reverse transcriptase [RevertAid, Thermo Scientific]). Samples were incubated for 10 minutes at 25^oC followed by 60 minutes at 42^oC. The reaction was terminated by heating at 70^oC for 10 minutes.

2.2.7.2 Quantitative Real Time Polymerase Chain Reaction (qPCR)

Most primer and TaqMan probe sets were already available in the lab. Those not already available were designed using OligoArchitect (Sigma-Aldrich, St. Louis, MO). Quantification was performed by multiplexing with 6-FAM (reporter) / TAMRA (quencher) and JOE (reporter) / BHQ1 (quencher) dyes for the target and the GAPDH endogenous control, respectively. This dye pair was chosen because the large difference in emission maximum gives the lowest spectral overlap. ROX reference dye (Invitrogen, #12223-012) was used as a passive reference dye to control for non-related fluctuations in the fluorescence. The amplification of the more abundant GAPDH was limited by the primer

concentration. This serves to spare common reagents (dNTPs, Mg^{2+}) for amplification of the target gene. The multiplex reaction mix was as follows:

Multiplex PCR Mix	µl per Reaction (25µ)	Concentration in Reaction
10X PCR Buffer	2.5	1X
dNTPs 2.5mM	3	300nM
$MgCl_2$ 50mM	2.5	5mM
Primers-F/R target gene (20µM)	1.125 ea.	900nM
Primers-F/R endogenous (20µM)	0.375 ea.	300nM
50X Rox Reference Dye	0.5	1X
Probes (10µM)	0.625 ea.	250nM
Taq	0.5	
DEPC H_20	4.25	
diluted cDNA (~1:20)	5	

To test for reaction efficiency, reactions were run in singleplex using a standard curve. The standard curve consisted of cDNA serially diluted ranging from 20pg-0.2fg. The reaction mix is as follows:

PCR Mix	per well (25µl)	Concentration in Reaction
10X PCR Buffer	2.5	1X
dNTPs 2.5mM	2.5	250nM
$MgCl_2$ 50mM	1.5	3mM
Primers-F/R 20µM	0.75 ea.	600nM
50X Rox Reference	0.5	1X
Probe 10µM	0.25	100nM
Taq	0.5	
DEPC H_20	10.75	
diluted cDNA (~1:20)	5	

The standard curve is plotted on a linear scale as C_T versus the concentration of the cDNA. The efficiency of the PCR can be determined from the slope of the standard curve using the formula:

$$Efficiency = 10\ x\ \frac{-1}{slope} - 1$$

Adequate efficiency was determined as having a slope between -3.58 and -3.10. The coefficient of correlation (R^2) was required to be at least 0.98.

Gene expression was analyzed using the ABI Prism® Sequence Detection System. Transcript levels were evaluated using the comparative C_T method ($\Delta\Delta C_T$ method), normalized to GAPDH as an endogenous control, and expressed as a fold difference from control (Biosystems, 2008). The comparative C_T method eliminates the need for a standard curve by instead using the relative difference between the control and treated samples. Samples were run in triplicate and average ΔC_T values for each sample for both the target gene and endogenous control was obtained through the software. All other calculations were performed in Microsoft® Excel. A simplified example:

Sample	GAPDH Avg. C_T	Target Avg. C_T	ΔC_T Target – GAPDH	$\Delta\Delta C_T$ ΔC_T - (Avg. Control ΔC_T)	Fold Difference* $2^{-\Delta\Delta CT}$
Control 1	15.791	16.202	0.411	-0.285	1.218
Control 2	16.667	17.329	0.662	-0.034	1.023
Sample 1	16.374	15.869	-0.505	-1.201	2.298
Sample 2	16.793	17.469	0.676	-0.02	1.013

*For derivation of the formula $2^{-\Delta\Delta CT}$, see Applied Biosystem's User Bulletin #2: http://www3.appliedbiosystems.com/cms/groups/mcb_support/documents/generaldocuments/cms_040980.pdf

2.2.7.3. Restriction Enzyme Digest of PKM2 PCR Product

Analysis of pyruvate kinase alternative splicing was performed as previously described with minor changes (Clower et al., 2010). Alternative splicing of exon 9 and 10 of the PKM gene results in two identical length isoforms, PKM1 and PKM2 (**Figure 2.2**). Mouse and human primer sets were designed to amplify exons 8 through 11. cDNA products were digested with PstI, NcoI (New England Biolabs, Ipswich, MA), both or left undigested. Products were run on a 5% native polyacrylamide gel [12mL 5X TBE (TrisBase, Boric acid, EDTA), 10mL 30% acrylamide/Bis solution, 38mL DDH_2O, 40ul TEMED, 400ul APS] at 30V in the cold room. The gel was post-stained with ethidium bromide [0.5ug/mL] for 20 minutes followed by two 20 minute washes with ddH_2O. Gels were imaged using a TD-1000R BiOVision dual-light transiluminator coupled to a camera. Images were analyzed using ImageJ.

2.2.7.4 Gene Expression Microarray

A gene expression microarray was performed by Vishnu Chintalgattu using a Mouse Genome 430 2.0 array gene chip purchased from Affymetrix (Santa Clara, CA). RNA from the hearts of mice treated with sunitinib or vehicle control for 3 or 7 days was used according to the manufacturer's protocol.

Table 2.2. Primer and Probe Sequences for PCR and qPCR.

Gene	Forward Primer (5'-3')	Reverse Primer (5'-3')	Probe (5'-3')
m PKM (exon 8-11)	GTCTGGAGAAACAGCCAAGG	CAACATCCATGGCCAAGTT	N/A
h PKM (exon 8-11)	AGAAACAGCCAAAGGGGACT	CATTCATGGCAAAGTTCACC	N/A
m PKM1	GCTGTTTGAAGAGCTTGTGC	TTATAAGAGGCCTCCACGCT	[6fam]CCAGTCACTCCACAGACC[tam]
m PKM2	CAGAGGCTGCCATCTACCAC	TCCTCGAATAGCTGCAAGTG	[6fam]GCCCGAGAGGCAGAGGCTGCC[tam]
h PKM1	AGCTGTTTGAAGAACTTG	CTCCGTCAGAACTATCAA	[6fam]GGAGTGCGTCTTGTGTCAGAA[tam]
h PKM2	GCCATCTACCACTTGCAA	CTTGGTGAGGACGATTATG	[6fam]CGGTGCATGCGTACTCCTTA[tam]
m GAPDH	GGTCTACATGTTCCAGTA	CCCATTTGATGTTAGTGG	[hex]ATTCAACGGCACAGTCAAGGC[bhq1]
m 18S	AGCTGAAACTTAAAGGAATTG	CACGGAATCGAGAAAGAG	[hex]TATCAATCTGTCAATCCTGTCCGTGT[bhq1]
m hnRNPA1	AGGAGGTTCTAATTACATACA	GCTGAGTTCACAAATCTG	[6fam]CTGTCACTTCTCTGGCTCTCCTC[tam]
m hnRNPA2	CTGTGAAGAAGCTGTTTG	CAGGATCATGGTCATCAA	[6fam]AAGGAAGATACTGAGGAACACCACC[tam]
m PTB	GGACCAAAGTTTAGCTTTC	CCCCACAGGTATAAAATCA	[6fam]ACTCTTCCACGCCTTCCACA[tam]
m c-myc	CGACTACGACTCCGTACAGC	GTAGCGACCGCAAACATAGGA	[6fam]CAGCAGAGCGAGCTGCAGCC[tam]
m GLUT4	TTCTGACCAACTAAGGGCGG	GTTCCTCCAGCACAGGACAC	[6fam]GCTGCCTATAAACACTGGTT [tam]
mr Hif1α	GGAAGCGAAAAATGGAACATC	TCACCTGGTTGCAGTAA	[6fam]TTCCAATTCCTGCTGCTTGAAAAAGGG[tam]
m PDK4	CTTTTCTGCGGCAAGAGCTG	TTCACTAAGCGGTCAGGCAG	[6fam]GGCCAATATCCTGAAGGAGA[tam]
m Angptl4	GGGACTGCCAGGAACTCTTC	GAAGTCCACAGAGCCGTTCA	[6fam]GGGAGCGGCACAGTGGACTT[tam]
m PHD3	AGGCAATGGTGGCTTGCTAT	GACCCCTCCGTGTAACTTGG	[6fam]CACCTGTATCTACTACCTGA[tam]
mr GLUT1	CATCGTCGTTGGGATCCTTA	GAGCAGTAGAGGCCACAAGTCT	[6fam]AGGTGTTCGGCTTAGACT[tam]
mr PDK1	GATCAGAAACCGGCACAATGA	AGGATGCACCCCGAAGCT	[6fam]CCATGGCCCAGGGTGTGACTGA[tam]

mr LDHa	CGACTGCACCATGATCGTG	TCCAGATTGCATCCACTTCC	[6fam]AGGCACACTGGCGTCGCCATGCT[tam]
mr αMHC	GCAAAGGAGGCAAGAAGAAAGG	TGAGGGTGGGTGGTCTTCAG	[6fam]ACAGTGTCTGCTCTCCACCGGGAA[tam]
mr βMHC	AGGGCGACCTCAACGAGAT	CAGCAGACTCTGGAGGCTCTT	[6fam]AGCTCAGCCATGCCAACCGTA[tam]
mr c-fos	GGTGCTGGATTGTATCTA	TGGTCGTTTCTAATTGGA	[6fam]CACGCTATTGCCAGGAACACAG[tam]
mr ANF	AGTGCGGTGTCCAACACAG	CTTCATCGGTCTGCTCGCT	[6fam]TCTGATGGATTTCAAGAA[tam]

Table 2.2 Primer and Probe Sequences for PCR/qPCR. Sequences are listed in the 5' to 3' direction. Dyes used for each probe are denoted in brackets. Species is specified as: m, mouse; h, human' r, rat.

Figure 2.2.

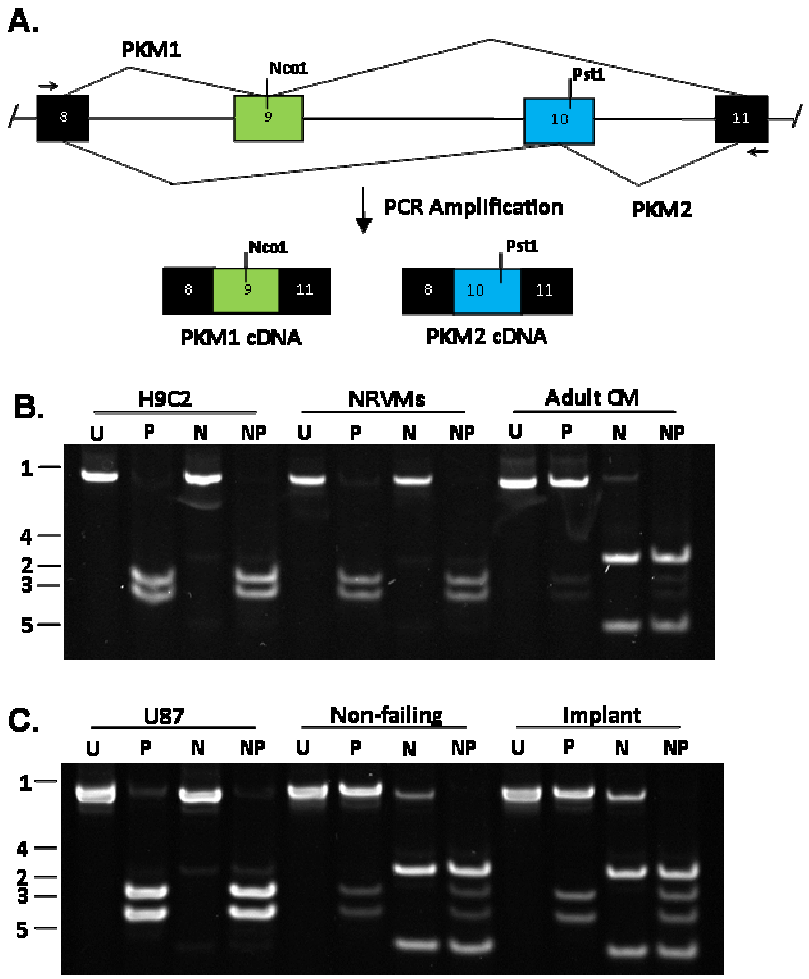

Figure 2.2 Analysis of the PKM splicing by restriction enzyme digestion. (A) Diagram displaying the cDNA products obtained using primers designed to amplify exon 8 through exon 11 of the PKM gene. (B) PKM isoform expression in the H9C2 rat cardiomyoblast cell line, isolated neonatal rat ventricular myocytes (NRVMs) or isolated adult mouse cardiomyocytes. The RT-PCR product was divided into four aliquots and left either uncut (U) or digested with PstI (P), NcoI (N) or PstI plus NcoI (NP). (C) PKM isoform expression in the U87 human glioblastoma cell line (as a positive control) or heart muscle samples from non-failing and failing human hearts.

2.2.8 Enzyme Activity Assays

Spectrophotometry was used to indirectly measure the rate of the appearance of a product of an enzymatic reaction. A spectrophotometer consists of two instruments, a light source (spectrometer) and a photometer, for capturing the light. A sample is placed in a liquid cuvette between the two instruments such that a light beam passes through the sample where a portion is absorbed. When light of a single wavelength passes through the solution, there is a direct relationship (Beer's Law) between the amount of light absorbed and the concentration of the reaction product (http://www.shimadzu.com/an/uv/support/fundamentals/structure.html):

Beer's Law: $I = I_o * 10^{-\varepsilon cl}$

Where I is the intensity of the light transmitted, ε is the reaction product's absorption coefficient, c is the concentration of the reaction product and l is the length of the light path. Because the light path is constant, the equation can be rewritten to

$I / I_o = 10^{-\varepsilon cl} = T$

T is the transmittance and there is a logarithmic relationship between the transmittance and the concentration of the reaction product such that

$-\log T = \log 1/T = \varepsilon cl$ = Optical density (absorbance)

Enzymes were extracted from whole tissue (~100mg) in 1mL of enzyme extraction buffer (50mM Tris-Base [pH 7.5], 100mM KCl, 5mM $MgCl_2$, 1mM EDTA [pH 7.6], 1% Triton X-100 and L-glutathione [153mg/50mL]) using a Dounce homogenizer. Samples were centrifuged for 5 minutes at 4°C and the supernatant recovered in a new tube. All enzyme activity assay protocols were adopted from Bergmeyer's Methods of Enzymatic Analysis (Bergmeyer, 2012).

2.2.8.1. Lactate Dehydrogenase Activity

Lactate dehydrogenase enzyme activity was measured in a phosphate buffer (0.1M, pH 7.0) containing pyruvate (2.5mg/mL) and NADH (10mg/mL). Activity was measured as the change in absorbance due to the oxidation of NADH at 340nm and normalized to protein content.

2.2.8.2. Pyruvate Kinase Activity

Pyruvate kinase activity was measured in a triethanolamine buffer (0.1M, pH 7.6) containing phosphoenolpyruvate, tri(cyclohexylammonium) salt (3.75mg/ml in 0.05M $MgSO_4$ /0.2M KCl buffer), ADP (30mg/mL, neutralized with KOH), NADH (10mg/mL) and LDH (from rabbit muscle, 32U/mL). Kinase activity was measured as the change in absorbance due to the oxidation of NADH at 340nm over the course of 12 minutes. Activity was normalized to protein concentration.

2.3 Statistical Analysis

Except where noted, results are expressed as the mean ± the standard error of the mean (SEM). Analysis was performed using ABI Prism Graphpad software using a two-tailed unpaired Student's t test or one-way ANOVA with a Tukey post hoc test. A *P* value of > 0.05 was considered statistically significant. In general, $*P < 0.05$, $**P < 0.01$ and $***P < 0.001$. *P* values that differ from this convention are indicated within the graph.

Chapter 3

MICROVASCULAR PERICYTES AS A PRIMARY TARGET OF SUNITINIB CARDIOTOXICITY

Notes

1. A considerable amount of the work presented in this chapter was performed by Vishnu Chintalgattu, PhD (currently a Senior Scientist in Cardiovascular Research at Amgen, Inc., San Francisco, CA). The work is presented here with the permission of both Dr. Chintalgattu and Dr. Aarif Khakoo

2. Some figures are recreated from Chintalgattu, V., Rees, M.L., Culver, J.C., Goel, A., Jiffar, T., Zhang, J., Dunner, K., Pati, S., Bankson, J.A., and Pasqualini, R. (2013). Coronary Microvascular Pericytes Are the Cellular Target of Sunitinib Malate–Induced Cardiotoxicity. Science translational medicine 5, 187ra169-187ra169. (Chintalgattu et al., 2013), with permission from the American Association for the Advancement of Science (license number 3466011035286).

3.1. Introduction

This chapter demonstrates that a primary cause of sunitinib cardiotoxicity is loss of coronary microvascular pericytes, resulting in coronary microvascular and cardiac contractile dysfunction. The data presented here show that loss of PDGFRβ signaling in the pericyte is a primary mechanism of sunitinib cardiotoxicity. Furthermore, I show that co-treatment with thalidomide preserves microvascular and contractile dysfunction without interfering with the anticancer efficacy of sunitinib.

3.1.1. Regulation of myocardial blood flow.

Sunitinib is foremost an inhibitor of angiogenesis and, as will be demonstrated in this chapter, sunitinib treatment leads to a disruption of myocardial vascular stability and function (Chintalgattu et al., 2013). Thus, a basic review of the regulation of myocardial blood flow is warranted. For an in-depth review of the regulation of blood flow in the coronary microcirculation, I refer to (Muller et al., 1996; Rubio and Berne, 1975).

Regulation of coronary blood flow is conceptually divided between regulation of the larger conduit vessels (>300μm in diameter), which confer little resistance to flow, and regulation of the smaller resistance vessels (<300μm in diameter) (Schelbert, 2010). **Figure 3.1.1** depicts the decline in blood flow velocity as a function of vessel cross-sectional area. The majority of coronary vascular resistance resides in the coronary arterioles less than 150μm in diameter (Chilian et al., 1986). It is important to note that there is considerable heterogeneity even within the small resistance vasculature. Vascular reactivity can differ substantially from the large to small arterioles as well as between the subendocardium—which is uniquely subject to the extravascular compressive forces of systole—and the subepicardium (Muller et al., 1996; Schelbert, 2010).

In the heart, the demand for oxygen is exactly matched by supply of oxygen through the coronaries. Unlike most other tissues, baseline extraction of oxygen is near maximal in the heart (**Figure 3.1.2**) (Gorlin, 1976). Accordingly, the primary mechanism to increase oxygen delivery to the myocardium is dilation of the small resistance vessels. At the same time, capillary pressure must remain constant to ensure efficient delivery of oxygen and nutrients (Muller et al., 1996). *Angina pectoris*—a painful tightening of the chest—occurs when myocardial oxygen demand exceeds coronary supply (Katz, 2010). It is important to note that oxygen delivery is also dependent on the hemoglobin content of the blood. For this reason, *angina pectoris* can result from severe anemia (Katz, 2010). Regulation of coronary vascular resistance is primarily controlled at local level, known as autoregulation, through myocardial production of metabolites, flow-mediated endothelial cell activation, and stimulation of the vascular smooth muscle (myogenic vasodilation) (Muller et al., 1996). The autonomic nervous system also controls vascular tone through activation of the alpha- and beta adrenergic receptors (Opie, 2004). The integration of signals leading to blood vessel dilation is summarized in **Figure 3.1.3.**

Myocardial demand for increased oxygen is thought to be transmitted through accumulation of adenosine, a degradation product of AMP and ADP (Schelbert, 2010). Adenosine readily diffuses out of the cell where it binds to receptors on vascular smooth muscle cells, leading to decreased intracellular calcium and relaxation (Lilly and School, 1998). Adenosine preferentially relaxes small arterioles compared to the larger vessels. Kantasuka and colleges demonstrated that rapid pacing of canine hearts led to dilation of both the large and small arterioles; however endogenous or exogenous supply of adenosine caused dilation in only the small arterioles (Kanatsuka et al., 1989). In addition to adenosine, other metabolic vasodilators include lactate, acetate and carbon dioxide (Katz, 2010).

Figure 3.1.1.

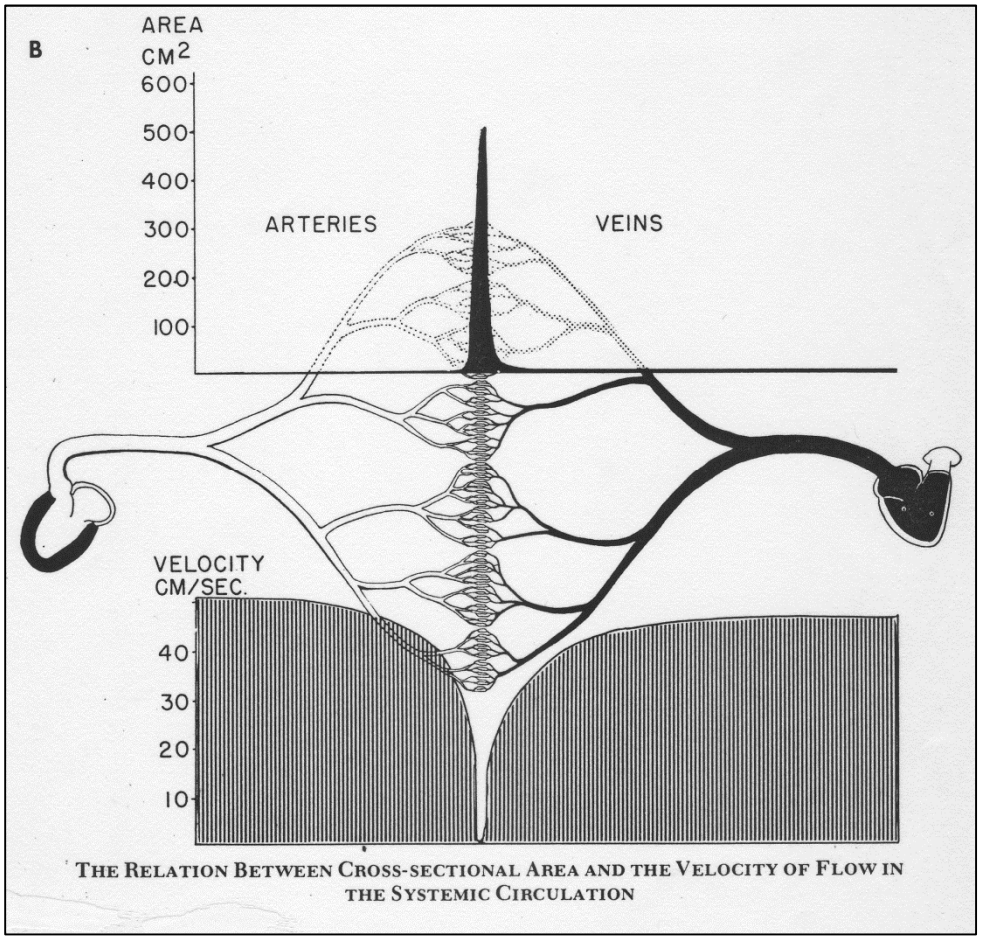

Figure 3.1.1. Relation between vessel cross-sectional area and blood flow velocity.

The largest resistance to blood flow in the heart is conferred by the smallest vessels in the heart. These vessels also account for the largest area in the heart. [Source: Rushmer, R.F. (1976). Cardiovascular Dynamics. (W.B. Saunders Company). (Rushmer, 1976)].

Figure 3.1.2.

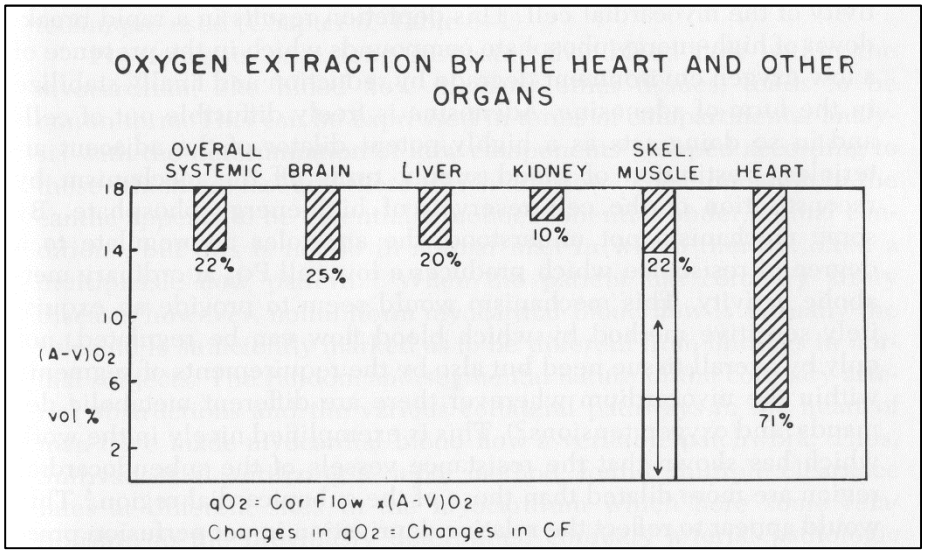

Figure 3.1.2. Oxygen consumption by the heart and other organs. The heart consumes more oxygen than any other organ at rest. Skeletal muscle can increase oxygen extraction during exercise but cardiac muscle oxygen extraction remains constant. Cardiac oxygen consumption per minute (qO_2) is equal to the difference between the arterial and venous percent oxygen multiplied by coronary flow. [Source: Gorlin, R. (1976). Coronary Artery Disease. (W.B. Saunders Company). (Gorlin, 1976)].

Figure 3.1.3.

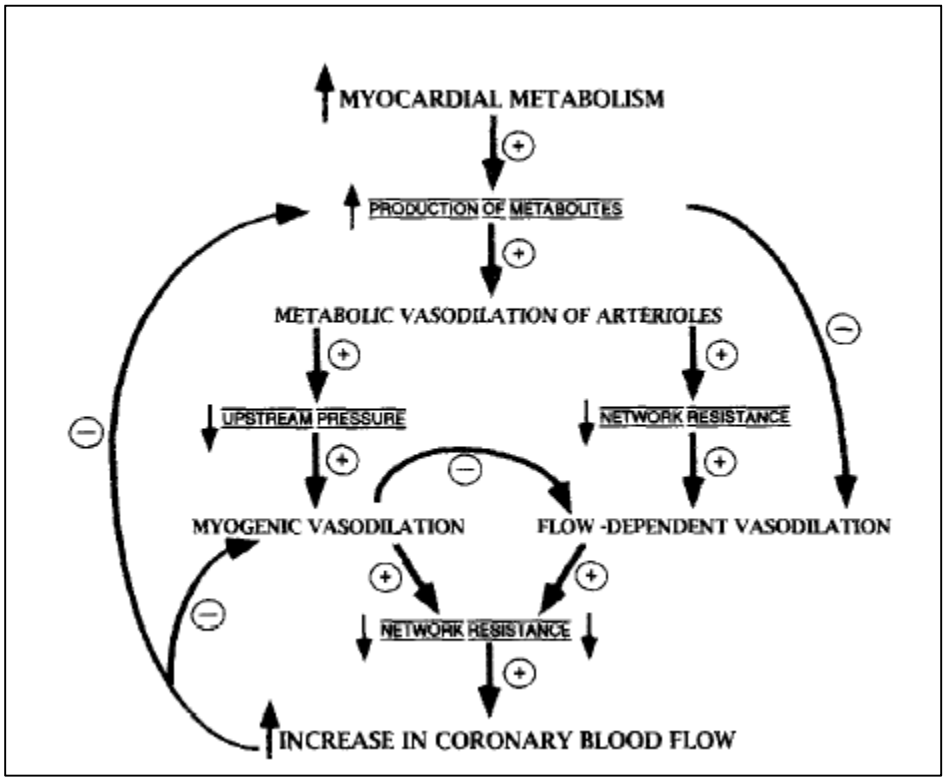

Figure 3.1.3. Integrated regulation of myocardial blood flow. Metabolic, myogenic and flow-dependent mechanisms act in a concerted manner to maintain proper oxygen delivery to the myocardium. [Source: Figure 5, Muller, J.M., Davis, M.J., and Chilian, W.M. (1996). Integrated Regulation of Pressure and Flow in the Coronary Microcirculation. Cardiovasc Res 32, 668-678. (Muller et al., 1996)]. Reused with permission from the journal.

In addition to of the effects of myocardial derived metabolites, microvascular tone is dependent on endothelial-mediated release of vasoactive compounds such as nitric oxide (NO), prostacyclin and endothelin-1. These factors are released from in endothelial cell in response to neural stimulation (i.e. acetylcholine), or shear-stress (also known as flow-mediated vasodilation). NO is the primary mechanism through which endothelial cells induce relaxation. NO is synthesized by endothelial NO synthase (eNOS) where it diffuses to the adjacent smooth muscle and activates guanylyl cyclase, which converts guanosine triphosphate (GTP) to cyclic guanosine monophosphate (cGMP). Increased intracellular cGMP leads to decreased Ca^{2+} levels and smooth muscle cell relaxation. Antagonism of eNOS with L-NG-nitroarginine methyl ester (L-NAME) in isolated porcine coronary microvessels produces constriction, indicating that there is tonic release of NO in the microvasculature (Kuo et al., 1991).

Ultimately, vascular tone is dependent on the contraction and relaxation of vascular smooth muscle cells. This results from calcium-dependent phosphorylation and dephosphorylation of myosin by the myosin light chain kinases (MLCK) and myosin light chain phosphatases, respectively. The dynamics of the actin-myosin interaction and crossbridge cycling in mediating mural cell contraction or relaxation is of indirect relation to the work presented here and is discussed in Katz' Physiology of the Heart or any other physiology textbook (Katz, 2010).

While the microvasculature confers the largest resistance to flow, it is consists of relatively little vascular smooth muscle. Instead, the structure and function of the microvasculature is supported by pericytes, which are discussed in detail below (Armulik et al., 2005).

3.1.2. Microvascular Pericytes

Pericytes were first described by Carl Josef Eberth in 1871. However, their discovery is attributed to Charles-Marie Benjamin Rouget who in 1873 described “a population of cells closely associated with the endothelial cells of the microcirculation” (Armulik et al., 2005). Rouget cells were subsequently named pericytes nearly 50 years later by Karl Wilhelm Zimmermann, alluding to their perivascular location.

Despite being the second most abundant cell type in the heart (Nees et al., 2012), evaluation of pericyte function in the heart has been limited until relatively recently. Pericytes have now been successfully isolated from a number or organs, including the heart (Nees et al., 2013). Due to their pluripotent nature pericytes are of particular interest in regenerative medicine, specifically post myocardial infarction (Gómez-Gaviro et al., 2012).

Most pericytes originate from the mesenchyme (Armulik et al., 2011). However, central nervous system and thymus pericytes are derived from the neural crest. Coronary pericytes arise from epicardial mesothelium (Armulik et al., 2011) where they undergo epithelial-to-mesenchymal transition, migrate into the interstitial space of the myocardium and fully differentiate. It is known that pericytes proliferate in vitro and in the CNS and may also differentiate from proliferating vascular smooth muscle cells (Nehls and Drenckhahn, 1993). While the developmental origin of pericytes is well studied, much less is known about their origin and proliferation during angiogenesis in the adult.

Pericytes are difficult to define as there is no single unequivocal marker that distinguishes them from other mesenchymal cells such as vascular smooth muscle cells and myofibroblasts. Nor is expression of any pericyte marker stable in its expression (discussed in more detail below). Therefore identification of pericytes relies on a combination of morphology, location, degree of vessel coverage and protein expression patterns. Key to their definition is that pericytes are embedded within the vascular basement membrane

which is continuous with the endothelial basement membrane (Armulik et al., 2005). Thus, definitive identification of pericyte requires detailed electron microscopy. Even then, pericytes are not always embedded in the basement membrane such as during active angiogenesis or certain disease states (Gomez et al., 2005).

Pericytes consist of a single cell body with long processes that extend the abluminal length of multiple endothelial cells, attaching to the endothelial cells through peg-socket type contacts (**Figure 3.1.4**). Pericytes also contact endothelial cells though N-cadherin based adhesion plaques and possibly also through gap junctions (Armulik et al., 2005; Cuevas et al., 1984). Secondary processes extend perpendicular to the primary processes, circling around the endothelial tube and aiding with capillary contraction. The degree of pericyte coverage varies between organ types and exhibits a strong positive correlation with the barrier function of the tissue, ranging from 1:1 (pericyte: endothelial cell) in the blood brain barrier to as low as 1:10 in skeletal muscle (Diaz-Flores et al., 2009).

Pericytes are ubiquitously expressed in all microvessels, principally in the capillaries but extending into both the precapillary arterioles and postcapillary venules (Nees et al., 2013). The exact point at which pericyte coverage shifts to vSMC is controversial due to the fact that definitive distinction between the two cell types is challenging. Others have proposed that pericyte coverage extends into the largest coronary vessels, existing within the extracellular matrix between the endothelial tube and internal elastic membrane as well as supporting the vasa vasorum of the larger coronary arteries (Diaz-Flores et al., 2009).

Figure 3.1.4.

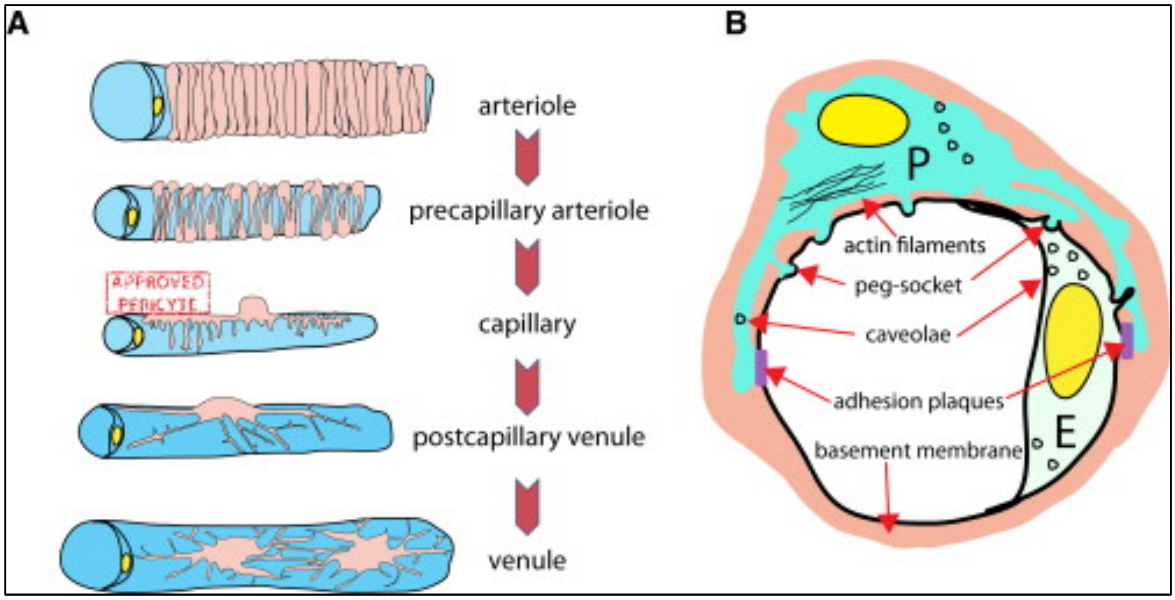

Figure 3.1.4. Vascular pericyte coverage and pericyte anatomy.

(A) A single layer of vascular smooth muscle cells (vSMCs) surround the larger arterioles. Beginning at the precapillary arteriole and then throughout the capillary, postcapillary venule and venule, the vessel is supported by pericytes. As opposed to vSMCs, pericytes display a prominent rounded cell body and long cytoplasmic processes. **(B)** Pericytes and endothelial cells share a basement membrane and share many contacts [Source: Figure 1. Armulik, A., Genove, G., and Betsholtz, C. (2011). Pericytes: Developmental, Physiological, and Pathological Perspectives, Problems, and Promises. Dev Cell 21, 193-215. (Armulik et al., 2011). Used with permission from Elsevier, permission number 3581440915913].

Pericyte recruitment and stabilization of the endothelium is dependent on multiple signaling pathways, the complexity of which is demonstrated in **Figure 3.1.5** and briefly described in the following sections.

3.1.2.1 PDGF-B and PDGFRβ

The platelet-derived growth factor (PDGF) family consists of three dimers comprised of two different disulfide linked polypeptide chains, PDGF-A and PDGF-B. The dimers most often exist as homodimers, PDGF-AA or PDGF-BB, however it was the heterodimer, PDGF-AB, that was first discovered in activated platelets (Andrae et al., 2008). Recently, two additional PDGF factors, PDGF-C and PDGF-D have also been described (Bergsten et al., 2001; Larochelle et al., 2001; Li et al., 2000). The PDGFs act in a paracrine manner, binding to heparin and heparin sulfate proteoglycans in the extracellular matrix through an essential C-terminal retention motif.

PDGFs act via two structurally related tyrosine kinase receptors, platelet-derived growth factor receptor α and β (PDGFRα and PDGFRβ). PDGFRα can bind either PDGF-A or PDGF-B. However, PDGFRβ appears to bind only PDGF-B (Leveen et al., 1994). Binding induces receptor dimerization and activation of the downstream pathways Ras/MAPK, PI3K/Akt and PKC. This results in actin reorganization, cell growth, migration and inhibition of apoptosis (Andrae et al., 2008).

During angiogenesis, PDGF-BB is produced by the endothelial tip cells and binds to PDGFRβ on the surface of developing pericytes (Gaengel et al., 2009). This process is dependent on retention of PDGF-BB in the extracellular matrix as deletion of this motif in mice ($pdgfb^{ret/ret}$) leads to pericyte detachment from the vessel wall and vascular malformations in the kidney and retina (Lindblom et al., 2003). Similarly, knockout of the N-deacetylase/N-sulfotransferase (NDST)-1 enzyme, leading to a reduction of N-sulfated

heparin sulfate, also results in pericyte detachment (Abramsson et al., 2007). Deletion of PDGF-B or PDGFRβ leads to almost identical perinatal lethality due to vascular malformations resulting in widespread hemorrhage and edema (Armulik et al., 2011; Leveen et al., 1994; Soriano, 1994). Loss of PDGF-B or PDGFRβ in an *in* vivo model of brain angiogenesis resulted in endothelial cell hyperplasia, abnormal endothelial shape and increased vascular permeability. Embryos from PDGF-B deficient mice also display pronounced dilation of all chambers of the heart as well as significant enlargement of the thoracic aorta (Leveen et al., 1994).

Only recently has the importance of PDGF-B/PDGFRβ signaling in maintaining pericyte coverage in the adult been explored. These investigations have focused mainly on tumor angiogenesis, diabetic retinopathy and neurobiology (Fernandez-Klett et al., 2010; Gee et al., 2003; Song et al., 2005; Winkler et al., 2011). Furthermore, my previous lab has reported that inducible cardiomyocyte-specific knockout of PDGFRβ in the adult mouse results in ventricular dilation and heart failure in response to pressure overload stress (Chintalgattu et al., 2010). This was correlated with impaired angiogenesis and microvascular dysfunction in the adult heart.

3.1.2.2 Angiopoietin-1/Tie2

Angiopoeitin-1/Tie2 paracrine signaling exists in a reciprocal orientation to PDGF-B/PDGFRβ. That is, pericytes produce angiopoietin-1 which binds to the endothelial Tei2 receptor, a receptor tyrosine kinase. Similar to PDGF-B/PDGFRβ, Angiopoeitin-1/Tie2 signaling promotes vessel maturation and stability (Falcon et al., 2009; Gaengel et al., 2009) and reduced vessel leakiness (Thurston et al., 1999). Furthermore, angiopoeitin-1/Tie2 signaling is essential for normal cardiac development (Armulik et al., 2011). Genetic deletion of either angiopoietin-1 or Tie2 leads death in utero due to cardiovascular abnormalities,

Figure 3.1.5.

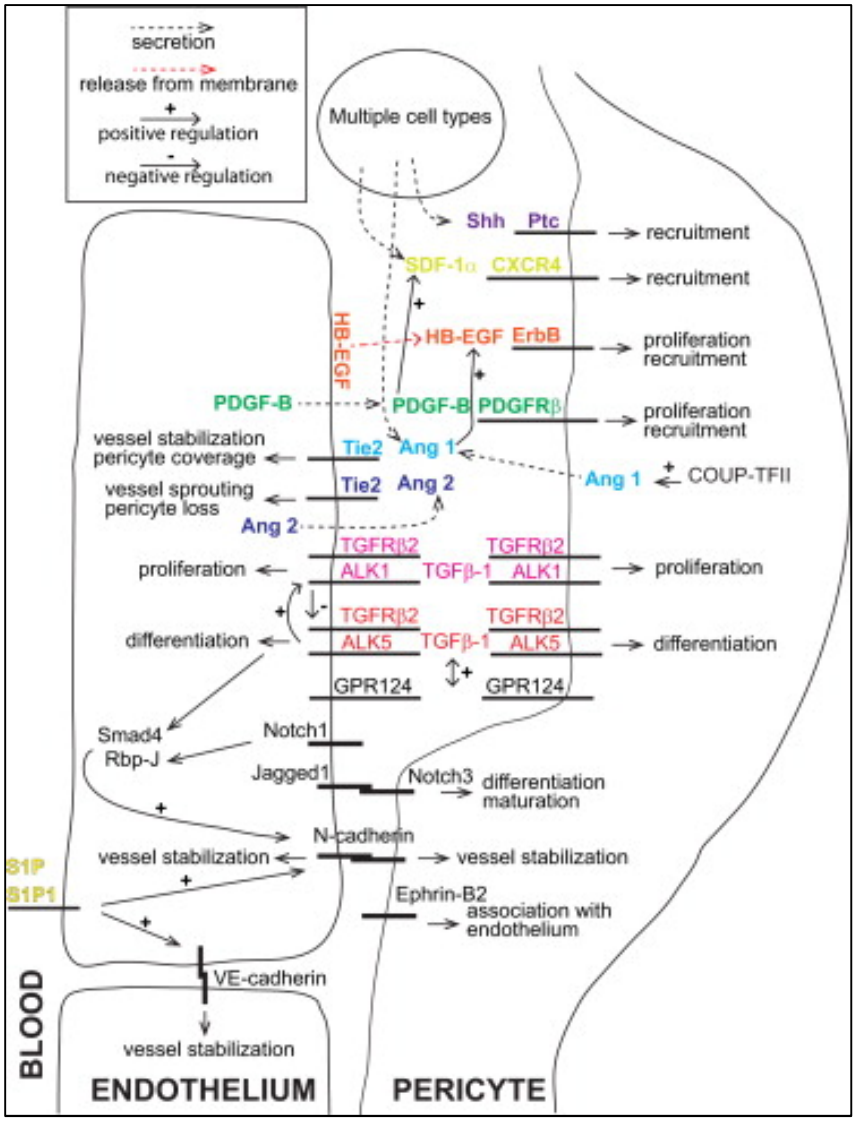

Figure 3.1.5. Signaling pathways mediating pericyte-endothelial cell interactions. The close interaction between endothelial cells and pericytes is regulated by a large number of pathways. However, the PDGF-B/PDGFRβ and Ang1/Tie2 interactions appear to be the most important. [Source: Figure 4. Armulik, A., Genove, G., and Betsholtz, C. (2011). Pericytes: Developmental, Physiological, and Pathological Perspectives, Problems, and Promises. Dev Cell 21, 193-215. (Armulik et al., 2011) Used with permission from Elsevier, permission number 3581440915913].

characterized by detachment of the endocardium from the underlying myocardial wall and absence of trabeculae (Jones et al., 2001; Patan, 1998). Similarly, missense mutations in the human *Tie2* receptor result in vascular malformations, resulting in multifocal bluish lesions on the skin and mucosa (Limaye et al., 2009; Vikkula et al., 1996). Multiple cell types produce angiopoietin-1, including other mesenchymal cells, cardiomyocytes, and hematopoietic cells; however the end result is much the same, promoting vascular stability and higher-order structure and reducing leakiness, reviewed by (Jones et al., 2001).

3.1.2.3 Transforming growth factor beta

Both endothelial and mural cells produce transforming growth factor beta (TGFβ). Signaling between the two is bidirectional and results in differentiation and maturation of the vessel. TGFβ induces a mural cell fate in undifferentiated mesenchymal cells, a process that is dependent on connexin-43 gap junction formation (Hirschi et al., 2003). TGFβ signals through two receptors in vascular cells activin receptor-like kinase (Alk)-1 and Alk-5, which have nearly opposing roles. Alk-5 activation inhibits migration and promotes mural cell differentiation, whereas Alk-1 phosphorylation induces a more proliferative state, reviewed in (Armulik et al., 2011). The two receptors are also regulated temporally, with Alk-1 dominating early development and Alk-5 inducing differentiation in later phases (Schmierer and Hill, 2007). Deletion of downstream components of the TGFβ signaling pathway such as *smad4* (Lan et al., 2007)*, smad5* (Chang et al., 1999) and *endoglin* (Li et al., 1999) result in embryonic lethality and vascular abnormalities.

3.1.3. Strategies to increase pericyte coverage and vessel normalization.

Tumor vasculature is structurally and functionally abnormal. Vessels are dilated, tortuous, leaky and have absent or detached pericytes. This often results in interstitial

hypertension, acidosis and hypoxia (Jain, 2005). Paradoxically, depletion of tumor pericytes results in accelerated tumor growth and metastasis (Ramaswamy et al., 2003; Sennino et al., 2007). Recent work has demonstrated that increasing pericyte coverage prevents tumor growth. This process has been termed “vessel normalization”, because the vasculature reverts to a near-normal phenotype.

3.1.3.1. Inhibition of VEGF-A

Treatment with bevacizumab, a monoclonal antibody directed against VEGF-A results in a pruning of poorly formed vessels, specifically ones lacking pericyte coverage (Winkler et al., 2004). Attempts to induce vessel normalization in cancer have focused primarily on inhibition of VEGF-A signaling. Interestingly, cardiotoxicity is not associated with agents that only inhibit VEGF-A signaling, such as bevacizumab (Khakoo et al., 2011). Vessel normalization also occurs with deletion of the pericyte marker, regulator of G-protein signaling 5 (RGS5), resulting in reduced leakiness and alleviation of hypoxia through an unknown mechanism (Hamzah et al., 2008). The only other strategy that has proved effective in normalizing tumor vasculature has been treatment with thalidomide.

3.1.3.2. Thalidomide

Thalidomide, a derivative of glutamic acid, was developed in the 1950s by the German company, Chemie Grünenthal, and used primarily to combat morning sickness in pregnant women. Though never approved by the FDA, thalidomide treatment led to severe birth defects (malformed limbs) in between 8,000 and 12,000 children born in Europe, Australia, Asia and South America (Bartlett et al., 2004). Thalidomide-induced teratogenicity is due to a direct inhibition of cereblon (CRBN) (Ito et al., 2010). CRBN forms an E3 ligase complex with damaged DNA binding protein 1 (DDB1) and Cul4A to target unidentified

Figure 3.1.6.

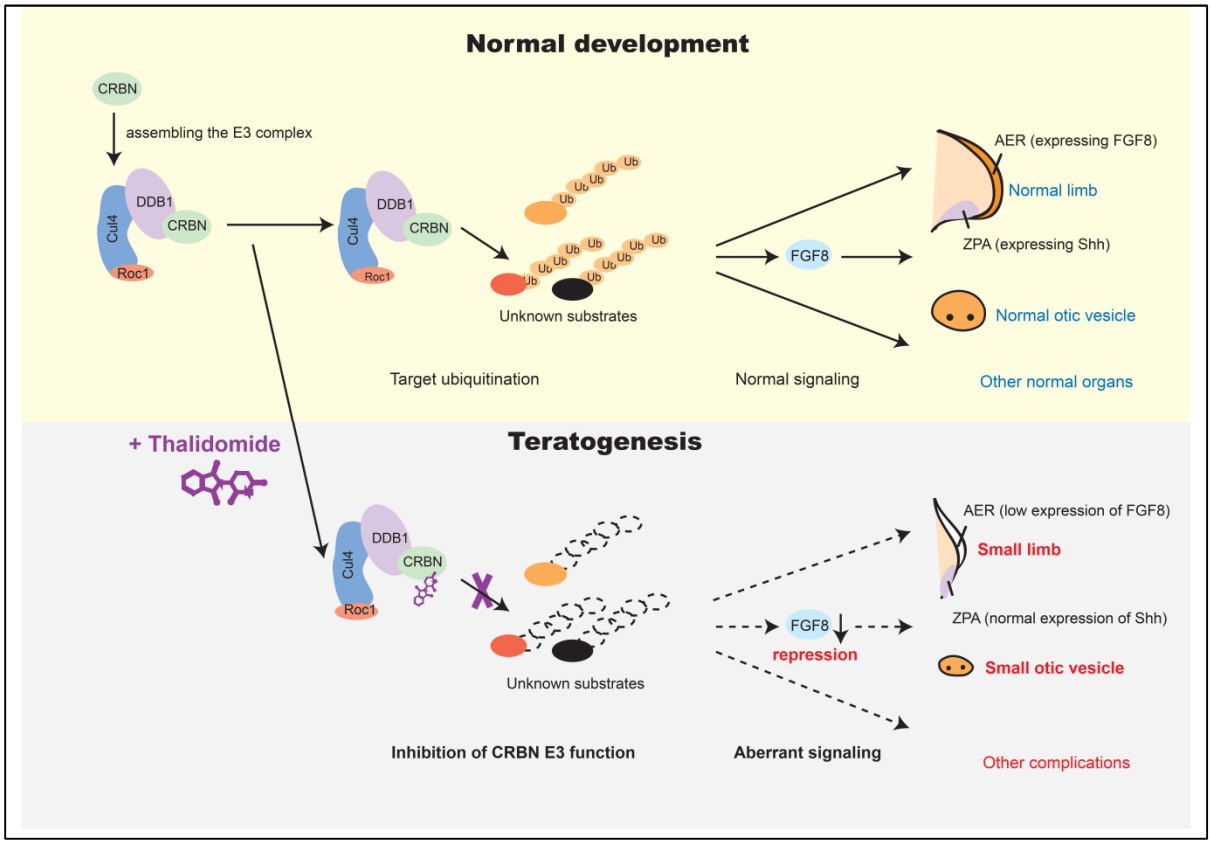

Figure 3.1.5. CRBN is the primary target of thalidomide teratogenicity. Cereblon (CRBN) forms an E3 ligase complex with damaged DNA binding protein 1 (DDB1) and Cul4A to target unidentified substrates for degradation, leading to expression of fibroblast growth factor 8 (FGF8) and normal limb outgrowth. Thalidomide directly binds to CRBN and inhibits this process. [Source: Supplemental Figure 19 from Ito, T., Ando, H., Suzuki, T., Ogura, T., Hotta, K., Imamura, Y., Yamaguchi, Y., and Handa, H. (2010). Identification of a Primary Target of Thalidomide Teratogenicity. Science 327, 1345-1350. (Ito et al., 2010) Used with permission from the journal, license number: 3586070673111].

substrates for degradation, leading to expression of fibroblast growth factor 8 (FGF8) and normal limb outgrowth (**Figure 3.1.6**).

The catalyst for the current use of thalidomide occurred in 1964 when Israeli physician Jacob Sheskin discovered that it could heal lesions in patients with erythema nodosum leprosum, a complication of leprosy (Sheskin, 1964). Nearly 30 years later, it was found that thalidomide had strong anti-inflammatory properties, primarily through inhibition of monocyte-derived tumor necrosis factor alpha (TNFα) (Sampaio et al., 1991). Within that same decade, thalidomide was found to be antiangiogenic (D'amato et al., 1994) and to co-stimulate T-cells previously activated by T-cell receptor (Haslett et al., 1998). The TNFα-mediated anti-inflammatory properties of thalidomide has led to its use in several other immune-system related complications such as Kaposi's sarcoma (Little et al., 2000) and cachexia (Gordon et al., 2005). Thalidomide has also significantly improved survival in multiple myeloma, a B-cell derived malignancy that is associated with increased bone-marrow microvascular density. Furthermore, its co-treatment with dexamethasone led to full remission in 10% of patients and partial remission in a quarter, leading to a clinical response rate of 32% (Singhal et al., 1999).

Subsequently, two derivatives of thalidomide—lenalidomide and pomalidomide—were developed which display 50,000 times more potency towards TNFα than thalidomide (Bartlett et al., 2004). These derivatives do not appear to cause teratogenicity yet retain the ability block angiogenesis. However as with thalidomide, the mechanism is still not well understood (Lu et al., 2009). In a mouse model of hereditary hemorrhagic telangiectasia, thalidomide increased pericyte coverage and induced vessel stabilization as well as increased PDGF-B in endothelial cells (Lebrin et al., 2010). This chapter will demonstrate that co-treatment with thalidomide can protect from sunitinib-induced pericyte loss and preserve contractile function in mice.

3.2 Results

3.2.1 Sunitinib induces cardiomyocyte hypertrophy.

Mice were treated with sunitinib for 21 days, a schedule that mimics the three weeks on, one week off, clinical treatment schedule (see methods). Sunitinib treatment did not result in increased heart weight to body weight ratios, which is normally indicative of cardiac hypertrophy (**Figure 3.2.1A**). Nor was there evidence of pulmonary edema, as indicated by normal lung weight to body weight ratios (**Figure 3.2.1B**). However, the increased cardiomyocyte cross-sectional area (**Figure 3.2.1C**) suggests that there is cellular hypertrophy despite no change in overall heart size.

Because sunitinib causes severe hypertension, mean-arterial pressure (MAP) was measured over the course of treatment. Mice do not readily develop hypertension. Therefore it was not much of a surprise that there was no increase in MAP (**Figure 3.2.1D**). This indicated that sunitinib-induced cardiotoxicity may be the result of a direct cellular effect, and not secondary to hemodynamic stress.

3.2.2 Sunitinib-induced cardiac contractile dysfunction is associated with coronary microvascular dysfunction.

Measurement of left-ventricular ejection fraction by cardiac MRI revealed a progressive decline over the course of 21 days (**Figure 3.2.2A**). This was associated with decreased cardiac contractility in response to the inotropic agent dobutamine (**Figure 3.2.2B**), measured by the maximum developed pressure in the left ventricle over time (dP/dt_{max}).

Figure 3.2.1.

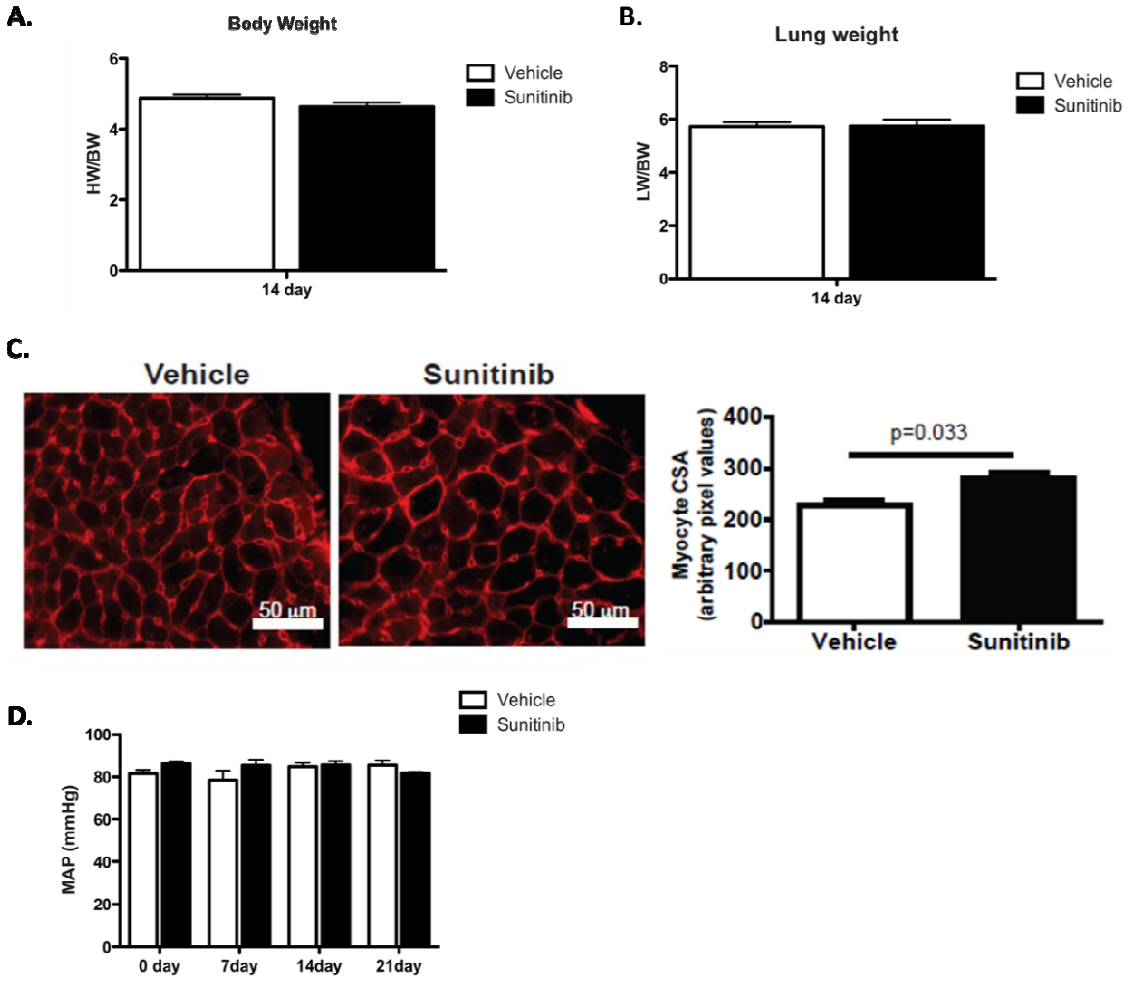

Figure 3.2.1. Sunitinib increases cardiomyocyte cross-sectional area despite no evidence of increased heart size. (A) Heart weight to body weight ratio. **(B)** Lung weight to body weight ratio. **(C)** Lectin-TRITC staining to demark cardiomyocyte cell boarders and cardiomyocyte cross-sectional area quantified to the right. **(D)** Mean arterial pressure over the course of the 21 day treatment.

Figure 3.2.2.

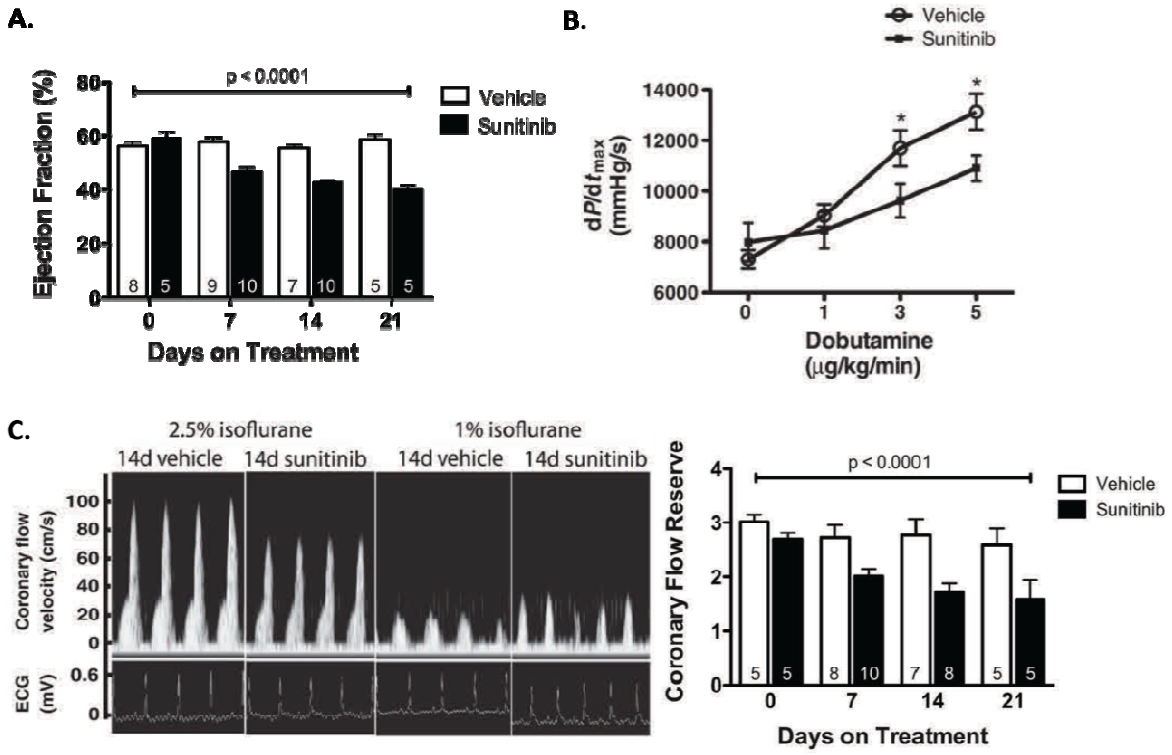

Figure 3.2.2. Sunitinib treatment leads to contractile and microvascular dysfunction. **(A)** Cardiac ejection fraction as assessed by cardiac MRI. **(B)** Maximum developed pressure over time (dP/dt_{max}) in the left ventricle in response to increasing concentration of dobutamine. **(C)** Representative ultrasound tracings of stimulated and basal coronary flow in the left-anterior descending coronary artery after 14 days of sunitinib treatment. Average CFR (dilated:basal) over the 21 day treatment protocol. *P < 0.05.

Coronary flow reserve (CFR), the change in blood flow velocity in the coronary artery in response to a hyperemic stimulus, is clinically relevant measure that has been eloquently adapted for the mouse heart (Hartley, Ultrasound in Medicine and Biology, 2008). Baseline coronary flow is often elevated under load-induced cardiac hypertrophy in order to support increased cardiac work (Hartley et al., 2011; Hartley et al., 2008). Consequentially, the absolute rise to maximal coronary blood flow velocity, the coronary flow reserve, in blunted in diseased states. Baseline coronary flow (1% isoflurane) was elevated in the sunitinib-treated and blunted upon stimulation (elevation of isoflurane levels to 2.5%), resulting in a significantly decreased CFR in the sunitinib treated mice (**Figure 3.2.2C**). Collectively, these results indicate that sunitinib-induced cardiotoxicity is associated with microvascular dysfunction.

3.2.3. Sunitinib treatment results in reduced vascular reactivity.

Acetylcholine stimulation of the endothelium leads to activation of endothelial nitric oxide synthase (eNOS) and consequent endothelium-dependent vascular relaxation and increase in blood flow. Similar to isoflurane, acetylcholine infusion revealed that sunitinib treatment leads to decreased CFR *in vivo* (**Figure 3.2.3A**). The same result was obtained when acetylcholine-mediated increases in total coronary flow were measured using the *ex vivo* Langendorff perfused heart preparation (**Figure 3.2.3B**). *Ex vivo* total coronary flow was also decreased upon stimulation with the direct nitric oxide (NO) donor, sodium nitroprusside (**Figure 3.2.3C**). As a direct donor of NO, sodium nitroprusside bypasses the endothelium to directly induce vasorelaxation. Therefore, sodium nitroprusside is useful to determine if the defect in vascular function resides in the ability of the mural cells to respond to NO. Given the fact

Figure 3.2.3.

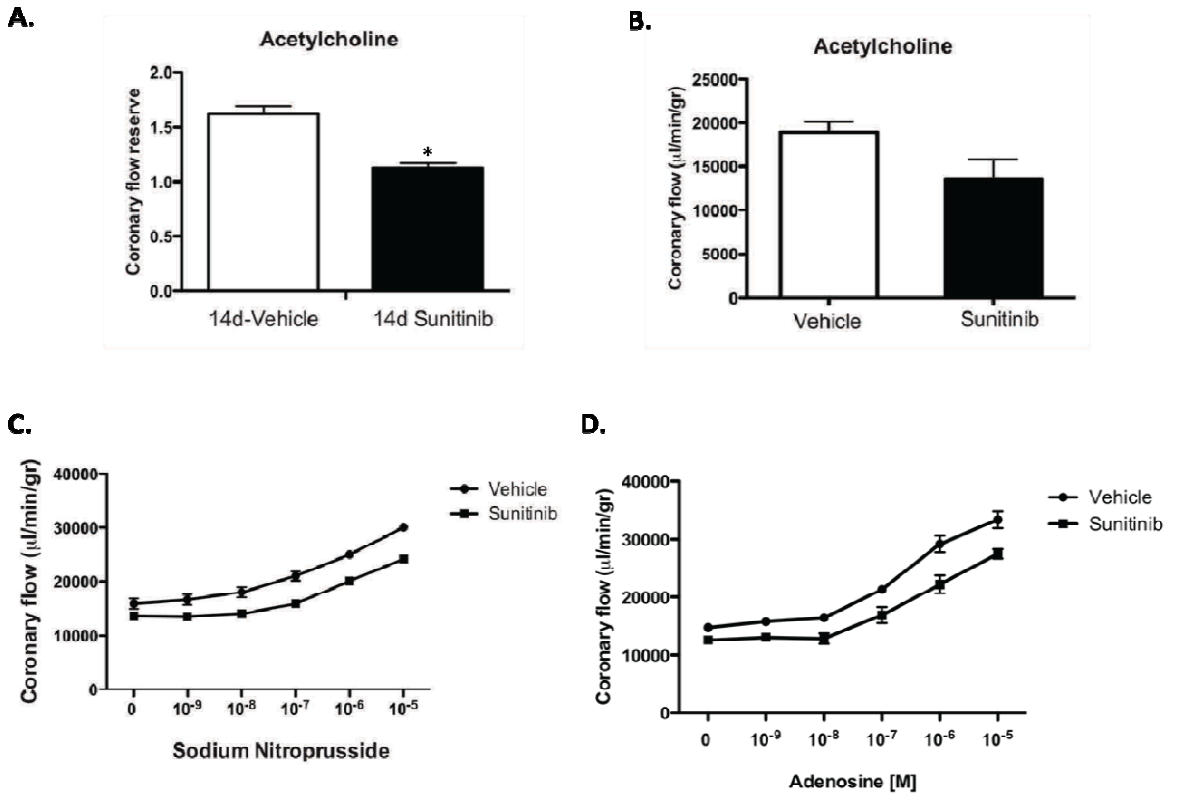

Figure 3.2.3. Sunitinib is associated with decreased vascular reactivity. (A) Acetylcholine-stimulated coronary flow reserve in mice treated with sunitinib or vehicle for 14 days measured *in vivo*. **(B)** Acetylcholine-stimulated *ex vivo* total coronary flow in mice treated with sunitinib for 14 days. **(C)** and **(D)** Total coronary flow in response to increasing concentration of sodium nitroprusside or adenosine measured in *ex vivo* Langendorff perfused hearts from mice treated with sunitinib or vehicle.

that *ex vivo* total coronary flow was also decreased in response to adenosine (endothelium-dependent) (**Figure 3.2.3D**), it appeared that sunitinib-induced microvascular dysfunction might be due to vSMC or pericyte dysfunction.

In order to determine if sunitinib treatment also leads to macrovascular dysfunction, vascular reactivity was assessed in isolated thoracic aortas with the help of Dr. Nathan Bryan at The University of Texas' Institute of Molecular Medicine. Isolated thoracic aortas from mice treated with sunitinib or vehicle were exposed to phenylephrine or acetylcholine to measure vascular constriction and relaxation, respectively (**Figure 3.2.4A and Figure 3.2.4B**). Sunitinib treatment had no effect on vasoconstriction or vasorelaxation of the large vessels. However, there was a significant decrease in cardiac nitrite concentrations, a byproduct of NO breakdown (**Figure 3.2.4C**). This indicated that sunitinib somehow alters the ability of the cardiac vasculature to metabolize NO. Interestingly, there was no difference in skeletal muscle nitrite levels, suggesting that sunitinib-induced vascular dysfunction may be specific to the heart.

3.2.4. Sunitinib treatment leads to loss of microvascular pericytes and microvascular abnormalities.

As described above, the largest resistance to flow in the heart is conferred by the cardiac microvasculature. Supporting these small vessels are pericytes which, similar to smooth muscle cells on larger vessels, provide structural and functional support. Scanning electron microscopy revealed a loss of microvascular pericytes in sunitinib-treated hearts (**Figure 3.2.5A**). This was confirmed by immunofluorescent microscopy of cardiac sections stained for the proteoglycan neural/glial 2 (NG2), an established marker for pericytes

Figure 3.2.4.

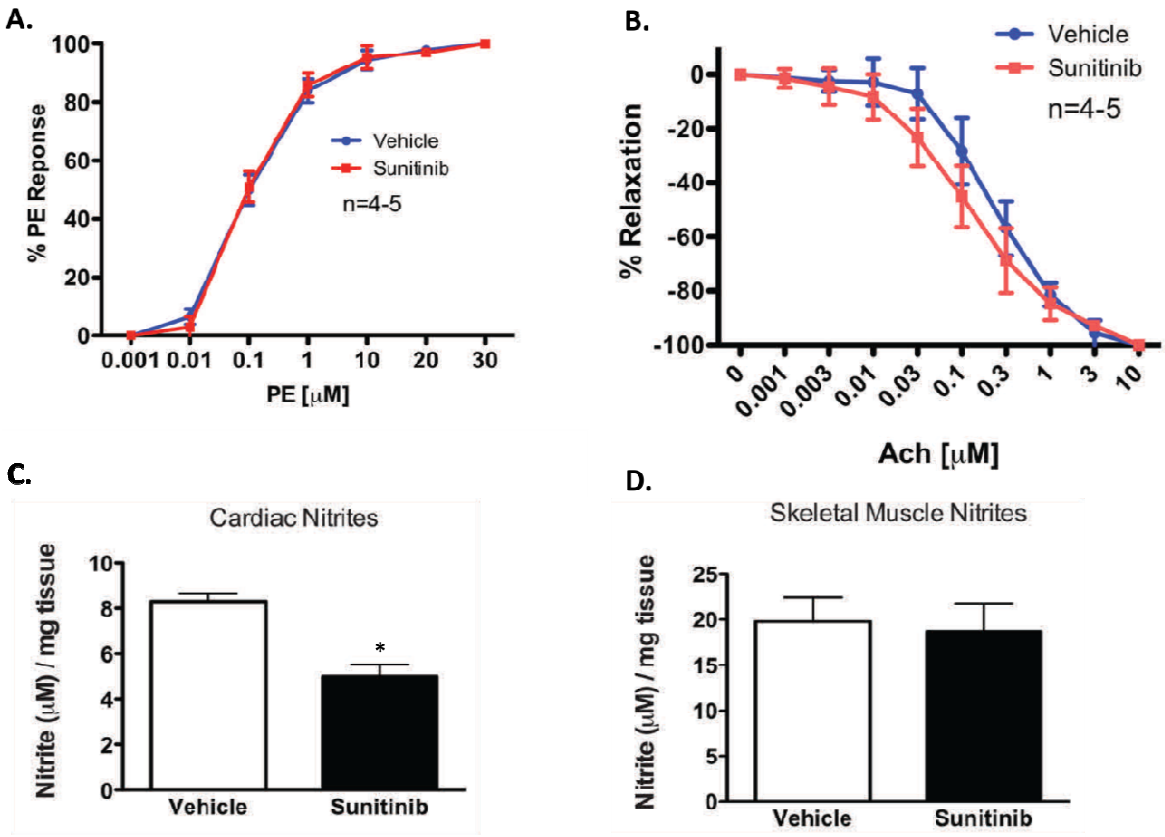

Figure 3.2.4. Sunitinib does not affect large-vessel reactivity. (A) and **(B)** Percent contraction or relaxation of isolated thoracic aortas from mice treated with sunitinib or vehicle stimulated with phenylephrine (PE) or acetylcholine (Ach). **(C)** and **(D)** Nitrite concentration in cardiac and skeletal muscle tissue, respectively. *P < 0.05.

(Ozerdem et al., 2001). Decreased NG2 expression was also observed by western blot (**Figure 3.2.5C**).

Next, the functional consequence of pericyte loss in the heart was determined. Pericyte loss has been linked to increased vascular permeability in both the blood-brain barrier and tumors (Lindahl et al., 1997; Mccarty et al., 2007). Perfusion of isolated mouse hearts with fluorescently labeled cadaverine, which in a healthy vasculature would remain within the vessel, suggested that sunitinib treatment leads to increased vascular permeability in the heart (**Figure 3.2.6A**). Absence of pericytes is also associated with immature, poorly formed vessels which can be assessed by measuring vascular tortuosity (Gaengel et al., 2009; Higuchi et al., 2000). Vascular tortuosity was significantly increased in hearts from sunitinib-treated mice, as measured by a blinded third party (Dr. Jim Culver, as a graduate student in the lab of Dr. Mary Dickinson at Baylor College of Medicine). Together these data suggest that pericyte loss leads to a leaky, poorly formed vasculature. They also indicate that the cardiac vasculature is dynamic, continuously remodeling in response to stress.

3.2.5. Cardiac pericyte loss is also observed with the structurally distinct PDGFRβ inhibitor, CP-673,451.

Noting that PDGFRβ signaling is essential for pericyte survival, it appeared that sunitinib-induced pericyte loss might be due to inhibition of PDGFRβ. CP-673,451 is a potent and specific PDGFRβ inhibitor that is structurally distinct from sunitinib (**Figure 3.2.7A**) (Roberts et al., 2005). Similar to sunitinib, treatment with CP-673,451 did not lead to increased heart weight to body weight or lung weight to body weight ratios (**Figure 3.2.7B**). However, a similar decline in left-ventricular ejection fraction was observed (**Figure 4.2.7C**)

Figure 3.2.5.

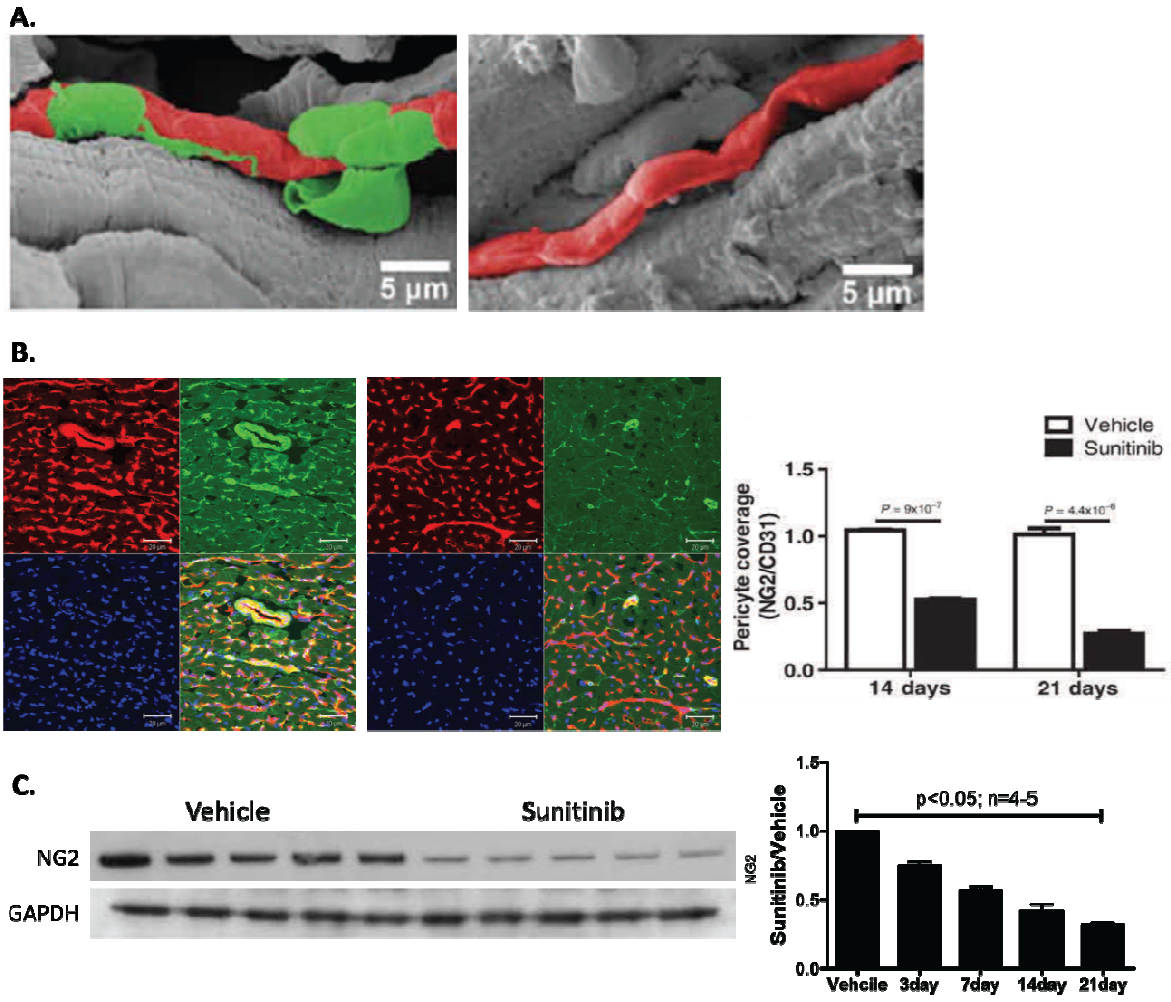

Figure 3.2.5. Sunitinib treatment induces loss of microvascular pericytes. (A) Representative scanning electron microscopy images of the cardiac microvasculature. Vessels and pericytes are psuedocolored red and green respectively. **(B)** Confocal images from cardiac sections showing staining for the endothelial cell marker CD31 (red), pericyte marker NG2 (green) or nuclear staining (DAPI, blue) and merged images (bottom left). Pericyte coverage quantified to the right as the relative intensity of NG2:CD31. **(C)** NG2 protein expression in mice treated with sunitinib or vehicle. Right, densitometric quantification.

Figure 3.2.6.

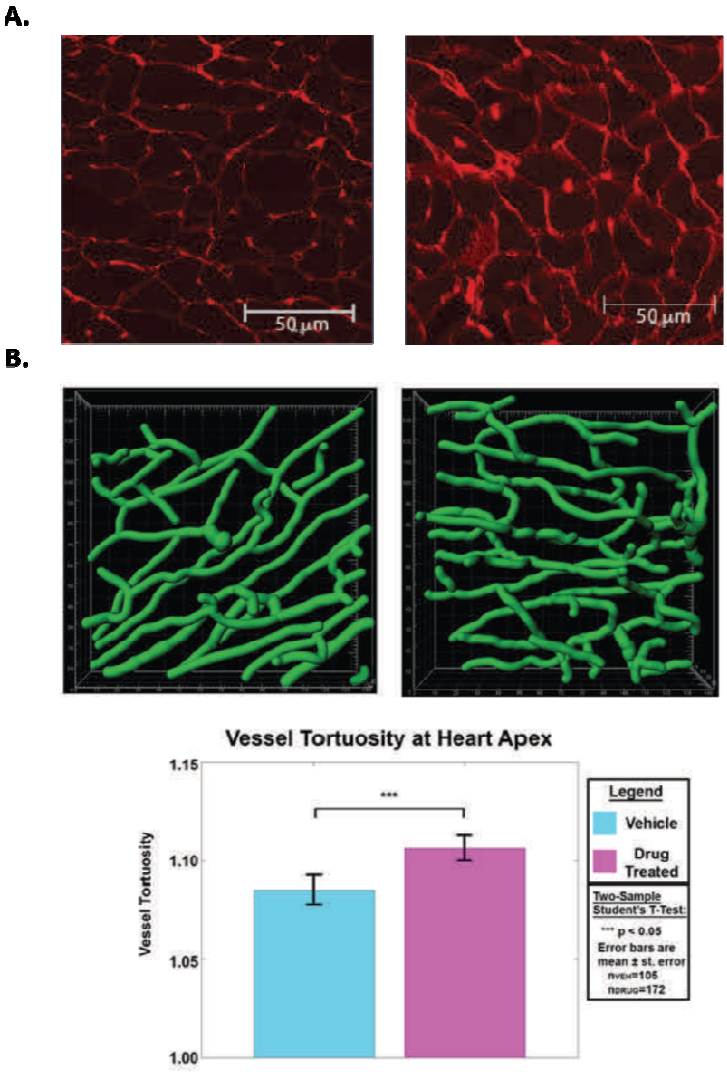

Figure 3.2.6. Pericyte loss leads to microvascular abnormalities. (A) Representative confocal images from mice treated with sunitinib and perfused with 0.9 kDa cadaverine conjugated to Alexa Fluor-555 demonstrating increased microvascular permeability. **(B)** Computer-based reconstruction of the cardiac vasculature derived from the apex hearts perfused with 70-kD tetramethylrhodamine-labeled dextran and (below) quantification of vascular tortuosity. ***P < .01.

Figure 3.2.7.

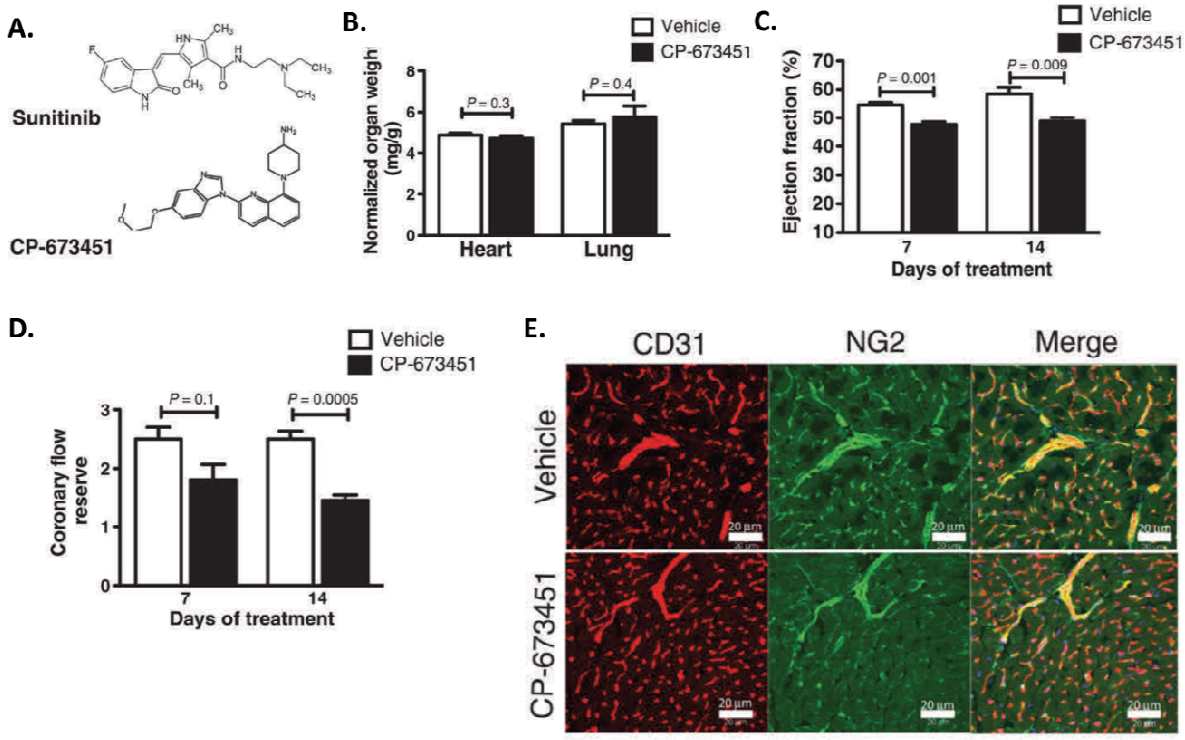

Figure 3.2.7. Coronary microvascular dysfunction and pericyte loss are recapitulated with the structurally distinct PDGFRβ inhibitor, CP-673451. (A) Chemical structures of sunitinib and CP-673451. **(B)** Heart weight to body weight and lung weight to body weight ratios for mice treated with CP-673451. **(C)** Cardiac ejection fraction at 7 and 14 days of treatment as measured by cardiac MRI. **(D)** Coronary flow reserve at day 7 and 14 of CP-673451 treatment. **(E)** Representative confocal micrographs showing staining for the vascular marker CD31 (red) or the pericyte marker NG2 (green) and merged images.

and coronary flow reserve (**Figure 3.2.7D**). Most strikingly, CP-673,451 treatment resulted in a similar loss of cardiac microvascular pericytes (**Figure 3.2.7E**). These data suggest that loss of PDGFRβ signaling underlies the development of contractile and microvascular toxicity due to sunitinib.

3.2.6. Pericyte loss is not a general feature of cardiotoxicity.

As described in Chapter 1, doxorubicin is a general DNA intercalating agent that causes cardiac injury through the generation of reactive oxygen species. Both low dose (5mg/kg/wk.) and high dose (10mg/kg/wk.) doxorubicin treatment led to decline in left-ventricular ejection fraction (**Figure 3.2.8A**) and coronary flow reserve (**Figure 3.2.8B**). However, there was no observable loss of the pericyte marker NG2 by either western blot (**Figure 3.2.8C**) or immunofluorescence (**Figure 3.2.8D**). Therefore pericyte loss appears to be a specific feature of sunitinib cardiotoxicity and not a general feature of cardiac injury by chemotherapeutic agents.

3.2.7. Co-treatment with thalidomide ameliorates sunitinib-induced contractile dysfunction and pericyte loss.

To test whether sunitinib was directly toxic to pericytes *in vitro,* the viability of human placental pericytes treated with sunitinib was determined using an MTT colorimetric assay (see methods). Cell viability was inversely correlated with the concentration of sunitinib (**Figure 3.2.9A**). As described above, thalidomide is known to increase vascular pericyte coverage. Co-treatment of isolated pericytes with sunitinib and thalidomide significantly increased cell viability, though not to control levels (**Figure 3.2.9B**). Neither sunitinib alone

Figure 3.2.8.

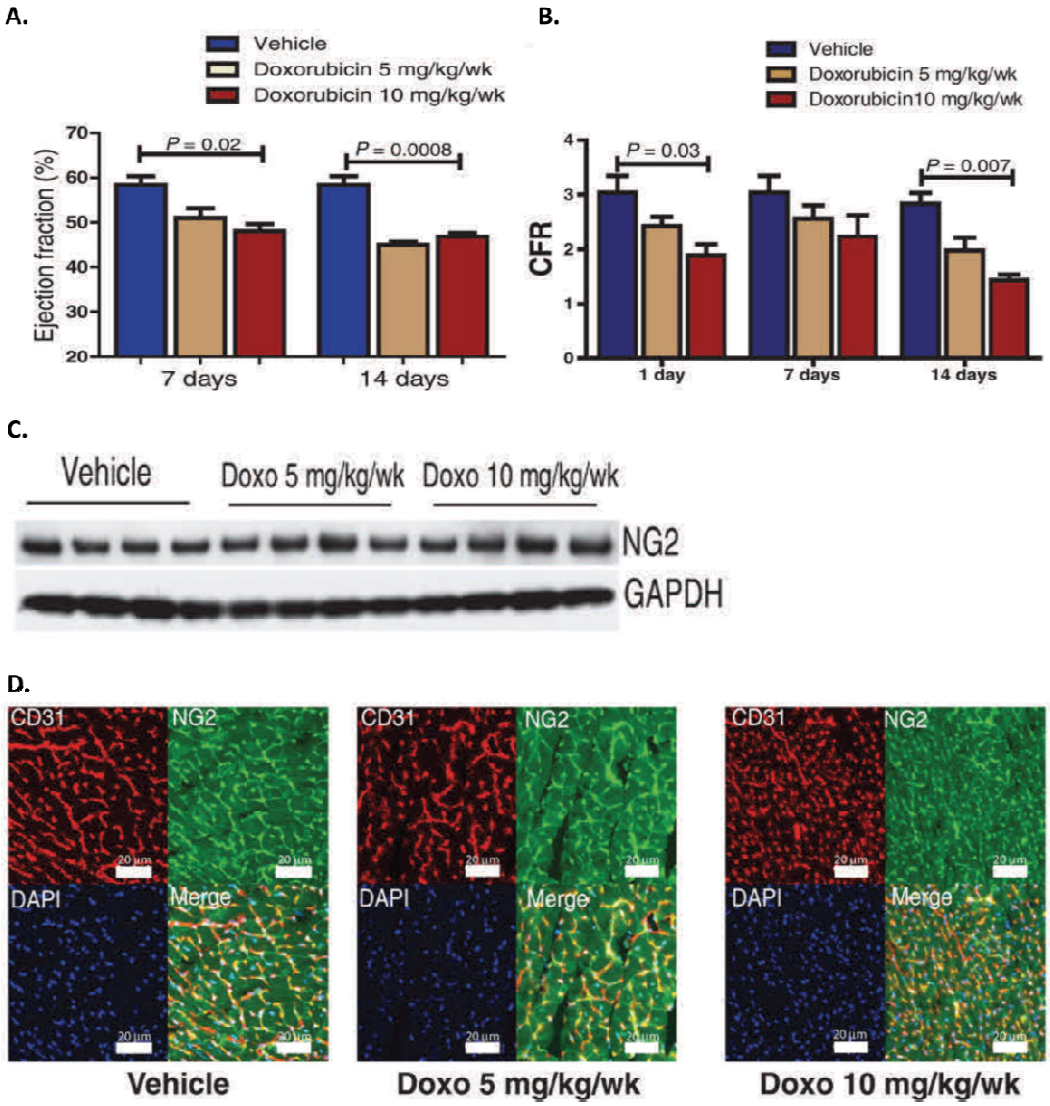

Figure 3.2.8. Doxorubicin treatment does not cause pericyte loss. (A) Cardiac ejection fraction in mice treated with doxorubicin or vehicle, measured by cardiac MRI. **(B)** Coronary flow reserve at day 1, 7 and 14 of treatment. **(C)** NG2 protein expression from cardiac lysates of mice treated with doxorubicin or vehicle. **(D)** Confocal micrographs stained for the endothelial marker CD31 (red), pericyte marker NG2 (green), nuclei (DAPI, blue) and merged images.

Figure 3.2.9

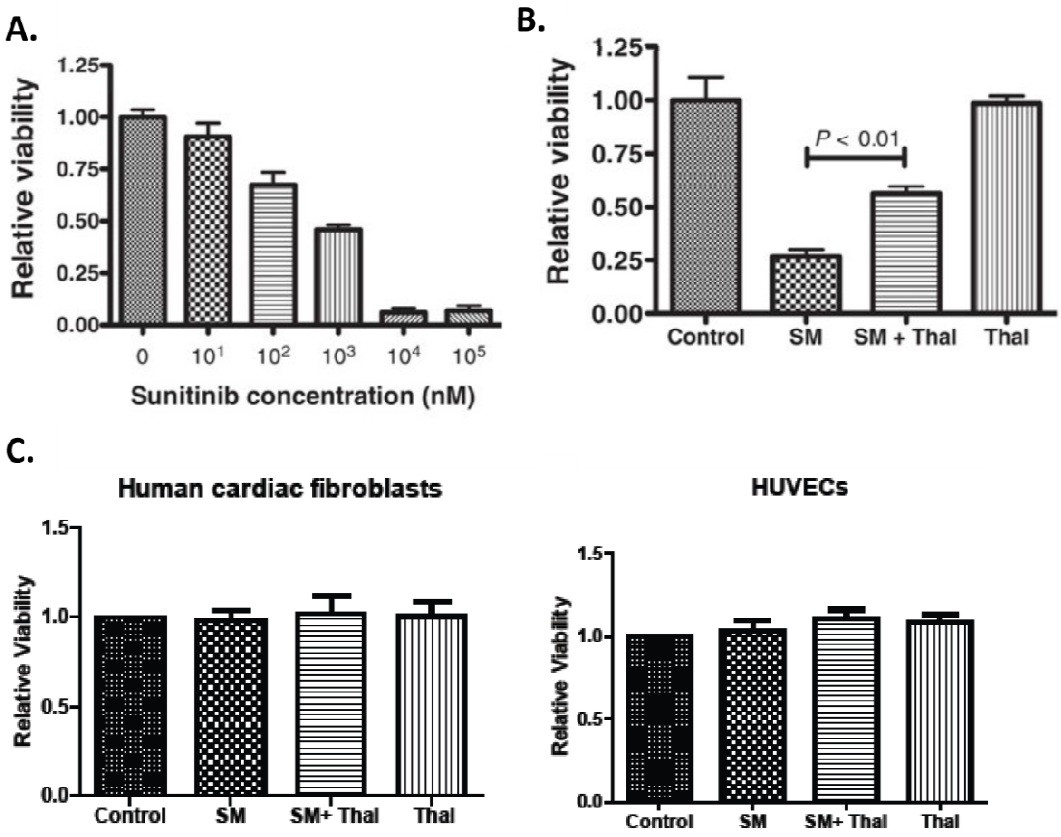

Figure 3.2.9. Sunitinib-induced pericyte death is rescued by thalidomide *in vitro*. (A) Pericyte viability measured by <TT assay after 24 hour treatment with increasing concentrations of sunitinib. **(B)** Pericyte viability after 24 hour treatment with sunitinib alone or plus thalidomide. **(C)** Neither sunitinib alone nor co-treatment with thalidomide affects fibroblast or endothelial cell viability.

nor co-treatment with thalidomide had any effect on fibroblast or endothelial cell viability (**Figure 3.2.9C**). This suggests that sunitinib-induced cardiotoxicity may be directly related to its effects on pericytes and that pericytes are specifically protected by thalidomide.

Therefore, if thalidomide could restore pericyte coverage in the heart, sunitinib induced cardiotoxicity might be prevented. Mice were treated with sunitinib alone or sunitinib plus thalidomide for 14 days followed by 14 days of recovery. Thalidomide protected from both sunitinib-induced reductions in both contractile (**Figure 3.2.10A**) and microvascular (**Figure 3.2.10B**) dysfunction during the treatment phase and this protection extended into the recovery period. Lastly, confocal microscopy revealed that thalidomide co-treatment preserved pericyte coverage of coronary microvessels (**Figure 3.2.10C**). These findings demonstrate that sunitinib-induced pericyte depletion may be directly responsible for sunitinib-induced cardiac dysfunction.

3.2.8. Thalidomide does not alter the anti-tumor efficacy of sunitinib.

To determine whether thalidomide may represent a novel strategy for cardioprotection during sunitinib treatment, the ability of sunitinib to halt tumor growth was evaluated in the presence of thalidomide. As a single treatment, thalidomide only mildly slowed tumor growth compared to sunitinib in a human renal cell carcinoma xenograft model (**Figure 3.2.11A**). However more importantly, the rate of tumor growth with co-administration of thalidomide and sunitinib was no different than sunitinib alone. As observed in non-tumor bearing mice, co-treatment with thalidomide protected from sunitinib-induced contractile dysfunction (**Figure 3.2.11B**) and decrease in coronary flow reserve (**Figure 3.2.11C**). Collectively, this data demonstrates that co-treatment with thalidomide may be a viable strategy for cardioprotection in patients receiving sunitinib.

Figure 3.2.10.

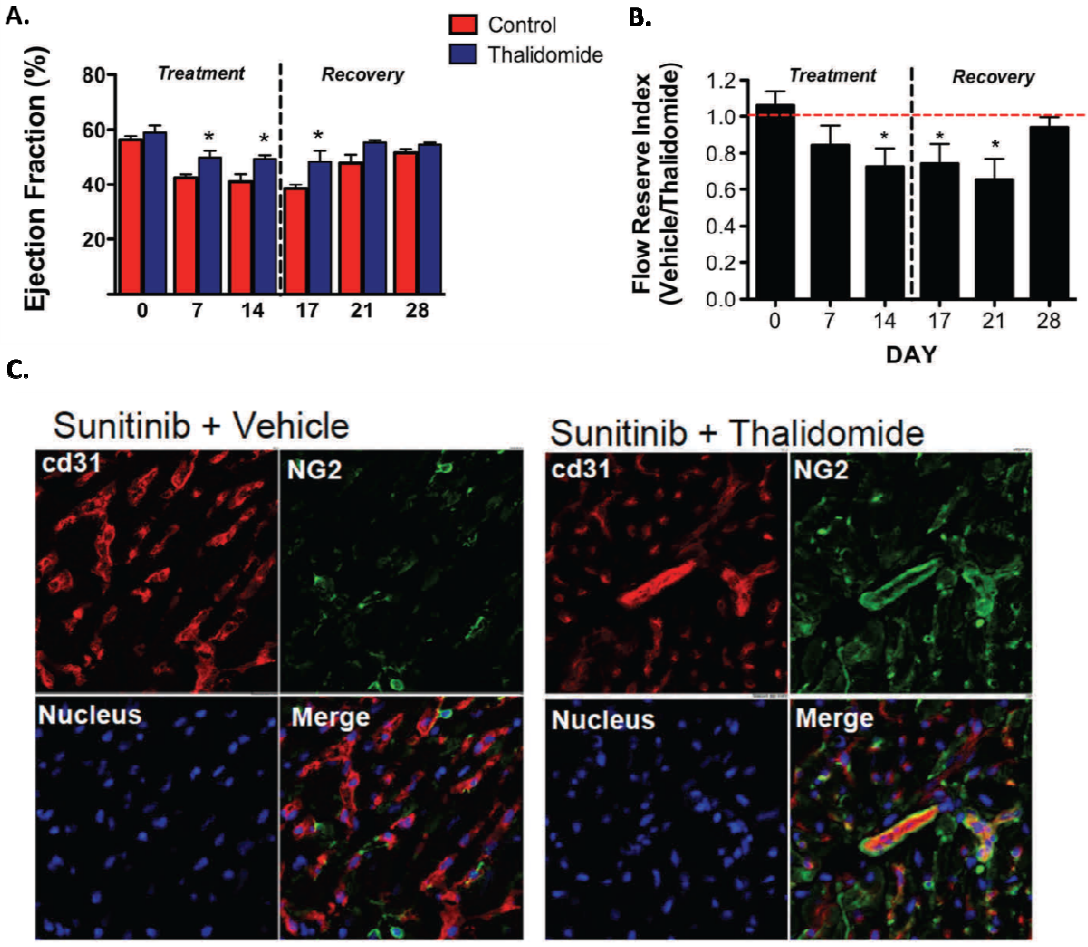

Figure 3.2.10. Co-treatment with thalidomide prevents sunitinib-induced cardiovascular dysfunction and pericyte loss. (A) Left-ventricular ejection fraction in mice treated with sunitinib alone (control) or sunitinib plus thalidomide (thalidomide) for 14 days followed by a 14 day recovery period. **(B)** Coronary flow reserve in mice treated with sunitinib alone or sunitinib plus thalidomide. Data is shown as the flow reserve index, or the ratio of mice treated with sunitinib alone to mice treated with sunitinib plus vehicle. **(C)** Confocal micrographs stained for the endothelial marker CD31 (red), pericyte marker NG2 (green), nuclei (DAPI, blue) and merged images. *$P < 0.05$.

Figure 3.2.11.

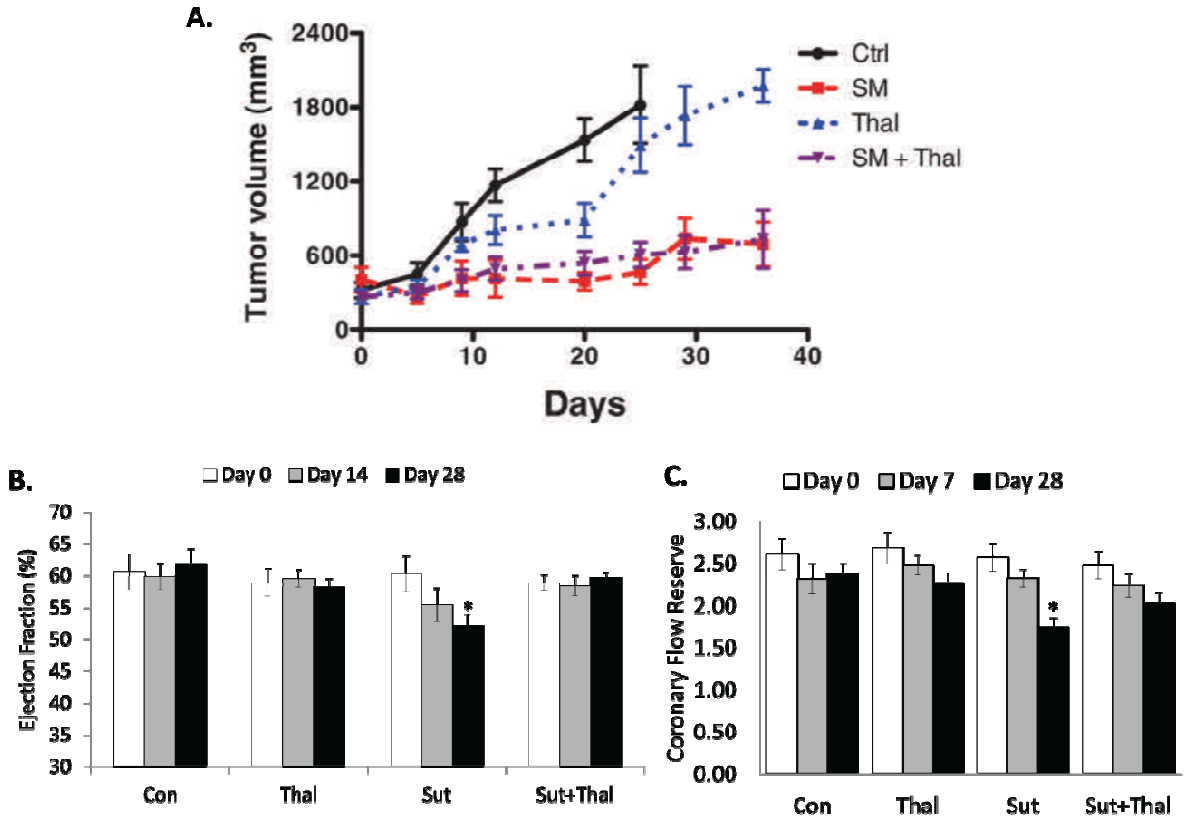

Figure 3.2.11. Co-treatment with thalidomide does not alter the anti-tumor capability of sunitinib. (A) Average tumor volume over time in untreated mice or mice treated with sunitinib alone, thalidomide alone or sunitinib plus thalidomide. **(B)** and **(C)** Left-ventricular ejection fraction and coronary flow reserve in tumor-bearing mice at day 0, 14 and 28 of treatment. *P < 0.05.

4. Discussion

The data presented here indicate that the primary cellular target of sunitinib is the pericytes surrounding the coronary microvasculature. Furthermore, pericyte loss leads to vascular abnormalities and cardiac dysfunction in the adult heart. It is known that pericyte loss leads to abnormal cardiac development and death during development (Bjarnegard et al., 2004; Jeansson et al., 2011). The data I presented here suggest that pericyte survival is similarly essential in the adult heart.

Sunitinib-induced cardiac dysfunction is mostly reversible with drug withdrawal (Uraizee et al., 2011); both cardiac and microvascular dysfunction slowly return to normal, suggesting that pericyte coverage also increases (**Figure 3.2.10**). It remains to be determined whether sunitinib treatment induces pericyte apoptosis *in vivo*, similar to pericyte loss in diabetic retinopathy (Geraldes et al., 2009). Or, whether the pericytes dedifferentiate and migrate away from the endothelium as occurs during cerebral ischemia (Thomas, 1999). My *in vitro* experiments (**Figure 3.2.9**) reveal a direct toxic effect of sunitinib on pericytes, suggesting that sunitinib treatment leads to pericyte cell death in the heart. Thus, the restoration of pericyte coverage may be the result of the transdifferentiation of myofibroblasts, smooth muscle cells or even endothelial cells in the heart (Deruiter et al., 1997; Nehls and Drenckhahn, 1993). Future studies may take advantage of cellular fate mapping tools, such as endothelial cell-specific expression of a myristoylated mCherry fluorescent protein (Poche et al., 2009), to determine the source of pericytes in the recovering sunitinib-treated heart.

The mechanism by which thalidomide protects from sunitinib-induced pericyte death remains unknown. Loss of microvascular pericytes in rat models of both Type I (streptozotocin-induced) or Type II (Zucker Diabetic Fatty rat) diabetes is associated with

high levels of TNFα (Behl et al., 2008). TNFα was also associated with pericyte dedifferentiation and proliferation in an experimental model of autoimmune encephalomyelitis (Tigges et al., 2013). Furthermore, pharmacological blockade of TNFα is sufficient to prevent pericyte cell death both *in vitro* and *in vivo* (Behl et al., 2008; Joussen et al., 2009; Tigges et al., 2013). Blockade of TNFα is the primary mechanism by which thalidomide improves autoimmune diseases and slows growth in multiple myeloma. Therefore it's possible that protection of coronary microvascular pericyte from sunitinib-induced cell death may be due to inhibition of TNFα. It would be interesting to determine if specific inhibition of TNFα could protect from sunitinib-induced cardiotoxicity. Although the combination of sunitinib and thalidomide did not slow tumor growth beyond sunitinib treatment alone (**Figure 3.2.11**), it is possible that more potent inhibition of TNFα—such as with lenalidomide or pomalidomide—in combination with sunitinib would be beneficial. In fact, several clinical trials evaluating lenalidomide as a single treatment for metastatic renal cell carcinoma have demonstrated positive results (Amato et al., 2008; Choueiri et al., 2006; Pal et al., 2012). Additional clinical studies will be necessary to determine whether sunitinib-induced coronary microvascular dysfunction and pericyte loss also occur in humans, and whether thalidomide represents a rational cardioprotection strategy for patients at high risk for cardiotoxicity due to sunitinib.

Pericyte loss is not a general feature of cardiac injury (**Figure 3.2.8**). Nonetheless, pericyte loss occurs during cerebral ischemia and in the early phases of diabetic retinopathy (Geraldes et al., 2009; Thomas, 1999). Therefore, it would be interesting to determine whether pericyte loss occurs in other forms of heart failure such as ischemic cardiomyopathy or diabetic cardiomyopathy. Along that same line, the exact mechanism by which pericyte loss leads to cardiac dysfunction remains to be fully explored. To this end, my previous lab performed gene expression microarrays on mice treated with sunitinib or vehicle for 3 or 7

days (**Figure 3.2.12**). Of 51 genes upregulated by at least 15%, 14 genes are known to be regulated by hypoxia inducible factor 1 alpha (Hif1α). Of these 14 genes, *PHD3*, *BNIP3, c-myc, Angptl4, and EDN1* are specifically upregulated in the hypoxic heart. It is possible that sunitinib-induced microvascular dysfunction leads to myocardial hypoxia, inducing a state similar to the hibernating myocardium (Ammirati et al., 2011; Kloner et al., 1989). Hibernating myocardium is defined as dysfunctional but still viable tissue and is discussed most often in the setting of left ventricular systolic dysfunction due to coronary artery disease. My data presented in the next chapter will suggest a possible connection between pericyte loss, hypoxia and dysfunction.

Lastly, pericyte loss may not be the only mechanism by which sunitinib could cause cardiac dysfunction. As discussed in Chapter 1, sunitinib has also been shown to directly inhibit adenosine monophosphate activated kinase (AMPK) (Kerkela et al., 2009; Laderoute et al., 2010). Sunitinib-induced changes in cardiac metabolism, specifically increased glucose metabolism, are the subject of the next chapter.

Figure 3.2.12.

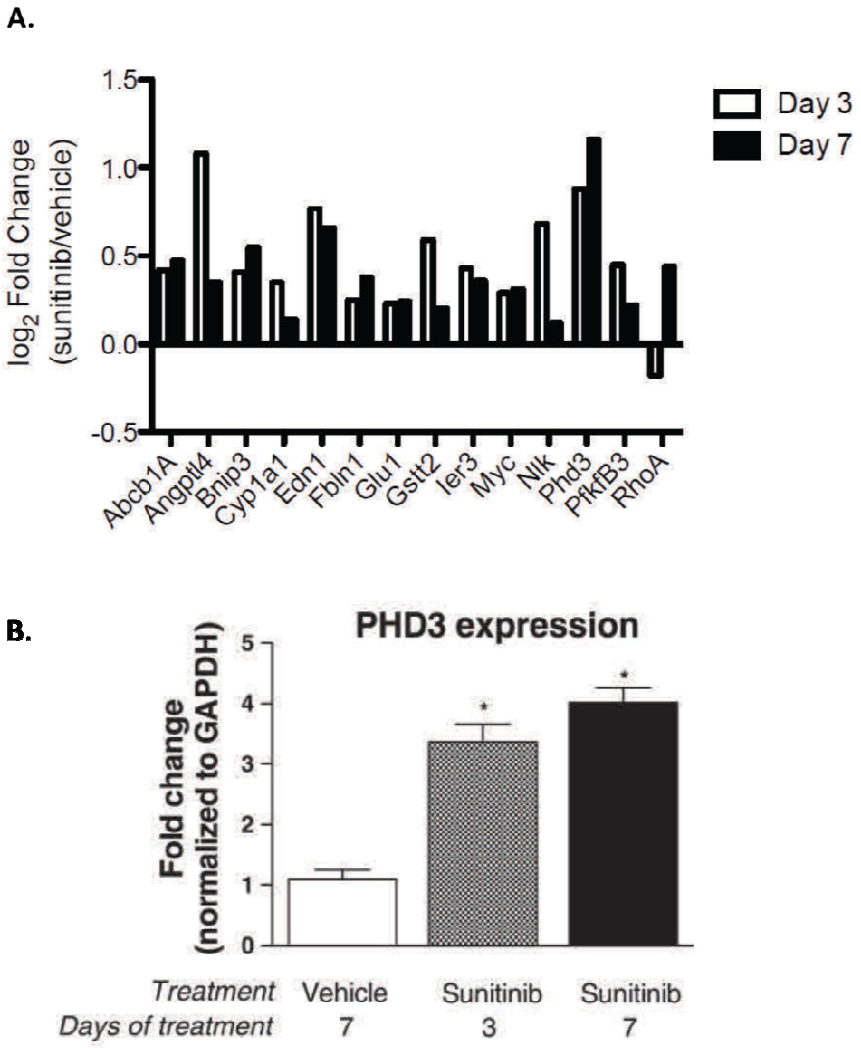

Figure 3.2.12. Microarray analysis of hearts from mice treated with sunitinib or vehicle for 3 or 7 days. (A) Fold change in expression of selected genes associated with hypoxia identified by the Affymetrix microarray. **(B)** qPCR confirmation of increased PHD3 expression in the hearts of mice treated with sunitinib for 3 or 7 days. *P<0.05.

Chapter 4

Altered Glucose Metabolism and a PKM2 Signature in the Failing Heart

Note: Several figures presented here are published in (Rees et al., 2015) Used with permission from Elsevier, license number: 500977596.

4.1 Introduction

4.1.1 Sunitinib lowers blood glucose levels in patients.

In addition to inducing cardiovascular dysfunction in a subset of patients, sunitinib dramatically lowers blood glucose levels in both diabetic and non-diabetic patients. Beginning as far back as 2004, a sprinkling of case reports have described a normalization of blood glucose levels in diabetic patients receiving sunitinib or the related receptor tyrosine kinase inhibitors imatinib, sorafenib and dasatinib (Billemont et al., 2008; Breccia et al., 2005; Breccia et al., 2004; Louvet et al., 2008; Mokhtari and Welsh, 2010; Templeton et al., 2008; Tsapas et al., 2008; Veneri et al., 2005). Agostino et al performed a retrospective study of blood glucose levels in both diabetic (17) and non-diabetic (61) patients treated with: imatinib (39), sunitinib (30), sorafenib (23) or dasatinib (8) (Agostino et al., 2011). The authors found significant decreases in blood glucose levels ranging from 53 mg/dL with dasatinib to 9 mg/dL with imatinib. Importantly, 47% (8/17) of the diabetic patients discontinued their medications, including some patients on insulin treatment.

Common to all these RTKIs is inhibition of PDGFRβ, Accordingly, the proposed mechanism for this phenomenon has thought to be the preservation of pancreatic beta cells through inhibition of PDGFRβ. In the most prominent paper promoting this hypothesis, the authors found that only drugs whose targets include the PDGFRβ (imatinib, sunitinib and a PDGFRβ-Ig) could both reverse and prevent the development of diabetes in the NOD mouse model of type I diabetes (Louvet et al., 2008). This was compared to specific inhibition of c-kit with PLX647, a monoclonal antibody that has also been proposed to mediate glycemic control (Mokhtari and Welsh, 2010). Several other investigators demonstrated preservation of pancreatic beta cells both in streptozotocin-treated rats and in the db/db mouse (Hagerkvist et al., 2008; Han et al., 2009). However this class of drugs,

specifically ones that target PDGFRβ, lower blood glucose levels in patients with type 2 diabetes as well, suggesting an alternative mechanism of glycemic control besides preservation of pancreatic beta cells, namely increased insulin action in the peripheral tissues. This concept is supported by the observation that imatinib increased insulin sensitivity and glucose disposal rates in rats fed a high fat diet (Hagerkvist et al., 2008).

Based on electron microscopy images demonstrating apparent mitochondrial structural abnormalities in the heart, Force et al proposed that cardiotoxicity due to imatinib and sunitinib may be due to mitochondrial defects (Force et al., 2007). Following this observation, a group at the pharmaceutical company Pfizer measured mitochondrial function in isolated rat mitochondria and H9C2 cells treated with imatinib, sunitinib, sorafenib and dasatinib (Will et al., 2008). Of the four kinase inhibitors tested, only sorafenib significantly affected isolated mitochondrial function and resulted in decreased ATP content in H9C2 cells. This indicated that mitochondrial dysfunction is most likely not the cause of sunitinib cardiotoxicity and confirmed the sentiment that the membrane whorls observed on transmission electron micrographs were most likely a freezing artifact (Dr. Michael Ewer, MD Anderson Cancer Center, personal communication).

4.1.2 Increased glucose metabolism and induction of the fetal gene program in the failing heart.

Mounting evidence from our lab and others indicates that glucose uptake in excess of the heart's capacity to oxidize glucose contributes to cardiovascular dysfunction. For instance, the ACCORD trial found that intensive glucose lowering therapies (targeted HbA1C levels below 6%) actually increase the incidence of death from cardiovascular disease in patients with type 2 diabetes. Given this high association between intensive

glucose lowering and cardiovascular dysfunction, I asked whether sunitinib similarly drives glucose uptake in excess of the heart's oxidative capacity.

A hallmark of the fetal heart is the use of carbohydrate substrates as the primary source of energy (Rajabi et al., 2007). The greater efficiency of carbohydrate substrates per mole of oxygen allows the fetal heart to withstand its low oxygen environment, rapidly changing hemodynamic load and demand for growth (Rajabi et al., 2007). Shortly after birth, as the maternal supply of nutrients is lost, the heart is exposed to a period of starvation where it rapidly depletes its glycogen stores and promptly switches to the oxidation of fatty acids. This process appears to require the induction of autophagy as deletion of the autophagasome elongation factor, ATG5, results in rapid post-natal lethality (Kuma et al., 2004). Though displaying a preference for fatty acids, the adult heart is an omnivore, capable of utilizing a wide range of additional carbon sources, such as lactate and ketone bodies, in response to metabolic milieu and hemodynamic load (Taegtmeyer, 1994).

The failing heart returns to predominant glucose utilization for energy provision. This is achieved, in part, through induction of the fetal gene program. The primary argument for this effect relates to the higher efficiency of glucose oxidation compared to the oxidation of fatty acids. The most convincing evidence for this comes from a study in the isolated working rat heart subjected to an abrupt increase in cardiac work (Goodwin et al., 1998) and a study by Korvald et al (Korvald et al., 2000). In this study, myocardial oxygen consumption and cardiac performance were measured *in vivo* using anesthetized pigs. For the same amount of cardiac work, oxygen consumption was 48% higher when pigs were infused with intralipid-heparin (IH) compared to infusion of glucose, insulin and potassium (GIK). Alternatively stated, for the same amount of oxygen consumed, glucose supports significantly more cardiac work. For this reason, activation of the fetal gene program is

thought to be mostly adaptive, provided glucose uptake and oxidation are matched (Rajabi et al., 2007).

Prominent features of the fetal gene program include myosin heavy chain (MHC) isoform switching from MHCα to MHCβ, expression of atrial naturietic factor (ANF) and activation of the transcription factors c-myc and c-fos (Rajabi et al., 2007). The switch to glucose oxidation results from primarily from the downregulation of adult genes such as GLUT4, pyruvate dehydrogenase kinase 2 (PDK2), muscle carnitine palmitoyl transferase 1 (mCPT-1) and medium-chain acyl-CoA decarboxylase (MCAD), (Barger and Kelly, 1999; Razeghi et al., 2001). In the course of work on my dissertation I have shown that induction of another fetal gene, the M2 isoform of pyruvate kinase (PKM2), may provide a link between activation of the fetal gene program and upregulation of glycolysis.

4.2 Results

4.2.1. Sunitinib treatment results in increased insulin sensitivity.

In order to test whether sunitinib affects blood glucose levels regardless of diabetic status, I tested insulin sensitivity in non-diabetic C57BL/6J mice. Sunitinib treated mice had decreased serum glucose levels (**Figure 4.2.1A**) despite significantly decreased circulating insulin levels (**Figure 4.2.1B**). This suggested to me that sunitinib increases insulin sensitivity as both groups consumed the approximately same number of calories per mouse per day (**Figure 4.2.1C**). Significantly increased insulin sensitivity was confirmed by an insulin tolerance test (**Figure 4.2.1D**) as well as by the slightly enhanced glucose clearance observed in an oral glucose tolerance test (**Figure 4.2.1E**).

Based on these findings, hyperinsulinemic euglycemic clamp studies were performed in the Mouse Metabolism Core at Baylor College of Medicine. The hyperinsulinemic

euglycemic clamp is considered the gold standard by which to characterize insulin sensitivity (Defronzo et al., 1979). Measurement of tissue-specific glucose uptake can be achieved using [U-^{14}C]-2-deoxyglucose (2DG), or the related tracer, 2-deoxy-2-[^{18}F]fluoro-D-glucose (FDG) (**Figure 4.2.2A**).

2DG and FDG are readily taken up by the cell and phosphorylated but not further metabolized, permitting an estimation of tissue glucose uptake (Nguyen et al., 1990). It is important to note, however, that glucose uptake is underestimated when 2DG is used, making assessment of myocardial glucose uptake with 2DG is qualitative rather than quantitative. Under non-steady state conditions, (i.e. the presence of insulin, competing substrates or ischemia) there is a discordant affinity of hexokinase for glucose versus FDG, with a stronger preference for glucose (Doenst and Taegtmeyer, 1998; Hariharan et al., 1995). Non-steady state conditions lead to a change in the lumped constant (LC), which is, in fact, not a constant but rather a conversion factor used to convert the rates of tracer uptake to the rates of tracee uptake. However, the LC can be predicted using a time-activity curve generated from the measured rates of [2-3H]glucose and FDG glucose uptake under the same conditions (Bøtker et al., 1999).

The steady-state glucose infusion rate was significantly increased in the sunitinib group (**Figure 4.2.2B**). Once steady-state conditions are reached, the rate of glucose infusion is equal to the rate of glucose disposal and the rate of peripheral glucose uptake can be approximated. The glucose disposal rate was significantly increased in the sunitinib group (**Figure 4.2.2C**) and [U-^{14}C]-2DG uptake revealed a fivefold and sevenfold increase in the heart and skeletal muscle, respectively (**Figure 4.2.2D**).

Figure 4.2.1.

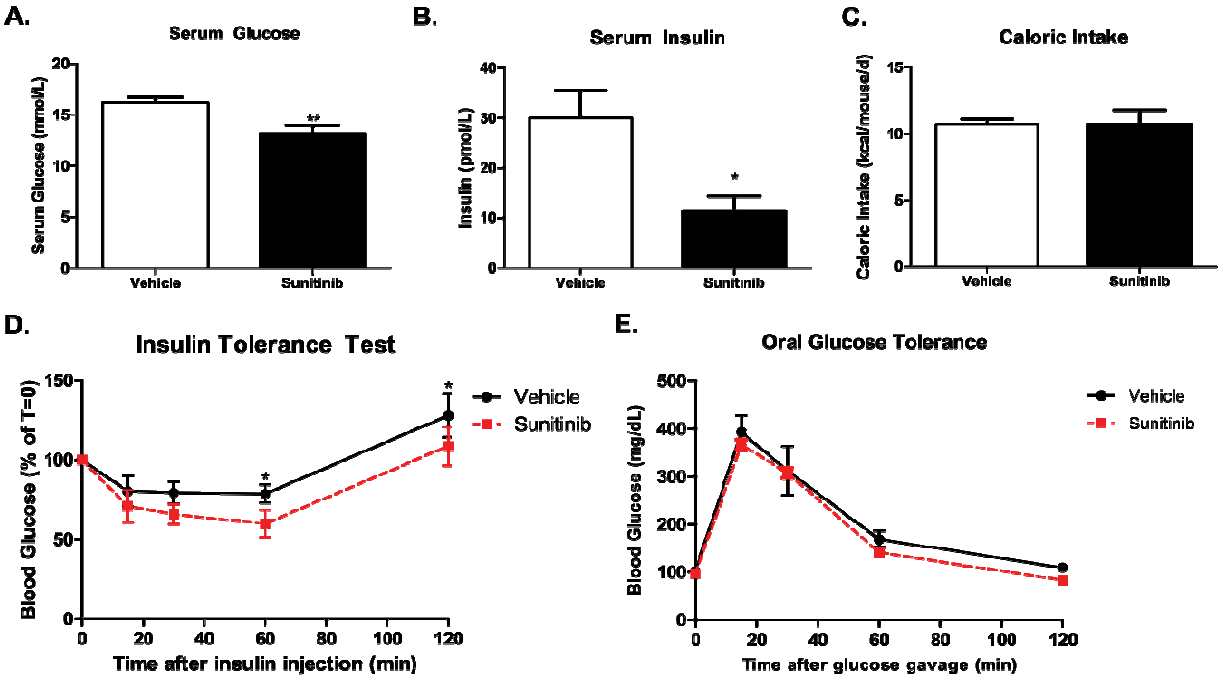

Figure 4.2.1. Sunitinib increases systemic insulin sensitivity. (A) Non-fasted serum glucose levels. **(B)** Non-fasted serum insulin. **(C)** Average caloric intake per day over the course of treatment. **(D)** Insulin tolerance test. **(E)** Oral glucose tolerance test. *P < 0.05 and **P < 0.01.

Figure 4.2.2.

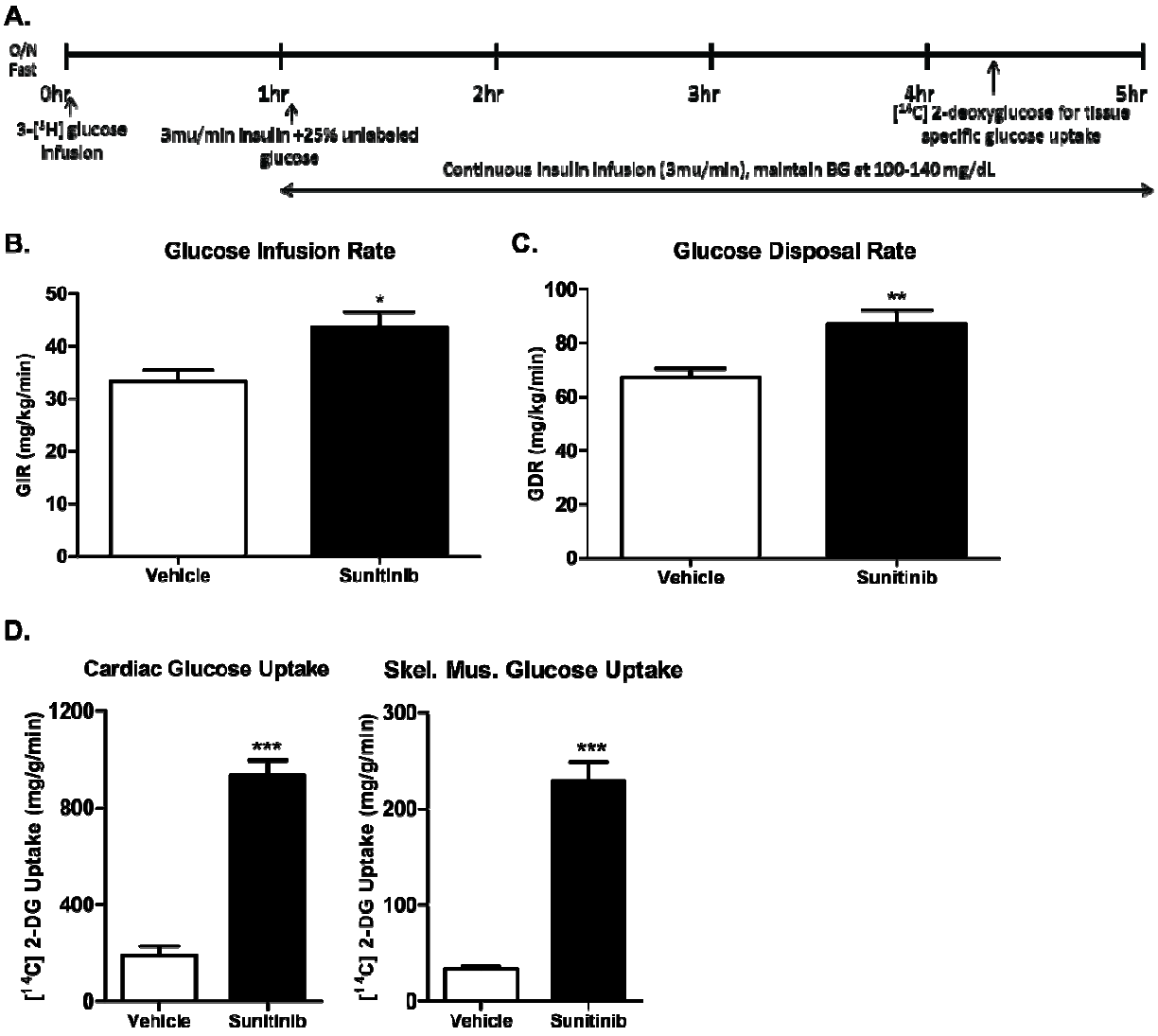

Figure 4.2.2. Hyperinsulinemic euglycemic clamp procedure in mice treated with sunitinib. (A) Summary of the clamp procedure. **(B)** Steady-state glucose infusion rate. **(C)** Glucose disposal rate calculated from the steady-state glucose disposal rate. **(D)** [U-14C]-2-deoxyglucose uptake in the heart and skeletal muscle. *P < 0.05, **P < 0.01 and ***P < 0.001.

A hallmark of the fetal heart is the reliance on glucose metabolism as the primary source of energy provision. The greater efficiency of glucose oxidation permits the fetal heart to adapt to its low oxygen environment and demand for growth. With exposure to the oxygen-rich post-natal environment and the rapid depletion of endogenous substrate stores, the heart rapidly switches to fatty acid oxidation. However, a salient feature of the failing heart is metabolic remodeling from predominant fatty acid oxidation to carbohydrate metabolism.

Transcript analysis by qPCR revealed a significant upregulation of glycolytic genes, specifically pointing to the redirection of glucose towards lactate production (**Figure 4.2.3A**). This corresponded to reduced enzyme activity of pyruvate kinase (**Figure 4.2.3B**) and increased lactate dehydrogenase activity (**Figure 4.2.3C**). Hallmarks of the fetal gene program, which include a switch in the contractile protein isoforms from myosin heavy chain α (MHCα) to MHCβ and increased expression of atrial naturetic factor (ANF), c-myc and c-fos (Rajabi et al., 2007), were increased in the sunitinib-treated hearts (**Figure 4.2.3D**). Thus, sunitinib treatment leads to upregulation of the fetal gene program in the heart. Upregulation of the fetal gene program and increased glycolysis are intimately linked with cardiac hypertrophy. Correspondingly, I observed an increase in cardiomyocyte cross-sectional area in sunitinib-treated mice (**Figure 4.2.3E**). Interestingly, I did not observe an increase in the heart weight to body weight ratio, which suggests that cardiac hypertrophy and apoptosis occurs side-by-side and may be a unique feature of sunitinib cardiotoxicity (**Figure 4.2.3F**).

4.2.3. Glucose is redirected into secondary pathways of metabolism.

Glycogen occupies about 2% of the cell volume in the adult cardiomyocyte, however comprises nearly a third of the cell volume in the fetal heart (Rajabi et al., 2007).

Figure 4.2.3.

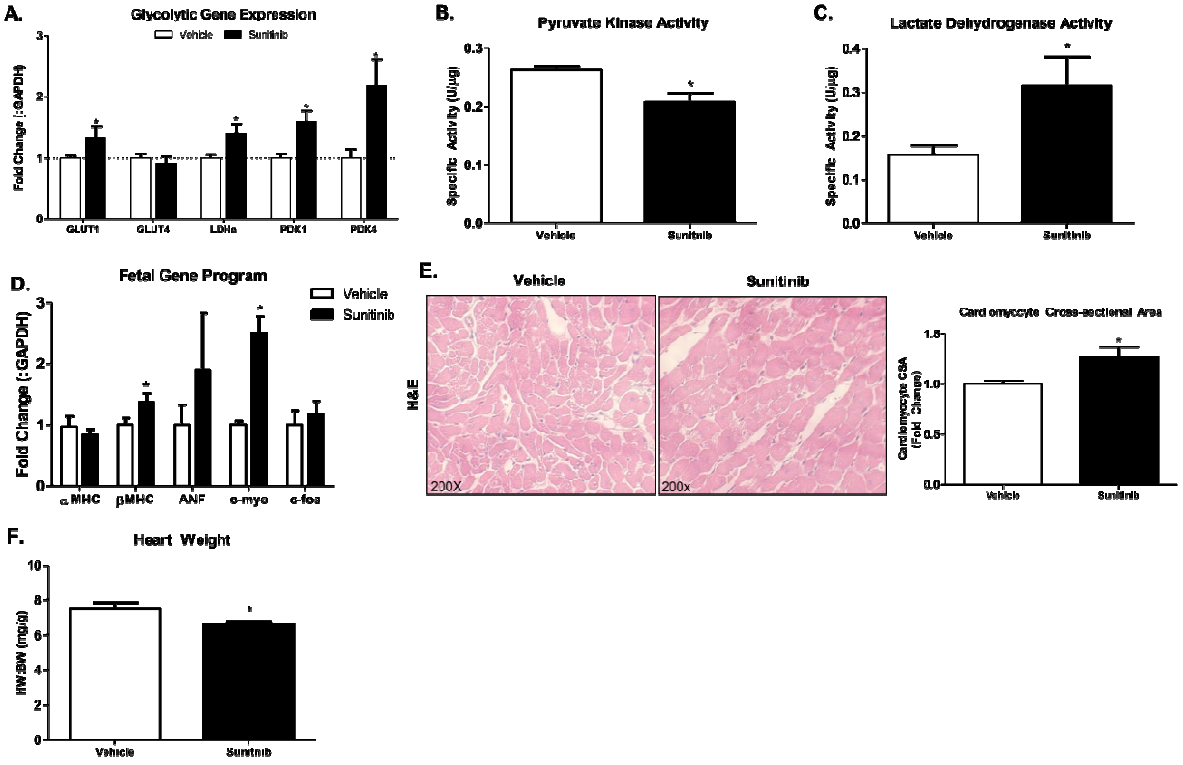

Figure 4.2.3. Sunitinib treatment increases glycolysis in the heart. (A) Transcript analysis by qPCR of key glycolytic genes. **(B)** Enzyme activity of pyruvate kinase. **(C)** Lactate dehydrogenase enzyme activity. **(D)** qPCR analysis demonstrating activation of the fetal gene program **(E)** Hemotoxylin and Eosin (H&E) staining of cross sections from mice treated with sunitinib or vehicle. Cardiomyocyte cross-sectional area is quantified to the right. **(F)** Ratio of heart weight to body weight. *P < 0.05.

Correspondingly, I observed significant glycogen accumulation in sunitinib treated hearts (**Figure 4.2.4A**). This was suggestive of an overflow of glucose into secondary pathways of glucose metabolism. Accordingly, I observed a significant increase in O-Linked β-N-acetylglucosamine (O-GlcNAc) modification of cardiac proteins (**Figure 4.2.4B**). O-GlcNAc is a product of the hexosamine biosynthetic pathway and results from conversion of glucose 6-phosphate to fructose 6-phosphate, glucosamine-6-phosphate and ultimately to UDP-GlcNAc (Ngoh et al., 2010; Watson et al., 2010). Similar to phosphorylation, it is rapidly cycled on and off proteins via the action of O-GlcNAc transferase and O-GlcNAcase. Sunitinib-induced cardiotoxicity is a unique model of cardiac dysfunction and it is unclear what the role of O-GlcNAcylation is in the sunitinib-treated heart.

It is of note that in the hearts from sunitinib-treated animals, the levels of glucose-6-phosphate are significantly decreased (**Figure 4.2.4C**). I have verified these measurements by repeated assays. The results suggest that G6P is metabolized by at least three different pathways: glycolysis, glycogen synthesis and the hexosamine biosynthetic pathway. Future work may determine the flux rates through the individual pathways.

4.2.4. Sunitinib treatment leads to induction of PKM2.

Increased glycolysis, slowed pyruvate kinase activity and redirection of glucose into secondary pathways of metabolism were reminiscent of the Warburg Effect in cancer. Since its first description by Otto Warburg, reviewed by (Warburg, 1956), the Warburg Effect has evolved to describe the upregulation of glycolysis by cancer cells and the redirection of glucose-derived carbons into biosynthetic pathways (Vander Heiden et al., 2009). One of the drivers of the Warburg Effect in cancer is the induction of the fetal, M2 isoform of pyruvate kinase (PKM2). Because I had observed activation of the fetal gene program in the sunitinib

Figure 4.2.4.

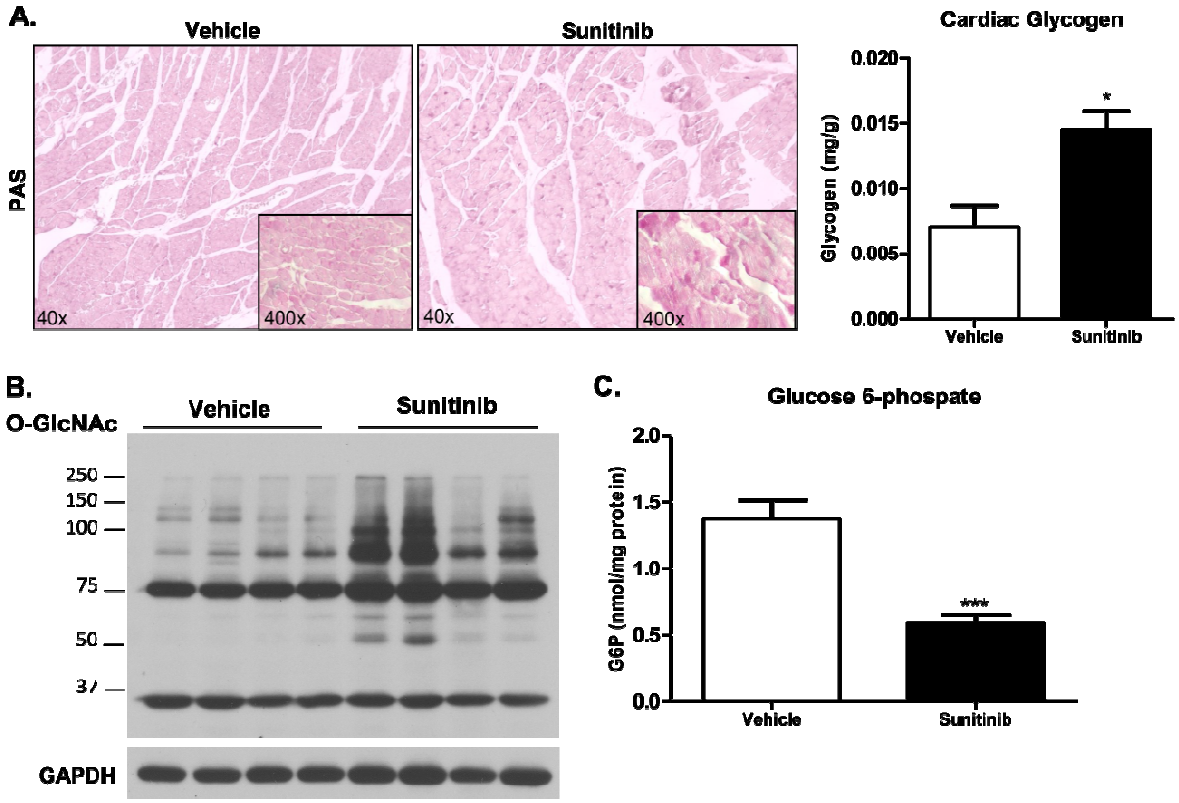

Figure 4.2.4. Glucose is redirected into secondary pathways of glucose metabolism. **(A)** Cardiac glycogen content as assessed by Periodic Acid-Schiff staining and quantified to right by tissue extraction and enzyme-coupled spectroscopy. **(B)** Western blot demonstrating increased O-GlcNAcylation of cardiac proteins. **(C)** Cardiac glucose 6-phosphate levels. *P < 0.05 and ***P < 0.001.

treated heart, I asked whether PKM2 induction also occurs with sunitinib treatment. Digestion of the PKM cDNA product with the restriction enzyme Pst1 (**Figure 4.2.5A**) revealed a significant increase in the percentage of PKM2 in the heart (**Figure 4.2.5B**). This was confirmed by both western blot (**Figure 4.2.5C**) and qPCR (**Figure 4.2.5D**). Thus, in hearts from sunitinib treated mice, PKM2 is upregulated like in cancer cells.

4.2.5. Sunitinib treatment leads to activation of Hif1α and c-myc.

Under normoxic conditions, the master hypoxia response factor, hypoxia inducible factor 1α (Hif1α) is hydroxylated by a family of prolyl-hydroxylases and subsequently targeted for ubiquitin-mediated proteasomal degradation by the von Hippel–Lindau protein (VHL). When the oxygen level in the cell falls, Hif1α translocates into the nucleus where it heterodimerizes with Hif1β and activates a host of genes, including PKM2. Hydroxylated PKM2, in turn, upregulates Hif1α expression in a positive feed-forward loop.

Sunitinib treatment resulted in increased Hif1α protein expression in the nuclear fraction of hearts from mice treated with sunitinib (**Figure 4.2.6A**) as well as an upregulation of Hif1α transcript levels (**Figure 4.2.6B**) and transcript levels of Hif1α-induced genes (**Figure 4.2.6C**). This suggests that activation of Hif1α may be an important contributor to the induction of PKM2 in the heart.

Alternative splicing of the PKM gene is dependent on three heterogeneous nuclear ribonucleoprotein (hnRNP) proteins: polypyrimidine tract binding protein (PTB, also known as hnRNPI), hnRNPA1 and hnRNPA2. At high levels, these factors bind to the intronic sequence flanking exon 9 and inhibit the inclusion of exon 9 (PKM1) in the mRNA product (Luo and Semenza, 2012). Upregulation of these factors is promoted by the oncogenic transcription factor c-myc (David et al., 2010). In the heart, c-myc is induced by pressure

Figure 4.2.5.

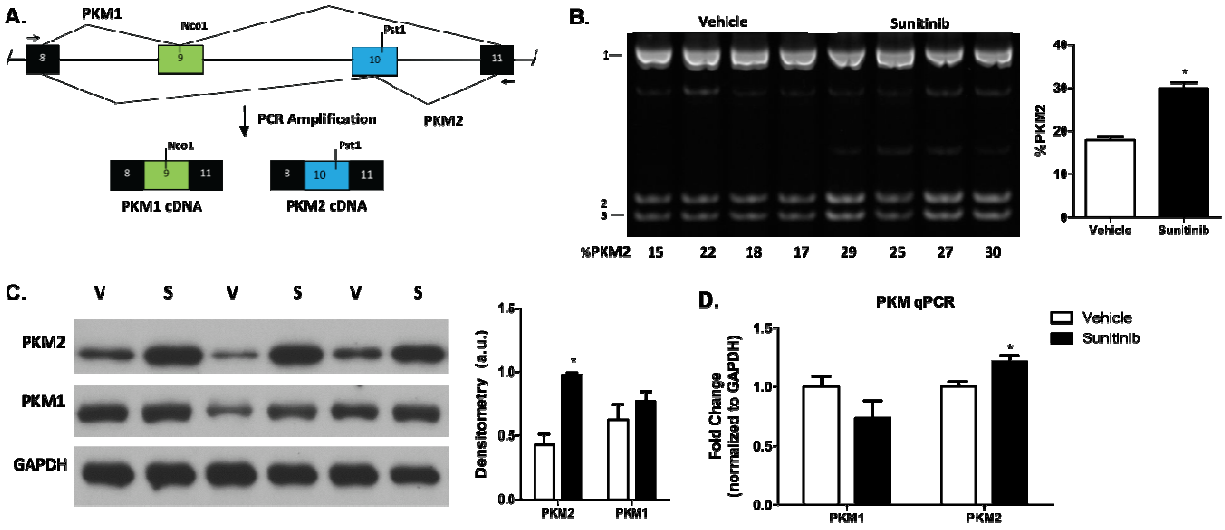

Figure 4.2.5. Sunitinib treatment results in induction of the M2 isoform of pyruvate kinase. (A) Diagram detailing the alternative splicing of the PKM gene and resulting cDNA products and restriction enzyme sites. **(B)** Pst1 digest of the PKM cDNA products and resulting percentage of PKM2, quantified to the right. **(C)** Western blotting of PKM2 and PKM1 mice treated with sunitinib (S) or vehicle (V). **(D)** qPCR quantification of PKM1 and PKM2 transcript levels. *P < 0.05.

Figure 4.2.6.

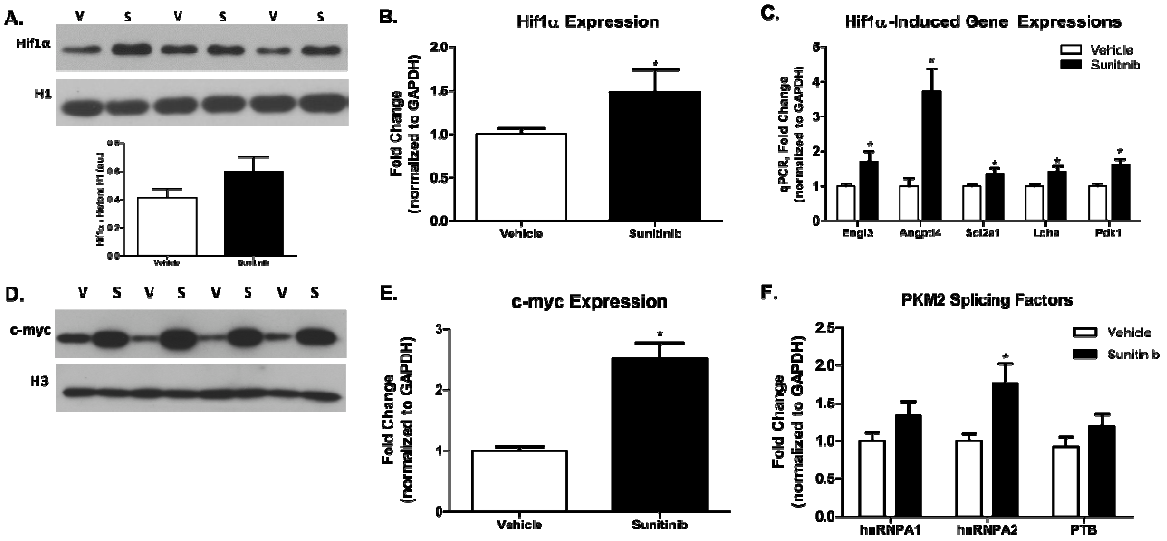

Figure 4.2.6. Sunitinib treatments results in the activation of Hif1α and c-myc. (A) Western blotting for Hif1α in the nuclear fraction of cardiac tissue lysates. **(B)** qPCR measurement of Hif1α and **(C)** Hif1α-target genes expression in the heart. **(D)** Western blot of c-myc protein expression in the nuclear fraction of cardiac tissue lysates. **(E)** Transcript analysis of c-myc and **(F)** of key PKM2 splicing factors induced by c-myc. *P < 0.05.

overload (Mulvagh et al., 1988). Additionally, coronary flow is a strong determinant of c-myc expression (Bauters et al., 1988). Nuclear c-myc protein (**Figure 4.2.6D**) and mRNA (**Figure 4.2.6E**) expression levels were significantly increased in sunitinib-treated hearts. Transcript levels of PTB, hnRNPA1 and hnRNPA2 were similarly increased in sunitinib treated hearts (**Figure 4.2.6F**). These findings further support the critical role of PKM2 expression (and the Warburg Effect) in hearts from sunitinib treated animals.

4.2.6. Hif1α activation results in PKM2 induction in the heart.

In order to determine directly whether hypoxia was sufficient to induce PKM2 expression in the heart, mice were housed in an 8% oxygen environment for 24 hours. As a result, PKM2 expression was increased in the heart, but not in skeletal muscle (**Figure 4.2.7A**). I next determined whether PKM2 induction could be induced *in vitro*. Not unexpectedly, the immortalized cardiac cell line H9C2 and neonatal rat ventricular myocytes (NRVMs) only express PKM2 whereas isolated adult mouse cardiomyocytes express primarily PKM1 **(Figure 4.2.7B**). Thus the isolated adult cardiomyocytes proved ideal to study the induction of PKM2 in the heart. Twenty-four hour exposure of isolated adult cardiomyocytes to 1% oxygen or to the pharmacological hypoxia mimetics, dimethyloxalylglycine (DMOG) and cobalt chloride, resulted in increased PKM2 expression compared to sunitinib treatment or untreated controls (**Figure 4.2.7C**). These results are important because they indicate that the pyruvate kinase isoform switch is mediated by oxygen deprivation and not as a direct effect of sunitinib.

4.2.7. PKM2 is induced in the failing human heart.

Figure 4.2.7.

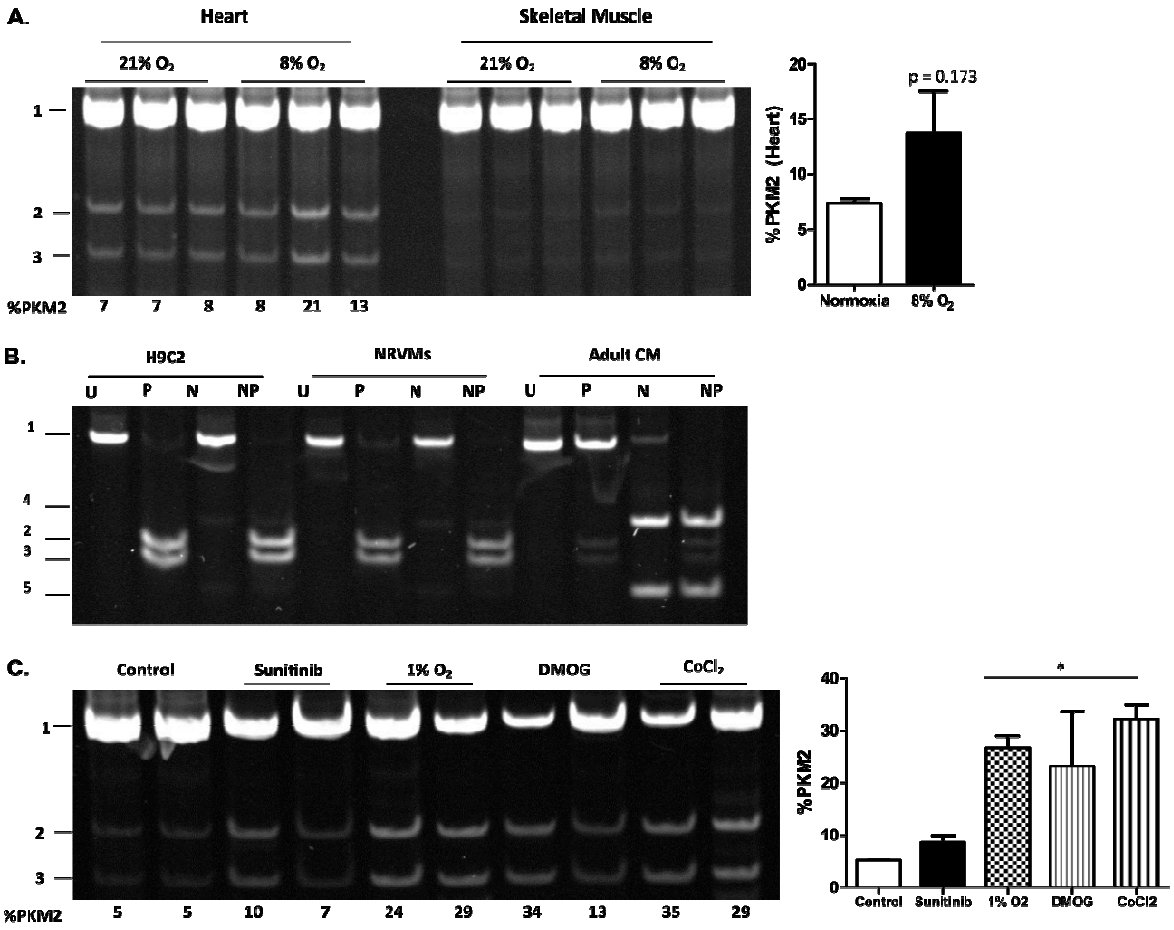

Figure 4.2.7. Hif1α activation results in PKM2 induction in the heart. (A) Percent PKM2 expression in mice subjected to normoxia (21% oxygen) or 8% oxygen for 24 hours. **(B)** Percent PKM2 expression in the H9C2 cell line, neonatal rat ventricular myocytes (NRVMs) or isolated adult cardiomyocytes. **(C)** Percent PKM2 expression in isolated adult cardiomyocytes exposed to 1% oxygen or treated with the pharmacological mimetics dimethyloxalylglycine (DMOG) or cobalt chloride ($CoCl_2$) for 24 hours. * $P < 0.05$.

To determine the clinical relevance of my findings I evaluated PKM2 expression in heart muscle samples from non-failing and failing human hearts, the latter before and after mechanical unloading with a left-ventricular assist device (LVAD). Compared to non-failing hearts, *PKM2* expression, assessed by qPCR, was significantly increased in the failing heart muscle samples (**Figure 4.2.8A**). This observation was confirmed by western blot (**Figure 4.2.8B**). It appeared that the induction of PKM2 regressed with mechanical unloading. I therefore evaluated PKM2 expression in a total of 13 paired samples and found a significant decrease in PKM2 expression in the explant heart muscle samples (**Figure 4.2.8C**). Similar to the mouse samples, PKM2 induction was correlated with O-GlcNAcylation of proteins in the human hearts (**Figure 4.2.8D**). The results confirm the lab's earlier observations that the failing human heart reverts to the fetal genotype (Razeghi et al., 2001). They also show, for the first time, a partial reversal with mechanical unloading.

4.3 Discussion

It has long been assumed that PKM2 is an oncogene, specifically selected by the tumor to drive growth. Yet the question remains why there is selection for PKM2 rather than a silencing or mutation of PKM1. A recent report from the Vander Heiden lab demonstrated that—surprisingly—deletion of PKM2 results in more aggressive tumors (Israelsen et al., 2013). It seems that selection for PKM2 permits metabolic flexibility, allowing for either pyruvate generation or a redirection of glucose-derived carbons into biosynthetic pathways for growth. In the postmitotic cardiomyocyte, the role of PKM2 induction in the failing heart may have a similar role.

Glucose metabolism in the hemodynamically stressed heart is finely regulated and can be both adaptive and maladaptive. For instance, overexpression of the glucose

Figure 4.2.8.

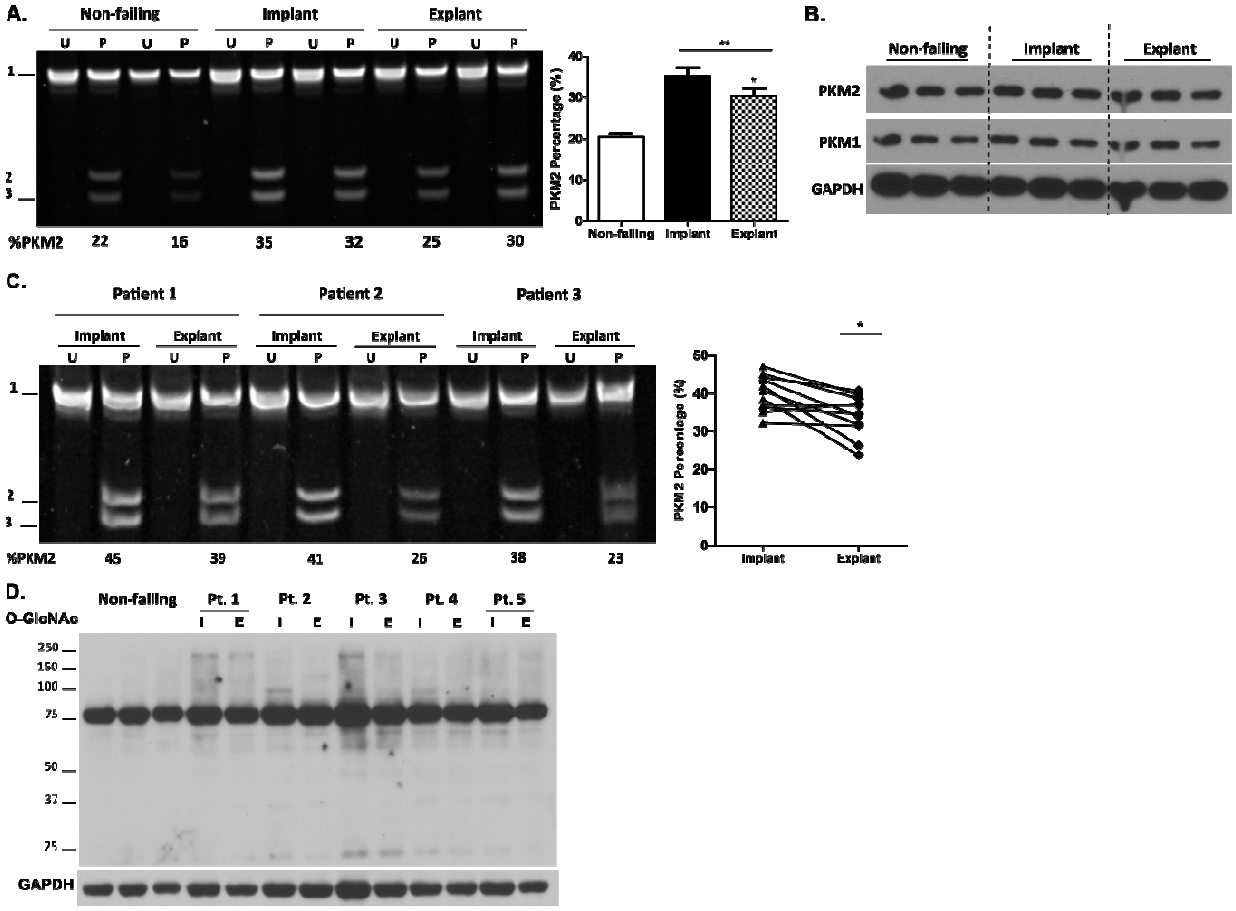

Figure 4.2.8. Induction of PKM2 in the failing human heart. (A) Percent PKM2 expression in non-failing, or failing human hearts before and after LVAD implantation. **(B)** Protein expression of PKM2 and PKM1 in heart muscle samples. **(C)** Percent PKM2 expression in paired heart muscle samples from before and after LVAD implantation. **(D)** Quantification of O-GlcNAcylated proteins in non-failing and paired failing human heart muscle samples at the time of LVAD implant (I) and explant (E) by Western Blot. *P < 0.05 and **P < 0.01.

transporter, GLUT1, prevents the development of heart failure in response to pressure overload stress as well as protects from ischemic injury in both young and aged mice (Liao et al., 2002; Luptak et al., 2007). Knockdown of acetyl-CoA carboxylase 2 (ACC2) enhances rates of fatty acid oxidation, prevents hypertrophy and preserves cardiac function (Essop et al., 2008; Kolwicz et al., 2012). Similarly, high fat feeding prevents hypertrophy-induced cardiac remodeling in rats (Okere et al., 2006). However in our lab's experience, preventing substrate switching via activation of peroxisome proliferator-activated receptor alpha (PPARα) exacerbates dysfunction in rat hearts subjected to pressure overload stress (Young et al., 2001).

The uncoupling of glycolysis from glucose oxidation may be where the process begins to unravel (Taegtmeyer, 2000). The lab has also demonstrated that myocardial glucose uptake in excess of the oxidative capacity of the heart leads to contractile dysfunction through the accumulation of glucose 6-phosphate, sustained activation of the mammalian target of rapamycin (mTOR) and endoplasmic reticulum stress (Sen et al., 2013).

A simple question is does induction of PKM2 allow the failing heart to respond to uncertain nutrient and oxygen availability or does PKM2 exacerbate pathological hypertrophy and adverse remodeling? I propose that PKM2 induction is part of the adaptive response in the stressed heart. Unlike PKM1, which exists as a near-constitutively active tetramer, PKM2 can exist as a dimer or tetramer and is uniquely subject to allosteric regulation and various post-translational modifications that determine its function as pyruvate kinase, protein kinase or transcription factor (Anastasiou et al., 2012; Wong et al., 2013). Importantly, the ability of PKM2 to rapidly cycle between a tetramer and dimer could be especially advantageous to the failing heart. In its tetramer form, PKM2 acts as a canonical pyruvate kinase, allowing pyruvate oxidation and ATP generation. The low

catalytic activity of the dimer form slows glycolysis and allows for the redirection of glucose-derived carbons into biosynthetic pathways promoting cell proliferation, in the case of cancer, or, in the case of the heart, intracellular self-renewal and hypertrophy. It will be important to determine if, similar to the Warburg effect in cancer, glucose-derived carbons support cardiac hypertrophy.

It has also been proposed that “cellular oncogenes drive the progression to heart failure” (Hoshijima and Chien, 2002). This is based on the observation that many of the pathways driving tumor growth also drive cardiomyocyte hypertrophy (Cheng and Force, 2010; Mulvagh et al., 1988). Induction of PKM2 in the hypertrophying heart would fit with this reasoning. Included in this original hypothesis was activation of the fetal gene, *c-myc*. In cancer, *c-myc* drives the expression of three heterogeneous nuclear ribonucleoprotein (hnRNP) proteins-polypyrimidine tract binding protein (PTB, also known as hnRNPI), hnRNPA1 and hnRNPA2-that are essential for preferential splicing of PKM2 (David et al., 2010). Because *c-myc* transcription was significantly induced in the sunitinib treated hearts (**Figure 4.2.6**), it is possible that c-myc might also be important for preferential PKM2 splicing in the heart. Furthering this hypothesis, changes in hemodynamic load induces c-myc in the remodeling heart (Depre et al., 1998). As PKM2 expression seems to correlate with hemodynamic load in the failing human heart (**Figure 4.2.8**), it seems likely that c-myc plays a role in promoting PKM2 induction, though the exact mechanism awaits elucidation. Hif1α and dysregulated c-myc have been shown to cooperatively promote transcription of key glycolytic genes in cancer (Wong et al., 2013). However, in the adult heart, Hif1α and c-myc seem to play opposing roles. Whether these two factors cooperate in the failing heart, or whether this is an anomaly of the sunitinib-treated heart, remains to be determined.

Vander Heiden and colleagues specifically deleted PKM2 in tumor cells by inserting flox sites flanking exon 10 of the PKM gene. Cre-induced recombination led to selective

expression of PKM1 and a nonfunctional, truncated version of the PKM gene, PKM-skip, which included neither exon 9 or 10. Interestingly, PKM2 is not required for tumor formation or progression. The obvious next experiment would be to delete PKM2 in the hearts of mice exposed to pressure-overload stress. This would determine whether PKM2 induction is adaptive or maladaptive feature of the stressed heart.

The reciprocal experiment would be to force PKM2 expression in the adult heart, perhaps by using a conditional deletion of PKM1 in the adult heart. This would address the "chicken or the egg" scenario with PKM2 expression and enhanced glucose uptake. Christofk and colleagues have demonstrated that knockdown of PKM2 in cancer cell lines decreased the rate of glycolysis and that reintroduction of PKM2 but not PKM1 enhanced glycolysis and xenograft tumor formation (Christofk et al., 2008). PKM2 induction in the heart is likely part of a coordinated response to hypoxic or hemodynamic stress in the heart. Furthermore, PKM2 induction is probably not the cause of the glycolytic switch but rather an important mediator.

PKM2 is subject to profound allosteric regulation and post-translational modifications that regulate its function as a pyruvate kinase, protein kinase or transcription factor. These nonmetabolic functions of PKM2 may be similarly important in the failing heart. For instance, oxidation of cysteine 358 decreases PKM2 activity, leading to a redirection of glucose into the pentose phosphate pathway and generation of reducing equivalents. Dimeric PKM2 can also translocate into the nucleus, for instance in response to EGFR stimulation, and transactivate transcription factors such as β-catenin or the stem cell factor Oct4 (Lee et al., 2008; Yang et al., 2011). PKM2 can use the high energy bonds from PEP to phosphorylate and activate proteins such as Stat3 (Gao et al., 2012). Stat3 is important for proper function of the electron transport chain (Wegrzyn et al., 2009), and cardiomyocyte-specific knockout of Stat3 accelerates inflammation-induced cardiac fibrosis (Jacoby et al., 2003).

Several small molecule activators of PKM2 have been developed and have proven to suppress tumor growth (Anastasiou et al., 2012; Parnell et al., 2013). Similar to the endogenous activator of PKM2, fructose-1,6-bisphopsphate (FBP), these molecules, namely DASA-58 (N, N′-diarylsulfonamide, NCGC001859) and TEPP-46 (thieno-[3,2-b]pyrrole [3,2-d]pyridazinone, NCGC00186528), stabilize the high-activity tetramer conformation of PKM2 allowing for flow of glucose through to pyruvate (Wong et al., 2013). Phosphorylation of tyrosine 105 by fibroblast growth factor receptor 1 (FGFR1) leads to FBP dissociation and destabilization of the tetramer formation. Importantly, small molecule activators of PKM2 that bind to this same FBP binding pocket are resistant to this phosphorylation (Wong et al., 2013). More recently small molecule activators of PKM2 have been developed which bind to a distinct site from FBP and appear to be more effective (Anastasiou et al., 2012). The question remains whether stabilization of PKM2 tetramer formation would be advantageous to the failing heart by better matching glucose uptake and oxidation. Forced fatty acid oxidation (i.e. activation of PPARs with fenofibrate (Chicco et al., 2007) exacerbates dysfunction in the failing heart. It is unclear whether normalization of PKM2 function in the failing heart would be similarly detrimental. It is important to note that while these activators restore the pyruvate kinase activity of PKM2, the potentially advantageous nuclear signaling and protein kinase activities are lost. Thus these inhibitors may be a useful tool to delineate the two function of PKM2 in the heart.

To my knowledge, this is the first evidence of PKM2 induction in any model of heart failure. The importance of secondary pathways of glucose metabolism in the heart is largely unrecognized beyond glycogen as an energetic store and redirection of glucose into the pentose phosphate pathways to maintain redox status in the failing heart (Doenst et al., 2013). PKM2 induction may be just the tip of the Warburg Effect iceberg in the failing heart.

Figure 4.2.9.

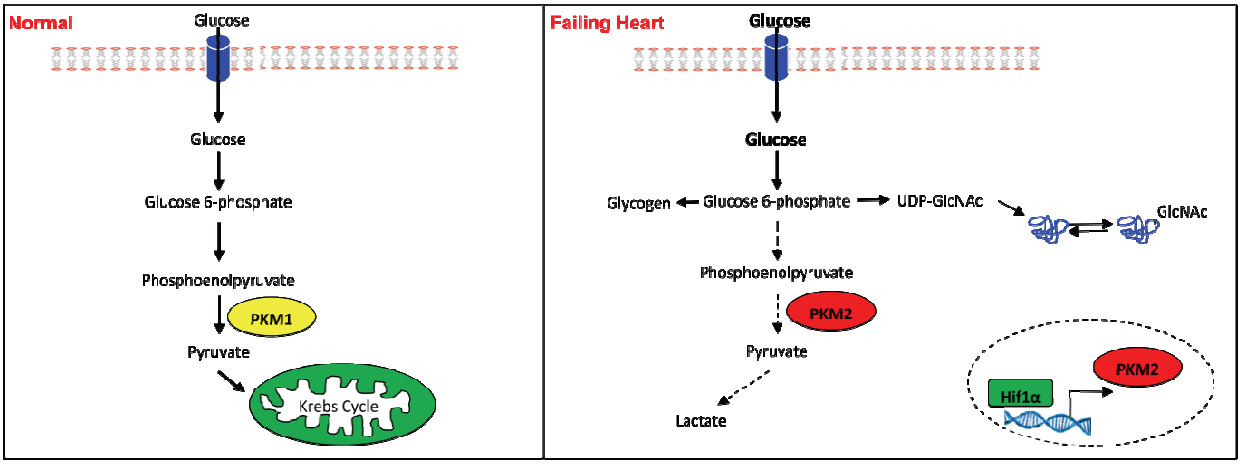

Figure 4.2.9. Summary. In the failing heart, activation of the hypoxia response factor Hlf1α results in induction of the M2 isoform of pyruvate kinase. This leads to a redirection of glycose into secondary pathways of metabolism including lactate production, glycogen accumulation on O-GlcNAcylation of proteins.

Chapter 5

CONCLUDING REMARKS AND FUTURE DIRECTIONS

5.1 Summary of findings

In my work, I explored mechanisms of cardiotoxicity due to the cancer chemotherapeutic agent, the receptor tyrosine kinase inhibitor sunitinib. My two major finding are that sunitinib denudes the coronary vasculature of an important constituent, its pericytes, and that sunitinib induces major metabolic changes in the heart which are consistent with metabolic and structural remodeling of the cardiomyocyte. I will now discuss the importance of my findings and how my findings may relate to each other.

Coronary microvascular pericytes are a primary target of sunitinib-induced cardiotoxicity. Work in my previous lab demonstrated that inhibition of the essential prosurvival signal, PDGFRβ, leads to cell death and coronary microvascular dysfunction. As I will discuss in detail below, microvascular dysfunction is associated with myocardial hypoxia and with the induction of the fetal gene program. My further work focused on sunitinib-induced metabolic changes in the heart and resulted in the discovery of an additional member of the fetal gene program, the M2 isoform of pyruvate kinase (PKM2). Most importantly, PKM2 induction is a signature of not only sunitinib cardiotoxicity but is also a striking feature of the failing human heart. To my knowledge, this is the first evidence of PKM2 induction in any model of heart failure.

This work began with the fact that cardiotoxicity due to cancer treatments is a major obstacle in effective cancer treatment. A patient may outlive his or her cancer only to succumb to heart failure in as little as five years (Go et al., 2013; Levy et al., 2002). The focus of my dissertation was therefore twofold: First, to elucidate the mechanism of sunitinib-induced cardiotoxicity in order to develop a cardioprotective strategy in patients receiving sunitinib and, secondly, to use sunitinib-induced cardiotoxicity as a tool to identify novel pathways that contribute to the progression of heart failure. I have demonstrated success in

both areas. Thalidomide, or perhaps one of its derivatives, may prove to be a viable treatment for patients at high risk of developing cardiac dysfunction while receiving sunitinib. Possible mechanisms for this protective effect are discussed in Chapter 3. Additionally, PKM2 may represent a novel metabolic target for the treatment of heart failure, although it remains to be determined whether the upregulation of PKM2 is adaptive or maladaptive to cardiac stress (discussed in Chapter 4).

The data presented here reveal two important things. First, microvascular pericytes are essential to maintain cardiac function in response to stress. This adds to a growing body of evidence suggesting that the coronary vasculature is more dynamic than previously recognized, reviewed by (Feigl, 1983) and (Gould et al., 2013). Secondly, PKM2 may be an important mediator of cardiac energy provision. However, the extent to which the Warburg Effect exists in the heart remains to be determined. The relevance of these two observations to non-chemotherapy related heart failure is still to be proven and beyond the scope of my thesis. Clearly, more work is necessary to elucidate the mechanisms driving these two observations. Particular areas of future work are discussed below.

5.2 Does pericyte loss result in myocardial hypoxia?

One of my most important observations was establishing the fact that sunitinib treatment alone does not induce PKM2 expression in isolated adult cardiomyocytes (**Figure 4.2.7**). This suggests that PKM2 induction through Hif1α may be secondary to the depletion of pericytes. In support of this hypothesis, deletion of either PDGF-B or PDGFRβ results in pericyte loss and leads to impaired perfusion and tissue hypoxia in the developing mouse brain (Hellström et al., 2001). Pericyte loss also leads to tissue hypoxia in a model of ischemic retinopathy (Wilkinson-Berka et al., 2004) and hypoxia-associated epithelial-to-

mesenchymal transition and increased metastasis was linked to pericyte loss in a mouse model of breast cancer (Cooke et al., 2012). Collectively, these studies demonstrate that pericyte loss can lead to tissue hypoxia, and my results now suggest the same may be true for the heart.

To induce deletion of pericytes in the breast tumors, the group of Cook et al. employed an inventive strategy, which could be used to determine whether PKM2 induction is secondary to pericyte loss and hypoxia in the heart (Cooke et al., 2012). The NG2 and, separately, PDGFRβ promoter was used to drive expression of the viral thymidine kinase (TK) in pericytes. Subsequent treatment with the antiviral drug ganciclovir led to selective cell death in TK-expressing cells, due to the fact that viral TK converts the nontoxic ganciclovir into a toxic metabolite (Barese et al., 2012). This approach may be advantageous over traditional methods that induce pericyte cell death, such as deletion of PDGF-B or PDGFRβ because the TK-ganciclovir approach would avoid the use of a Cre recombinase, which can be cardiotoxic at high levels (Buerger et al., 2006).

Thalidomide co-treatment may also be a useful tool to determine whether PKM2 induction is secondary to pericyte loss. In the first part of my thesis, I demonstrated that thalidomide can restore pericyte coverage. Thus, if protection of microvascular pericytes with thalidomide is sufficient to prevent induction of PKM2, it may be concluded that pericyte loss leads to PKM2 induction. However, there are several issues with this approach, particularly the non-specific nature of both sunitinib and thalidomide. Therefore a genetic approach, such as the TK-ganciclovir approach described above, would yield a more definitive answer, and I did not pursue this line of research.

In addition to the regulation of capillary diameter (discussed in chapter 3), the diffusion distance that oxygen much travel from its dissociation from hemoglobin, across the

endothelium and finally to the mitochondria is crucially important in determining oxygen levels within the cell. This is illustrated by the Krogh cylinder model, which relates the radius of a capillary to the radius of a theoretical cylinder of tissue to which it supplies oxygen (**Figure 5.1**) (Fishman, 1982). The ratio of the cross-sectional area of the capillary to the cross-sectional area of the cylinder is directly proportional to the decrease in oxygen pressure from the capillary to that point. For example in **Figure 5.1**, a cell 10 units away from a capillary that has a radius of 5 units results in a ratio of 1:4. Therefore, if the arterial pO_2 is 80 mmHg, the pO_2 at that cell would be 20 mmHg. However if this distance is doubled, the pO_2 at the level of the cell would only be 5 mmHg, which would be sufficient to induce Hif1α activation.

In my model of sunitinib-induced pericyte loss, this distance may increase due to interstitial edema resulting from increased vessel leakiness (**Figure 3.2.6**). Although it does not likely double, the extent of interstitial edema was not measured in my experiments. It is also important to stress that the pO_2 within the capillary does not remain constant along the length of the capillary. As oxygen is extracted by the tissue the intracapillary pO_2 declines. This, coupled to decreased oxygen gradients at more distal sites and turbulent flow, would suggest that there are areas within the sunitinib treated heart where the pO_2 falls to critically low levels.

The existence of hypoxia *in vivo* is prohibitively difficult to prove. Precise measurement of cellular PO_2 with an oxygen electrode is the definitive method to establish the presence of hypoxia (Krogh, 1919a, b). However, this is not always technically possible. Hypoxyprobe (pimonidazole HCl) is a commercially available tracer that can be used to label hypoxic areas *in vivo* (Hypoxyprobe, NPI Inc., Burlington, MA). Pimonidazole is stabilized under hypoxic conditions and binds to peptide thiols such as glutathione (Hodgkiss, 1998).

Figure 5.1

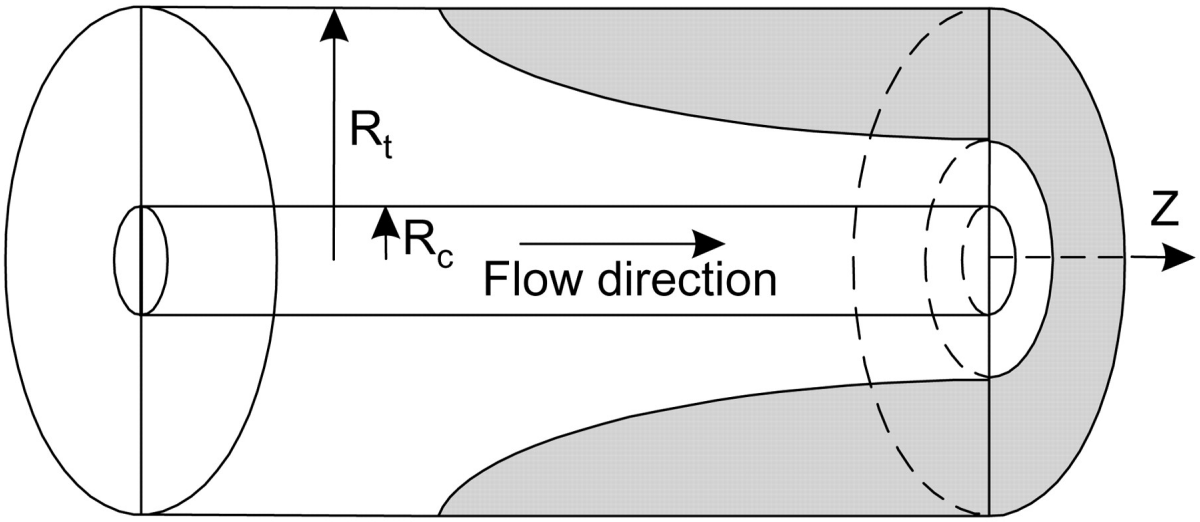

Figure 5.1. The Krogh cylinder model of an oxygen pressure field. The pO_2 at a given distance (R) from the capillary is directly proportional to the ratio of the capillary cross-sectional area to the cross-sectional area of the theoretical cylinder to which it supplies oxygen. For instance, at a point that is 10 units from a capillary that has a radius of 5 units results in a ratio of 1 to 4. Thus, if the capillary has a pO_2 of 80mmHg, the pO_2 at that point would be 20mmHg. Source: B. J. McGuire , T. W. Secomb. (1985) A theoretical model for oxygen transport in skeletal muscle under conditions of high oxygen demand. J Appl. Physiol. Reused with permission from the journal.

Fixed tissue sections or tissue lysates can then be probed with an antibody directed against pimonidazole. My attempt to use this probe in my sunitinib-treated mice resulted in false-positive staining in my control mice, perhaps due to incomplete washout of the probe before sacrifice. I therefore decided to abandon this approach.

Another approach could be to use positron emission tomography (PET) imaging with ^{18}F-fluoromisonidazole (Rasey et al., 1996). Similar to pimonidazole, fluoromisonidazole is stabilized under hypoxic conditions and has been used to image hypoxic regions in both human and mouse tumors (Bentzen et al., 2002; Rajendran et al., 2004). Use of this probe in sunitinib treated mice or in conjunction with a model of pericyte loss, such as the TK-ganciclovir approach suggested above, would help establish whether pericyte loss results in myocardial hypoxia.

Still, it is entirely possible that sunitinib treatment leads to Hif1α stabilization irrespective of a change in cellular PO_2. Sustained mTOR activation through loss of TSC2 has been shown to stabilize Hif1α and induce PKM2 expression in mouse kidney tumors (Sun et al., 2011). Similarly, preliminary evidence from my lab indicates that conditional deletion of tuberous sclerosis 2 (TSC2), and therefore activation of mTOR, in the adult heart leads to PKM2 induction (Davogustto, unpublished observations). Additionally, oleanolic acid has been shown to repress PKM2 expression in isolated cancer cell lines (Liu et al., 2014). In addition to inducing pressure overload stress (discussed in Chapter 4), it will be interesting to determine whether other mechanisms, such as mTOR activation or metabolic stress, can induce PKM2 in the heart.

5.3 Sunitinib as an insulin sensitizing agent.

The induction of PKM2 is not likely the cause of enhanced systemic insulin sensitivity during sunitinib treatment. As discussed in the previous chapter, it has been proposed that sunitinib decreases blood glucose levels though preservation of pancreatic beta cells (Hagerkvist et al., 2008; Han et al., 2009; Louvet et al., 2008). However, sunitinib also reduces blood glucose levels in both non-diabetic mice and in humans (Billemont et al., 2008; Breccia et al., 2005; Breccia et al., 2004; Louvet et al., 2008; Mokhtari and Welsh, 2010; Templeton et al., 2008; Tsapas et al., 2008; Veneri et al., 2005). Therefore, it seems likely that sunitinib increases peripheral insulin sensitivity. In normal insulin responsive cells, such as cardiomyocytes, activation of the PI3K-Akt signaling cascade by the binding of insulin to the insulin receptor leads to increased glucose uptake though trafficking of glucose transporters (primarily GLUT4) to the cell surface (James et al., 1989). However, similar to the VEGFRs and PDGFRs, the insulin receptor is a receptor tyrosine kinase, making it unlikely that sunitinib would increase insulin sensitivity through activation of the insulin receptor. However sunitinib may alter increase GLUT4 translocation or inhibit its endocytosis from the plasma membrane (Martin et al., 1999).

In the treatment of diabetes, enhanced insulin sensitivity is achieved through pharmacological modulation of several pathways. The group of insulin-sensitizing agents known as thiazolidinediones (TZDs), improve insulin sensitivity by lowering plasma free fatty acids and activating peroxisome proliferator-activated receptor gamma (PPARγ). PPARγ regulates the expression of multiple metabolic enzymes (Spiegelman, 1998). In rats, the TZD rosiglitazone increases GLUT4 expression (Oakes et al., 1994). Therefore, modulation of PPARγ could be a mechanism by which sunitinib increases insulin sensitivity.

Metformin also increases insulin sensitivity in the peripheral tissues. This is achieved primarily though decreasing hepatic gluconeogenesis (Stumvoll et al., 1995). However, metformin also activates AMP-activated protein kinase (AMPK) (Zhou et al., 2001a) and has

been shown to increase glucose uptake *in vitro* (Bertrand et al., 2006). Conversely, sunitinib may directly inhibit AMPK (Kerkela et al., 2009; Laderoute et al., 2010). Sunitinib treatment is also associated with increased hepatic glucose production, as measured during the hyperinsulinemic euglycemic clamp procedure (**Figure 4.2.2**). Therefore, it is not likely that sunitinib enhances insulin sensitivity in a manner similar to metformin.

It is, however, possible that sunitinib-induced pericyte loss directly enhances insulin sensitivity. The laboratory of Alan Attie at The University of Wisconsin-Madison has suggested that pericyte loss leads to increased transendothelial transport of insulin, allowing enhanced delivery of insulin to the muscle cell (Raines et al., 2011; Richards et al., 2010). In support of this hypothesis, pericyte loss in a rat model of diabetic retinopathy is associated with increased expression of genes involved in vesicular transport such as caveolin-1 and plasmalemmal vesicle associated protein-1 (PV-1) (Klaassen et al., 2009).

Alternatively, because sunitinib is a highly promiscuous kinase inhibitor, it's entirely possible that a unique combination of kinase inhibition leads to enhanced insulin sensitivity and glucose uptake in the sunitinib-treated animal. For this reason, I suspect that a proteomic approach would be useful to elucidate the mechanism of enhanced insulin sensitivity associated with sunitinib treatment. This is, however, beyond the scope of my thesis.

5.4. Why do only a fraction of sunitinib-treated patients develop cardiac dysfunction?

A vexing question is why only approximately 20% of patients develop cardiac dysfunction while on sunitinib. Assuming sunitinib also induces pericyte loss in humans, what is unique about the vasculature of these patients that makes them sensitive to sunitinib? Interestingly, patients who develop hypertension while receiving sunitinib have

significantly better responses to treatment and longer progression-free survival, suggesting that there is something different about the vasculature of these patients (Bono et al., 2011; Rini et al., 2011)). Yet the question remains, how do we determine what that difference is, and how can it be used to better inform treatment strategies?

This question is of course not limited to sunitinib cardiotoxicity. Predicting whether a patient will respond to a given treatment spans all avenues of human disease and is the foundation of personalized medicine. My previous lab attempted to answer a similar question: what determines the time of transplant-free survival in a patient with new onset non-ischemic cardiomyopathy. That is, what determines whether a patient will remain stable for some time or will rapidly decompensate, in need of mechanical assist and/or need cardiac transplantation. By performing microRNA profiling on endomyocardial biopsies obtained from a small number of patients (10), my previous lab found that differential regulation of three microRNAs was predictive of outcome (unpublished data). Similarly, my current lab found that lower expression of two microRNAs, miRs 23a and 195, was associated with functional recovery in patients placed on a LVAD compared to patients who remained LVAD-dependent (Ramani et al., 2011). However, other tools may be more predictive of the development of cardiac dysfunction with sunitinib such as proteomics or epigenetic analysis. None of this has been attempted as yet.

5.5. Future Directions

My dissertation work revealed two important new findings: the necessity of microvascular pericyte coverage in preserving cardiac function and the induction of PKM2 in the failing heart. Sunitinib cardiotoxicity is, admittedly, not a robust model of heart failure because, due to the nonspecific nature of the drug, the mechanisms driving certain

observations are difficult to discern. Furthermore, it is unclear whether inhibition of these pathways is relevant to other models of heart failure.

Irrespective of any mechanisms, my findings indicate extensive remodeling of the heart, akin to the remodeling observed in cancer cells. In cancer cells, glucose metabolism is redirection from oxidation, and to some extent also from glycolysis, to a host of biosynthetic pathways including the pentose phosphate pathway (**Figure 5.2**) and reviewed by (Vander Heiden et al., 2009). Increased flux through the pentose phosphate provides reducing equivalents (NADPH) and precursors for nucleotide synthesis (ribose) and nonessential amino acids, both of which are necessary for cell growth and division. Furthermore, the increased reliance on glutamine by cancer cells leads to production of acetyl-CoA for lipid biosynthesis via cycling through citrate. Mutations in key regulators of these pathways, such as in LKB1, p53 and c-myc, enable cancer cells to redirect glucose and glutamine into these biosynthetic pathways and proliferate uncontrollably.

The main difference between the Warburg Effect in cancer and in the heart is that cancer cells hypertrophy and proliferate (Vander Heiden et al., 2009) while heart muscle cells hypertrophy and fail (Sen et al., 2013). However the pathways driving cellular hypertrophy in both cases may be very much the same. In addition to providing a more efficient fuel source, the switch to predominant glucose metabolism in the stressed heart may also support hypertrophy. The Warburg Effect may not be entirely applicable to the hypoxic heart, such as in the case of sunitinib cardiotoxicity, because it seems unlikely that the heart would synthesize new proteins under conditions of limited oxygen availability. However, increased O-GlcNAcylation of proteins may be part of the hypoxic response. Increased hexosamine and protein O-GlcNAcylation is protective in the setting of ischemia-reperfusion (Jensen et al., 2012). Nonetheless, in response to other stresses such as pressure overload or even exercise, the Warburg Effect may be a previously unrecognized

Figure 5.2

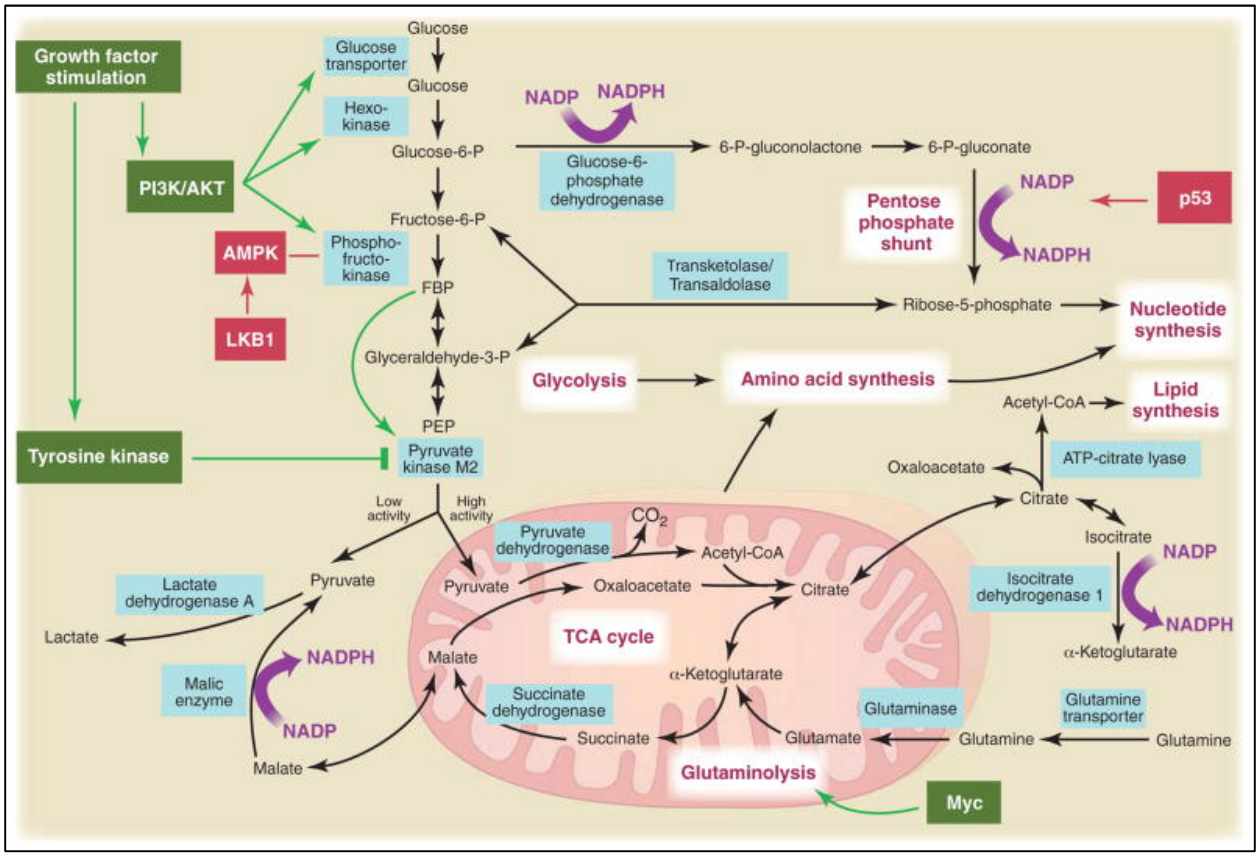

Figure 5.2. The Warburg Effect in cancer cells. The Warburg Effect is controlled by pathways involving known oncogenes and tumor suppressors. [Source: Vander Heiden, M.G., Cantley, L.C., and Thompson, C.B. (2009). Understanding the Warburg Effect: The Metabolic Requirements of Cell Proliferation. Science 324, 1029-1033. (Vander Heiden et al., 2009), reprinted with permission from the AAAS].

mechanism through which the heart obtains carbons and reducing equivalents for cardiac hypertrophy.

An important future experiment would be to trace glucose-derived carbons during pressure overload induced hypertrophy. The specifics of this experiment would be difficult to perform *in vivo* because cardiac hypertrophy requires at least a couple of weeks. It might be possible to introduce [U-^{13}C]glucose into the chow of mice that have undergone transverse aortic banding. However, analysis of these findings may be confounded by the dynamic nature of protein turnover in the heart (Razeghi et al., 2003). Examination of the Warburg Effect in cancer does not have this problem because cancer cells rapidly proliferate in culture. As little as 6 hours of incubation with [U-^{13}C]glucose or [U-^{13}C]glutamine was sufficient to trace the incorporation of these carbons into biosynthetic pathways via gas chromatography-mass spectrometry (Mullen et al., 2012). A similar experiment could be performed in cultured cardiomyocytes. Cultured neonatal rat cardiomyocytes hypertrophy in response to norepinephrine (Simpson, 1983; Simpson, 1985). However as my work has demonstrated, neonatal rat cardiomyocytes already express PKM2, a hallmark of the Warburg Effect (**Figure 4.2.7**). Therefore, this experiment would need to be performed in isolated adult cardiomyocytes. Stimulation of isolated adult feline cardiomyocytes with TNF-α is sufficient to induce hypertrophy (Yokoyama et al., 1997) and therefore these experiments are feasible. Additionally, the Warburg Effect is highly reliant on glutamine for citrate and acetyl-CoA for the synthesis of fatty acids (Mullen et al., 2012). Future experiments evaluating the Warburg Effect in the hypertrophying heart may also focus on glutamine metabolism.

Assuming that glucose- or glutamine-derived carbons support cardiac hypertrophy, the next step would be to determine the mechanisms driving this effect. For instance, our lab has demonstrated that sustained activation of mTOR leads to uncontrolled protein synthesis

and endoplasmic reticulum stress in the heart (Sen et al., 2013). Based on these findings, we developed mice in which the negative regulator of mTOR, TSC2, can be conditionally deleted. Preliminary evidence suggests that this leads to an induction of PKM2 in the heart. AMPK may also mediate the Warburg Effect. As my lab has shown, AMPK regulated protein turnover through the E3 ligases Atrogin-1 and MuRF1 (Baskin and Taegtmeyer, 2011). Finally, as discussed in Chapter 4, I also predict that c-myc plays an important role in mediating the Warburg Effect in the heart. It will be interesting to determine if driving c-myc expression in the heart is sufficient to induce the Warburg Effect in the heart.

Further work will determine how these findings will be leveraged for the development of novel treatments for human heart failure. At this point, there are certainly more questions than answers. Yet, in the words of Albert Einstein, *"scientific endeavor is a natural whole the parts of which mutually support one another in a way which, to be sure, no one can anticipate"* (Einstein, 2011).

Figure 5.3

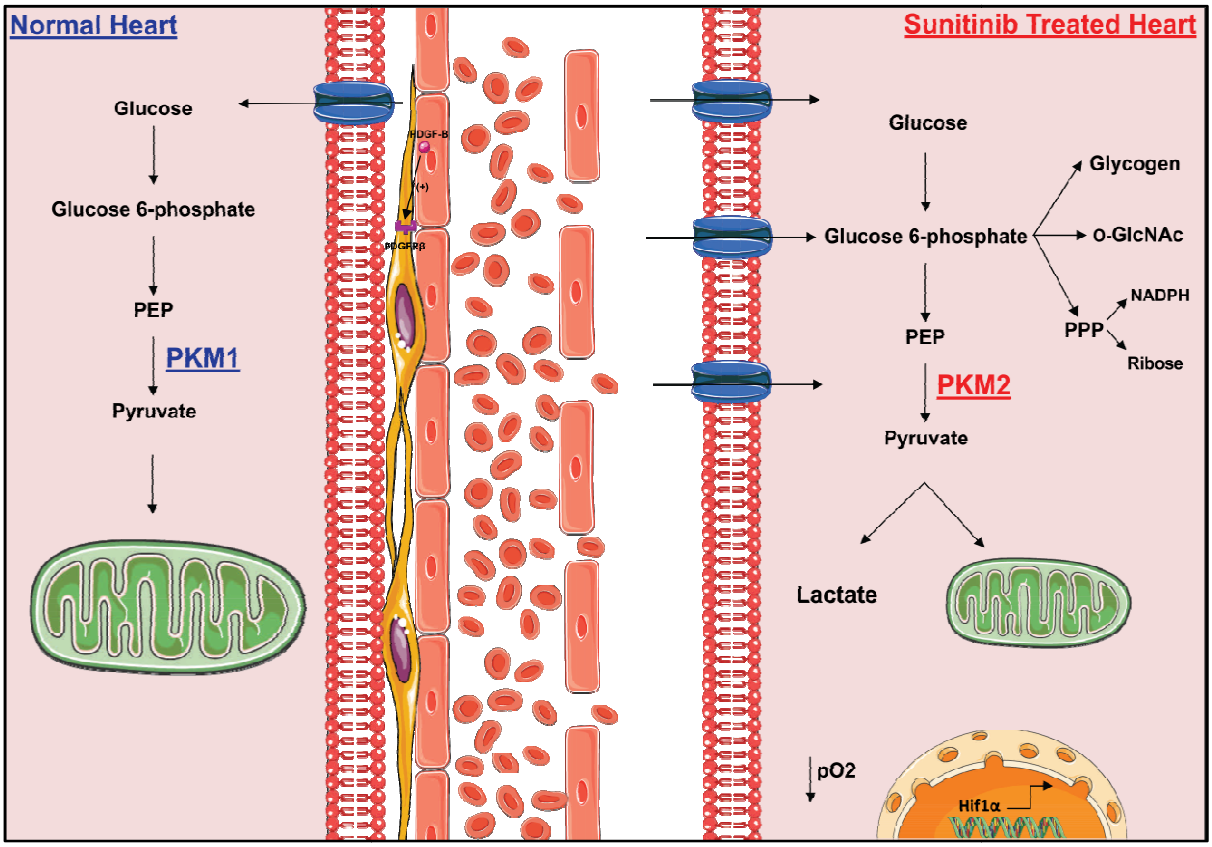

Figure 5.3 Summary of findings.

Sunitinib induces microvascular pericyte loss through inhibition of the platelet derived growth factor receptor beta (PDGFRβ), resulting in microvascular dysfunction and myocardial hypoxia. Subsequent activation of hypoxia inducible factor 1 alpha (Hif1α) leads to induction of the M2 isoform of pyruvate kinase (PKM) and switch to predominant glycolysis and a redirection of glucose-derived carbons into bio. PEP, phosphoenolpyruvate; PPP, pentose phosphate pathway; O-GlcNAc, O-Linked β-N-acetylglucosamine.

REFERENCES

Abràmoff, M.D., Magalhães, P.J., and Ram, S.J. (2004). Image Processing with Imagej. Biophotonics international *11*, 36-43.

Abramsson, A., Kurup, S., Busse, M., Yamada, S., Lindblom, P., Schallmeiner, E., Stenzel, D., Sauvaget, D., Ledin, J., and Ringvall, M. (2007). Defective N-Sulfation of Heparan Sulfate Proteoglycans Limits Pdgf-Bb Binding and Pericyte Recruitment in Vascular Development. Genes Dev *21*, 316-331.

Agostino, N.M., Chinchilli, V.M., Lynch, C.J., Koszyk-Szewczyk, A., Gingrich, R., Sivik, J., and Drabick, J.J. (2011). Effect of the Tyrosine Kinase Inhibitors (Sunitinib, Sorafenib, Dasatinib, and Imatinib) on Blood Glucose Levels in Diabetic and Nondiabetic Patients in General Clinical Practice. J Oncol Pharm Pract *17*, 197-202.

Amato, R.J., Hernandez-Mcclain, J., Saxena, S., and Khan, M. (2008). Lenalidomide Therapy for Metastatic Renal Cell Carcinoma. American journal of clinical oncology *31*, 244-249.

Ammirati, E., Rimoldi, O.E., and Camici, P.G. (2011). Is There Evidence Supporting Coronary Revascularization in Patients with Left Ventricular Systolic Dysfunction? Circulation Journal *75*, 3-10.

Anastasiou, D., Yu, Y., Israelsen, W.J., Jiang, J.-K., Boxer, M.B., Hong, B.S., Tempel, W., Dimov, S., Shen, M., and Jha, A. (2012). Pyruvate Kinase M2 Activators Promote Tetramer Formation and Suppress Tumorigenesis. Nature chemical biology *8*, 839-847.

Andrae, J., Gallini, R., and Betsholtz, C. (2008). Role of Platelet-Derived Growth Factors in Physiology and Medicine. Genes Dev *22*, 1276-1312.

Armulik, A., Abramsson, A., and Betsholtz, C. (2005). Endothelial/Pericyte Interactions. Circulation Research *97*, 512-523.

Armulik, A., Genove, G., and Betsholtz, C. (2011). Pericytes: Developmental, Physiological, and Pathological Perspectives, Problems, and Promises. Dev Cell *21*, 193-215.

Barese, C.N., Krouse, A.E., Metzger, M.E., King, C.A., Traversari, C., Marini, F.C., Donahue, R.E., and Dunbar, C.E. (2012). Thymidine Kinase Suicide Gene-Mediated Ganciclovir Ablation of Autologous Gene-Modified Rhesus Hematopoiesis. Molecular Therapy *20*, 1932-1943.

Barger, P.M., and Kelly, D.P. (1999). Fatty Acid Utilization in the Hypertrophied and Failing Heart: Molecular Regulatory Mechanisms. The American journal of the medical sciences *318*, 36.

Bartlett, J.B., Dredge, K., and Dalgleish, A.G. (2004). The Evolution of Thalidomide and Its Imid Derivatives as Anticancer Agents. Nature Reviews Cancer *4*, 314-322.

Baskin, K.K., and Taegtmeyer, H. (2011). Amp-Activated Protein Kinase Regulates E3 Ligases in Rodent Heart. Circulation Research *109*, 1153-1161.

Bauters, C., Moalic, J., Bercovici, J., Mouas, C., Emanoil-Ravier, R., Schiaffino, S., and Swynghedauw, B. (1988). Coronary Flow as a Determinant of C-Myc and C-Fos Proto-Oncogene Expression in an Isolated Adult Rat Heart. Journal of Molecular and Cellular Cardiology *20*, 97-101.

Behl, Y., Krothapalli, P., Desta, T., Dipiazza, A., Roy, S., and Graves, D.T. (2008). Diabetes-Enhanced Tumor Necrosis Factor-Alpha Production Promotes Apoptosis and the Loss of Retinal Microvascular Cells in Type 1 and Type 2 Models of Diabetic Retinopathy. Am J Pathol *172*, 1411-1418.

Bentzen, L., Keiding, S., Horsman, M.R., Grönroos, T., Hansen, S.B., and Overgaard, J. (2002). Assessment of Hypoxia in Experimental Mice Tumours by [18 F] Fluoromisonidazole Pet and Po 2 Electrode Measurements. Acta oncologica *41*, 304-312.

Bergmeyer, H.-U. (2012). Methods of Enzymatic Analysis. (Elsevier).

Bergsten, E., Uutela, M., Li, X., Pietras, K., Ostman, A., Heldin, C.H., Alitalo, K., and Eriksson, U. (2001). Pdgf-D Is a Specific, Protease-Activated Ligand for the Pdgf Beta-Receptor. Nat Cell Biol *3*, 512-516.

Bertrand, L., Ginion, A., Beauloye, C., Hebert, A.D., Guigas, B., Hue, L., and Vanoverschelde, J.-L. (2006). Ampk Activation Restores the Stimulation of Glucose Uptake in an in Vitro Model of Insulin-Resistant Cardiomyocytes Via the Activation of Protein Kinase B. American Journal of Physiology-Heart and Circulatory Physiology *291*, H239-H250.

Billemont, B., Medioni, J., Taillade, L., Helley, D., Meric, J.B., Rixe, O., and Oudard, S. (2008). Blood Glucose Levels in Patients with Metastatic Renal Cell Carcinoma Treated with Sunitinib. Br J Cancer *99*, 1380-1382.

Biosystems, A. (2008). Guide to Performing Relative Quantification of Gene Expression Using Real-Time Quantitative Pcr.

Bjarnegard, M., Enge, M., Norlin, J., Gustafsdottir, S., Fredriksson, S., Abramsson, A., Takemoto, M., Gustafsson, E., Fassler, R., and Betsholtz, C. (2004). Endothelium-Specific Ablation of Pdgfb Leads to Pericyte Loss and Glomerular, Cardiac and Placental Abnormalities. Development *131*, 1847-1857.

Bono, P., Rautiola, J., Utriainen, T., and Joensuu, H. (2011). Hypertension as Predictor of Sunitinib Treatment Outcome in Metastatic Renal Cell Carcinoma. Acta oncologica *50*, 569-573.

Bøtker, H.E., Goodwin, G.W., Holden, J.E., Doenst, T., Gjedde, A., and Taegtmeyer, H. (1999). Myocardial Glucose Uptake Measured with Fluorodeoxyglucose: A Proposed Method to Account for Variable Lumped Constants. Journal of nuclear medicine: official publication, Society of Nuclear Medicine *40*, 1186-1196.

Bray, G.A. (1960). A Simple Efficient Liquid Scintillator for Counting Aqueous Solutions in a Liquid Scintillation Counter. Anal Biochem *1*, 279-285.

Breccia, M., Muscaritoli, M., and Alimena, G. (2005). Reduction of Glycosylated Hemoglobin with Stable Insulin Levels in a Diabetic Patient with Chronic Myeloid Leukemia Responsive to Imatinib. Haematologica *90 Suppl*, Ecr21.

Breccia, M., Muscaritoli, M., Aversa, Z., Mandelli, F., and Alimena, G. (2004). Imatinib Mesylate May Improve Fasting Blood Glucose in Diabetic Ph+ Chronic Myelogenous Leukemia Patients Responsive to Treatment. J Clin Oncol *22*, 4653-4655.

Buerger, A., Rozhitskaya, O., Sherwood, M.C., Dorfman, A.L., Bisping, E., Abel, E.D., Pu, W.T., Izumo, S., and Jay, P.Y. (2006). Dilated Cardiomyopathy Resulting from High-Level Myocardial Expression of Cre-Recombinase. Journal of cardiac failure *12*, 392-398.

Cardiff, R.D., Miller, C.H., and Munn, R.J. (2014). Manual Hematoxylin and Eosin Staining of Mouse Tissue Sections. Cold Spring Harb Protoc *2014*, 655-658.

Cardinale, D., Sandri, M.T., Colombo, A., Colombo, N., Boeri, M., Lamantia, G., Civelli, M., Peccatori, F., Martinelli, G., and Fiorentini, C. (2004). Prognostic Value of Troponin I in Cardiac Risk Stratification of Cancer Patients Undergoing High-Dose Chemotherapy. Circulation *109*, 2749-2754.

Chang, H., Huylebroeck, D., Verschueren, K., Guo, Q., Matzuk, M.M., and Zwijsen, A. (1999). Smad5 Knockout Mice Die at Mid-Gestation Due to Multiple Embryonic and Extraembryonic Defects. Development *126*, 1631-1642.

Cheng, H., and Force, T. (2010). Molecular Mechanisms of Cardiovascular Toxicity of Targeted Cancer Therapeutics. Circulation Research *106*, 21-34.

Chicco, A.J., Mccune, S.A., Rees, M.L., Gardner, R.T., Moore, R.L., and Sparagna, G.C. (2007). Fenofibrate Exacerbates Aberrant Cardiolipin Profile and Mitochondrial Dysfunction in the Failing Shhf Rat Heart. Journal of Molecular and Cellular Cardiology *42*, S63-S64.

Chilian, W.M., Eastham, C.L., and Marcus, M.L. (1986). Microvascular Distribution of Coronary Vascular Resistance in Beating Left Ventricle. Am J Physiol *251*, H779-788.

Chintalgattu, V., Ai, D., Langley, R.R., Zhang, J., Bankson, J.A., Shih, T.L., Reddy, A.K., Coombes, K.R., Daher, I.N., Pati, S., Patel, S.S., Pocius, J.S., Taffet, G.E., Buja, L.M., Entman, M.L., and Khakoo, A.Y. (2010). Cardiomyocyte Pdgfr-Beta Signaling Is an Essential Component of the Mouse Cardiac Response to Load-Induced Stress. J Clin Invest *120*, 472-484.

Chintalgattu, V., Rees, M.L., Culver, J.C., Goel, A., Jiffar, T., Zhang, J., Dunner, K., Pati, S., Bankson, J.A., and Pasqualini, R. (2013). Coronary Microvascular Pericytes Are the Cellular Target of Sunitinib Malate–Induced Cardiotoxicity. Science translational medicine *5*, 187ra169-187ra169.

Choueiri, T.K., Dreicer, R., Rini, B.I., Elson, P., Garcia, J.A., Thakkar, S.G., Baz, R.C., Mekhail, T.M., Jinks, H.A., and Bukowski, R.M. (2006). Phase Ii Study of Lenalidomide in Patients with Metastatic Renal Cell Carcinoma. Cancer *107*, 2609-2616.

Christofk, H.R., Vander Heiden, M.G., Wu, N., Asara, J.M., and Cantley, L.C. (2008). Pyruvate Kinase M2 Is a Phosphotyrosine-Binding Protein. Nature *452*, 181-186.

Chu, T.F., Rupnick, M.A., Kerkela, R., Dallabrida, S.M., Zurakowski, D., Nguyen, L., Woulfe, K., Pravda, E., Cassiola, F., and Desai, J. (2007). Cardiotoxicity Associated with Tyrosine Kinase Inhibitor Sunitinib. The Lancet *370*, 2011-2019.

Clower, C.V., Chatterjee, D., Wang, Z., Cantley, L.C., Vander Heiden, M.G., and Krainer, A.R. (2010). The Alternative Splicing Repressors Hnrnp A1/A2 and Ptb Influence Pyruvate Kinase Isoform Expression and Cell Metabolism. Proceedings of the National Academy of Sciences *107*, 1894-1899.

Cohen, J., Babiarz, J., Abrams, R., Guo, L., Kameoka, S., Chiao, E., Taunton, J., and Kolaja, K. (2011). Use of Human Stem Cell Derived Cardiomyocytes to Examine Sunitinib Mediated Cardiotoxicity and Electrophysiological Alterations. Toxicology and applied pharmacology *257*, 74-83.

Cooke, V.G., Lebleu, V.S., Keskin, D., Khan, Z., O'connell, J.T., Teng, Y., Duncan, M.B., Xie, L., Maeda, G., and Vong, S. (2012). Pericyte Depletion Results in Hypoxia-Associated Epithelial-to-Mesenchymal Transition and Metastasis Mediated by Met Signaling Pathway. Cancer cell *21*, 66-81.

Cordero-Reyes, A.M., Youker, K., Estep, J.D., Torre-Amione, G., and Nagueh, S.F. (2014). Molecular and Cellular Correlates of Cardiac Function in End-Stage Dcm: A Study Using Speckle Tracking Echocardiography. JACC: Cardiovascular Imaging *7*, 441-452.

Cuevas, P., Gutierrez-Diaz, J.A., Reimers, D., Dujovny, M., Diaz, F.G., and Ausman, J.I. (1984). Pericyte Endothelial Gap Junctions in Human Cerebral Capillaries. Anat Embryol (Berl) *170*, 155-159.

D'amato, R.J., Loughnan, M.S., Flynn, E., and Folkman, J. (1994). Thalidomide Is an Inhibitor of Angiogenesis. Proc Natl Acad Sci U S A *91*, 4082-4085.

David, C.J., Chen, M., Assanah, M., Canoll, P., and Manley, J.L. (2010). Hnrnp Proteins Controlled by C-Myc Deregulate Pyruvate Kinase Mrna Splicing in Cancer. Nature *463*, 364-368.

Defronzo, R.A., Tobin, J.D., and Andres, R. (1979). Glucose Clamp Technique: A Method for Quantifying Insulin Secretion and Resistance. American Journal of Physiology-Gastrointestinal and Liver Physiology *237*, G214-G223.

Demetri, G.D., Van Oosterom, A.T., Garrett, C.R., Blackstein, M.E., Shah, M.H., Verweij, J., Mcarthur, G., Judson, I.R., Heinrich, M.C., and Morgan, J.A. (2006). Efficacy and Safety of Sunitinib in Patients with Advanced Gastrointestinal Stromal Tumour after Failure of Imatinib: A Randomised Controlled Trial. The Lancet *368*, 1329-1338.

Depre, C., Shipley, G.L., Chen, W., Han, Q., Doenst, T., Moore, M.L., Stepkowski, S., Davies, P.J., and Taegtmeyer, H. (1998). Unloaded Heart in Vivo Replicates Fetal Gene Expression of Cardiac Hypertrophy. Nature medicine *4*, 1269-1275.

Deruiter, M.C., Poelmann, R.E., Vanmunsteren, J.C., Mironov, V., Markwald, R.R., and Gittenberger-De Groot, A.C. (1997). Embryonic Endothelial Cells Transdifferentiate into Mesenchymal Cells Expressing Smooth Muscle Actins in Vivo and in Vitro. Circ Res *80*, 444-451.

Di Lorenzo, G., Autorino, R., Bruni, G., Carteni, G., Ricevuto, E., Tudini, M., Ficorella, C., Romano, C., Aieta, M., and Giordano, A. (2009). Cardiovascular Toxicity Following Sunitinib Therapy in Metastatic Renal Cell Carcinoma: A Multicenter Analysis. Annals of oncology *20*, 1535-1542.

Diaz-Flores, L., Gutierrez, R., Madrid, J.F., Varela, H., Valladares, F., Acosta, E., Martin-Vasallo, P., and Diaz-Flores, L., Jr. (2009). Pericytes. Morphofunction, Interactions and Pathology in a Quiescent and Activated Mesenchymal Cell Niche. Histol Histopathol *24*, 909-969.

Doenst, T., Nguyen, T.D., and Abel, E.D. (2013). Cardiac Metabolism in Heart Failure Implications Beyond Atp Production. Circulation Research *113*, 709-724.

Doenst, T., and Taegtmeyer, H. (1998). Profound Underestimation of Glucose Uptake by [18f] 2-Deoxy-2-Fluoroglucose in Reperfused Rat Heart Muscle. Circulation *97*, 2454-2462.

Dolci, A., Dominici, R., Cardinale, D., Sandri, M.T., and Panteghini, M. (2008). Biochemical Markers for Prediction of Chemotherapy-Induced Cardiotoxicity Systematic Review of the Literature and Recommendations for Use. American Journal of Clinical Pathology *130*, 688-695.

Edvardsen, T., and Sarvari, S.I. (2013). What Are the Best Tools for Early Diagnosis of Cancer Treatment–Induced Cardiotoxicity and What Is the Treatment?

Einstein, A. (2011). Out of My Later Years: The Scientist, Philosopher, and Man Portrayed through His Own Words. (Philosophical Library/Open Road).

Epstein, F.H. (2007). Mr in Mouse Models of Cardiac Disease. NMR in Biomedicine *20*, 238-255.

Erez, A., Nagamani, S.C., Shchelochkov, O.A., Premkumar, M.H., Campeau, P.M., Chen, Y., Garg, H.K., Li, L., Mian, A., and Bertin, T.K. (2011). Requirement of Argininosuccinate Lyase for Systemic Nitric Oxide Production. Nature medicine *17*, 1619-1626.

Essop, M.F., Camp, H.S., Choi, C.S., Sharma, S., Fryer, R.M., Reinhart, G.A., Guthrie, P.H., Bentebibel, A., Gu, Z., and Shulman, G.I. (2008). Reduced Heart Size and Increased Myocardial Fuel Substrate Oxidation in Acc2 Mutant Mice. American Journal of Physiology-Heart and Circulatory Physiology *295*, H256-H265.

Ewer, M.S., Vooletich, M.T., Durand, J.-B., Woods, M.L., Davis, J.R., Valero, V., and Lenihan, D.J. (2005). Reversibility of Trastuzumab-Related Cardiotoxicity: New Insights Based on Clinical Course and Response to Medical Treatment. Journal of Clinical Oncology *23*, 7820-7826.

Faivre, S., Demetri, G., Sargent, W., and Raymond, E. (2007). Molecular Basis for Sunitinib Efficacy and Future Clinical Development. Nature Reviews Drug Discovery *6*, 734-745.

Falcon, B.L., Hashizume, H., Koumoutsakos, P., Chou, J., Bready, J.V., Coxon, A., Oliner, J.D., and Mcdonald, D.M. (2009). Contrasting Actions of Selective Inhibitors of Angiopoietin-1 and Angiopoietin-2 on the Normalization of Tumor Blood Vessels. Am J Pathol *175*, 2159-2170.

Feigl, E.O. (1983). Coronary Physiology. Physiol Rev *63*, 1-205.

Feng, M., Whitesall, S., Zhang, Y., Beibel, M., D'alecy, L., and Dipetrillo, K. (2008). Validation of Volume–Pressure Recording Tail-Cuff Blood Pressure Measurements. American journal of hypertension *21*, 1288-1291.

Fernandez-Klett, F., Offenhauser, N., Dirnagl, U., Priller, J., and Lindauer, U. (2010). Pericytes in Capillaries Are Contractile in Vivo, but Arterioles Mediate Functional Hyperemia in the Mouse Brain. Proc Natl Acad Sci U S A *107*, 22290-22295.

Fishman, A.P., Richards, Dickinson W. (1982). Circulation of the Blood, Med and Ideas. (Bethesda, MD: American Physiological Society).

Folkman, J. (1971). Tumor Angiogenesis: Therapeutic Implications. New England Journal of Medicine *285*, 1182-1186.

Folland, E., Parisi, A., Moynihan, P., Jones, D.R., Feldman, C.L., and Tow, D. (1979). Assessment of Left Ventricular Ejection Fraction and Volumes by Real-Time, Two-Dimensional Echocardiography. A Comparison of Cineangiographic and Radionuclide Techniques. Circulation *60*, 760-766.

Force, T., Krause, D.S., and Van Etten, R.A. (2007). Molecular Mechanisms of Cardiotoxicity of Tyrosine Kinase Inhibition. Nature Reviews Cancer *7*, 332-344.

Fotakis, G., and Timbrell, J.A. (2006). In Vitro Cytotoxicity Assays: Comparison of Ldh, Neutral Red, Mtt and Protein Assay in Hepatoma Cell Lines Following Exposure to Cadmium Chloride. Toxicology Letters *160*, 171-177.

French, K.J., Coatney, R.W., Renninger, J.P., Hu, C.X., Gales, T.L., Zhao, S., Storck, L.M., Davis, C.B., Mcsurdy-Freed, J., and Chen, E. (2010). Differences in Effects on Myocardium and Mitochondria by Angiogenic Inhibitors Suggest Separate Mechanisms of Cardiotoxicity. Toxicologic pathology *38*, 691-702.

Gaengel, K., Genové, G., Armulik, A., and Betsholtz, C. (2009). Endothelial-Mural Cell Signaling in Vascular Development and Angiogenesis. Arteriosclerosis, thrombosis, and vascular biology *29*, 630-638.

Gao, X., Wang, H., Yang, J.J., Liu, X., and Liu, Z.-R. (2012). Pyruvate Kinase M2 Regulates Gene Transcription by Acting as a Protein Kinase. Molecular cell *45*, 598-609.

Gee, M.S., Makonnen, S., Al-Kofahi, K., Roysam, B., Payvandi, F., Man, H.-W., Muller, G.W., and Lee, W.M. (2003). Selective Cytokine Inhibitory Drugs with Enhanced Antiangiogenic Activity Control Tumor Growth through Vascular Inhibition. Cancer research *63*, 8073-8078.

Geraldes, P., Hiraoka-Yamamoto, J., Matsumoto, M., Clermont, A., Leitges, M., Marette, A., Aiello, L.P., Kern, T.S., and King, G.L. (2009). Activation of Pkc-Delta and Shp-1 by Hyperglycemia Causes Vascular Cell Apoptosis and Diabetic Retinopathy. Nat Med *15*, 1298-1306.

Go, A.S., Mozaffarian, D., Roger, V.L., Benjamin, E.J., Berry, J.D., Borden, W.B., Bravata, D.M., Dai, S., Ford, E.S., Fox, C.S., Franco, S., Fullerton, H.J., Gillespie, C., Hailpern, S.M., Heit, J.A., Howard, V.J., Huffman, M.D., Kissela, B.M., Kittner, S.J., Lackland, D.T., Lichtman, J.H., Lisabeth, L.D., Magid, D., Marcus, G.M., Marelli, A., Matchar, D.B., Mcguire, D.K., Mohler, E.R., Moy, C.S., Mussolino, M.E., Nichol, G., Paynter, N.P., Schreiner, P.J., Sorlie,

P.D., Stein, J., Turan, T.N., Virani, S.S., Wong, N.D., Woo, D., and Turner, M.B. (2013). Heart Disease and Stroke Statistics--2013 Update: A Report from the American Heart Association. Circulation *127*, e6-e245.

Gómez-Gaviro, M.V., Lovell-Badge, R., Fernández-Avilés, F., and Lara-Pezzi, E. (2012). The Vascular Stem Cell Niche. Journal of cardiovascular translational research *5*, 618-630.

Gomez, D.R., Missett, B.T., Wara, W.M., Lamborn, K.R., Prados, M.D., Chang, S., Berger, M.S., and Haas-Kogan, D.A. (2005). High Failure Rate in Spinal Ependymomas with Long-Term Follow-Up. Neuro Oncol *7*, 254-259.

Goodwin, G.W., Taylor, C.S., and Taegtmeyer, H. (1998). Regulation of Energy Metabolism of the Heart During Acute Increase in Heart Work. Journal of Biological Chemistry *273*, 29530-29539.

Gordon, J., Trebble, T., Ellis, R., Duncan, H., Johns, T., and Goggin, P. (2005). Thalidomide in the Treatment of Cancer Cachexia: A Randomised Placebo Controlled Trial. Gut *54*, 540-545.

Gorlin, R. (1976). Coronary Artery Disease. (Saunders).

Gould, K.L., Johnson, N.P., Bateman, T.M., Beanlands, R.S., Bengel, F.M., Bober, R., Camici, P.G., Cerqueira, M.D., Chow, B.J., Di Carli, M.F., Dorbala, S., Gewirtz, H., Gropler, R.J., Kaufmann, P.A., Knaapen, P., Knuuti, J., Merhige, M.E., Rentrop, K.P., Ruddy, T.D., Schelbert, H.R., Schindler, T.H., Schwaiger, M., Sdringola, S., Vitarello, J., Williams, K.A., Sr., Gordon, D., Dilsizian, V., and Narula, J. (2013). Anatomic Versus Physiologic Assessment of Coronary Artery Disease. Role of Coronary Flow Reserve, Fractional Flow Reserve, and Positron Emission Tomography Imaging in Revascularization Decision-Making. J Am Coll Cardiol *62*, 1639-1653.

Hagerkvist, R., Jansson, L., and Welsh, N. (2008). Imatinib Mesylate Improves Insulin Sensitivity and Glucose Disposal Rates in Rats Fed a High-Fat Diet. Clin Sci (Lond) *114*, 65-71.

Hahn, V.S., Lenihan, D.J., and Ky, B. (2014). Cancer Therapy–Induced Cardiotoxicity: Basic Mechanisms and Potential Cardioprotective Therapies. Journal of the American Heart Association *3*, e000665.

Hamzah, J., Jugold, M., Kiessling, F., Rigby, P., Manzur, M., Marti, H.H., Rabie, T., Kaden, S., Gröne, H.-J., and Hämmerling, G.J. (2008). Vascular Normalization in Rgs5-Deficient Tumours Promotes Immune Destruction. Nature *453*, 410-414.

Han, M.S., Chung, K.W., Cheon, H.G., Rhee, S.D., Yoon, C.H., Lee, M.K., Kim, K.W., and Lee, M.S. (2009). Imatinib Mesylate Reduces Endoplasmic Reticulum Stress and Induces Remission of Diabetes in Db/Db Mice. Diabetes *58*, 329-336.

Hariharan, R., Bray, M., Ganim, R., Doenst, T., Goodwin, G.W., and Taegtmeyer, H. (1995). Fundamental Limitations of [18f] 2-Deoxy-2-Fluoro-D-Glucose for Assessing Myocardial Glucose Uptake. Circulation *91*, 2435-2444.

Hartley, C.J., Reddy, A.K., Madala, S., Entman, M.L., Michael, L.H., and Taffet, G.E. (2011). Doppler Velocity Measurements from Large and Small Arteries of Mice. American Journal of Physiology-Heart and Circulatory Physiology *301*, H269-H278.

Hartley, C.J., Reddy, A.K., Madala, S., Michael, L.H., Entman, M.L., and Taffet, G.E. (2008). Doppler Estimation of Reduced Coronary Flow Reserve in Mice with Pressure Overload Cardiac Hypertrophy. Ultrasound in medicine & biology *34*, 892-901.

Hasinoff, B., Schnabl, K., Marusak, R., Patel, D., and Huebner, E. (2003). Dexrazoxane (Icrf-187) Protects Cardiac Myocytes against Doxorubicin by Preventing Damage to Mitochondria. Cardiovascular Toxicology *3*, 89-99.

Hasinoff, B.B., Patel, D., and O'hara, K.A. (2008). Mechanisms of Myocyte Cytotoxicity Induced by the Multiple Receptor Tyrosine Kinase Inhibitor Sunitinib. Molecular pharmacology *74*, 1722-1728.

Haslett, P.A., Corral, L.G., Albert, M., and Kaplan, G. (1998). Thalidomide Costimulates Primary Human T Lymphocytes, Preferentially Inducing Proliferation, Cytokine Production, and Cytotoxic Responses in the Cd8+ Subset. J Exp Med *187*, 1885-1892.

Hawthorne, F. (2010). Inside the Fda: The Business and Politics Behind the Drugs We Take and the Food We Eat. (Wiley).

Hellström, M., Gerhardt, H., Kalén, M., Li, X., Eriksson, U., Wolburg, H., and Betsholtz, C. (2001). Lack of Pericytes Leads to Endothelial Hyperplasia and Abnormal Vascular Morphogenesis. The Journal of cell biology *153*, 543-554.

Higuchi, K., Hashizume, H., Aizawa, Y., and Ushiki, T. (2000). Scanning Electron Microscopic Studies of the Vascular Smooth Muscle Cells and Pericytes in the Rat Heart. Arch Histol Cytol *63*, 115-126.

Hirschi, K.K., Burt, J.M., Hirschi, K.D., and Dai, C. (2003). Gap Junction Communication Mediates Transforming Growth Factor-B Activation and Endothelial-Induced Mural Cell Differentiation. Circulation Research *93*, 429-437.

Hodgkiss, R.J. (1998). Use of 2-Nitroimidazoles as Bioreductive Markers for Tumour Hypoxia. Anti-cancer drug design *13*, 687-702.

Hoshijima, M., and Chien, K.R. (2002). Mixed Signals in Heart Failure: Cancer Rules. The Journal of Clinical Investigation *109*, 849-855.

Institute, N.C. (2009). Common Terminology Criteria for Adverse Events V4.0 H.a.H. Services, ed.

Israelsen, W.J., Dayton, T.L., Davidson, S.M., Fiske, B.P., Hosios, A.M., Bellinger, G., Li, J., Yu, Y., Sasaki, M., and Horner, J.W. (2013). Pkm2 Isoform-Specific Deletion Reveals a Differential Requirement for Pyruvate Kinase in Tumor Cells. Cell *155*, 397-409.

Ito, T., Ando, H., Suzuki, T., Ogura, T., Hotta, K., Imamura, Y., Yamaguchi, Y., and Handa, H. (2010). Identification of a Primary Target of Thalidomide Teratogenicity. Science *327*, 1345-1350.

Jacoby, J.J., Kalinowski, A., Liu, M.-G., Zhang, S.S.-M., Gao, Q., Chai, G.-X., Ji, L., Iwamoto, Y., Li, E., and Schneider, M. (2003). Cardiomyocyte-Restricted Knockout of Stat3 Results in Higher Sensitivity to Inflammation, Cardiac Fibrosis, and Heart Failure with Advanced Age. Proceedings of the National Academy of Sciences *100*, 12929-12934.

Jain, R.K. (2005). Normalization of Tumor Vasculature: An Emerging Concept in Antiangiogenic Therapy. Science *307*, 58-62.

James, D.E., Strube, M., and Mueckler, M. (1989). Molecular Cloning and Characterization of an Insulin-Regulatable Glucose Transporter. Nature *338*, 83-87.

Jeansson, M., Gawlik, A., Anderson, G., Li, C., Kerjaschki, D., Henkelman, M., and Quaggin, S.E. (2011). Angiopoietin-1 Is Essential in Mouse Vasculature During Development and in Response to Injury. J Clin Invest *121*, 2278-2289.

Jensen, R.V., Zachara, N.E., Nielsen, P.H., Kimose, H.H., Kristiansen, S.B., and Bøtker, H.E. (2012). Impact of O-Glcnac on Cardioprotection by Remote Ischaemic Preconditioning in Non-Diabetic and Diabetic Patients. Cardiovasc Res, cvs337.

Jones, L.W., and Alfano, C.M. (2013). Exercise-Oncology Research: Past, Present, and Future. Acta oncologica *52*, 195-215.

Jones, N., Iljin, K., Dumont, D.J., and Alitalo, K. (2001). Tie Receptors: New Modulators of Angiogenic and Lymphangiogenic Responses. Nature Reviews Molecular Cell Biology *2*, 257-267.

Joussen, A.M., Doehmen, S., Le, M.L., Koizumi, K., Radetzky, S., Krohne, T.U., Poulaki, V., Semkova, I., and Kociok, N. (2009). Tnf-Alpha Mediated Apoptosis Plays an Important Role in the Development of Early Diabetic Retinopathy and Long-Term Histopathological Alterations. Mol Vis *15*, 1418-1428.

Kanatsuka, H., Lamping, K.G., Eastham, C.L., Dellsperger, K.C., and Marcus, M.L. (1989). Comparison of the Effects of Increased Myocardial Oxygen Consumption and Adenosine on the Coronary Microvascular Resistance. Circ Res *65*, 1296-1305.

Karaman, M.W., Herrgard, S., Treiber, D.K., Gallant, P., Atteridge, C.E., Campbell, B.T., Chan, K.W., Ciceri, P., Davis, M.I., and Edeen, P.T. (2008). A Quantitative Analysis of Kinase Inhibitor Selectivity. Nature biotechnology *26*, 127-132.

Katz, A.M. (2010). Physiology of the Heart. (Wolters Kluwer Health/Lippincott Williams & Wilkins Health).

Kerkela, R., Woulfe, K.C., Durand, J.B., Vagnozzi, R., Kramer, D., Chu, T.F., Beahm, C., Chen, M.H., and Force, T. (2009). Sunitinib-Induced Cardiotoxicity Is Mediated by Off-Target Inhibition of Amp-Activated Protein Kinase. Clinical and translational science *2*, 15-25.

Khakoo, A.Y., Liu, P.P., Force, T., Lopez-Berestein, G., Jones, L.W., Schneider, J., and Hill, J. (2011). Cardiotoxicity Due to Cancer Therapy. Texas Heart Institute Journal *38*, 253.

Klaassen, I., Hughes, J.M., Vogels, I.M., Schalkwijk, C.G., Van Noorden, C.J., and Schlingemann, R.O. (2009). Altered Expression of Genes Related to Blood–Retina Barrier Disruption in Streptozotocin-Induced Diabetes. Experimental eye research *89*, 4-15.

Kloner, R.A., Przyklenk, K., and Patel, B. (1989). Altered Myocardial States: The Stunned and Hibernating Myocardium. The American journal of medicine *86*, 14-22.

Knapton, A., Herman, E., Todd, J., Estis, J., and Zhang, J. (2013). An Exploration of Sunitinb-Induced Cardiotoxicity in Male Sprague-Dawley Rats. The FASEB Journal *27*, 652.651.

Kolwicz, S.C., Olson, D.P., Marney, L.C., Garcia-Menendez, L., Synovec, R.E., and Tian, R. (2012). Cardiac-Specific Deletion of Acetyl Coa Carboxylase 2 Prevents Metabolic Remodeling During Pressure-Overload Hypertrophy. Circulation Research *111*, 728-738.

Korashy, H.M., Al-Suwayeh, H.A., Maayah, Z.H., Ansari, M.A., Ahmad, S.F., and Bakheet, S.A. (2014). Mitogen-Activated Protein Kinases Pathways Mediate the Sunitinib-Induced Hypertrophy in Rat Cardiomyocyte H9c2 Cells. Cardiovascular Toxicology, 1-11.

Korvald, C., Elvenes, O.P., and Myrmel, T. (2000). Myocardial Substrate Metabolism Influences Left Ventricular Energetics in Vivo. American Journal of Physiology-Heart and Circulatory Physiology *278*, H1345-H1351.

Krogh, A. (1919a). The Number and Distribution of Capillaries in Muscles with Calculations of the Oxygen Pressure Head Necessary for Supplying the Tissue. J Physiol *52*, 409-415.

Krogh, A. (1919b). The Supply of Oxygen to the Tissues and the Regulation of the Capillary Circulation. J Physiol *52*, 457-474.

Kuma, A., Hatano, M., Matsui, M., Yamamoto, A., Nakaya, H., Yoshimori, T., Ohsumi, Y., Tokuhisa, T., and Mizushima, N. (2004). The Role of Autophagy During the Early Neonatal Starvation Period. Nature *432*, 1032-1036.

Kumar, R., Crouthamel, M., Rominger, D., Gontarek, R., Tummino, P., Levin, R., and King, A. (2009). Myelosuppression and Kinase Selectivity of Multikinase Angiogenesis Inhibitors. British journal of cancer *101*, 1717-1723.

Kuo, L., Chilian, W.M., and Davis, M.J. (1991). Interaction of Pressure- and Flow-Induced Responses in Porcine Coronary Resistance Vessels. Am J Physiol *261*, H1706-1715.

Laderoute, K., Calaoagan, J.M., Madrid, P.B., Klon, A.E., and Ehrlich, P.J. (2010). Su11248 (Sunitinib) Directly Inhibits the Activity of Mammalian 5'-Amp-Activated Protein Kinase (Ampk). Cancer biology & therapy *10*, 68-76.

Lan, Y., Liu, B., Yao, H., Li, F., Weng, T., Yang, G., Li, W., Cheng, X., Mao, N., and Yang, X. (2007). Essential Role of Endothelial Smad4 in Vascular Remodeling and Integrity. Molecular and cellular biology *27*, 7683-7692.

Larochelle, W.J., Jeffers, M., Mcdonald, W.F., Chillakuru, R.A., Giese, N.A., Lokker, N.A., Sullivan, C., Boldog, F.L., Yang, M., Vernet, C., Burgess, C.E., Fernandes, E., Deegler, L.L., Rittman, B., Shimkets, J., Shimkets, R.A., Rothberg, J.M., and Lichenstein, H.S. (2001). Pdgf-D, a New Protease-Activated Growth Factor. Nat Cell Biol *3*, 517-521.

Lash, L.H., and Jones, D.P. (2013). Mitochondrial Dysfunction: Methods in Toxicology. (Elsevier Science).

Lebrin, F., Srun, S., Raymond, K., Martin, S., Van Den Brink, S., Freitas, C., Bréant, C., Mathivet, T., Larrivée, B., and Thomas, J.-L. (2010). Thalidomide Stimulates Vessel Maturation and Reduces Epistaxis in Individuals with Hereditary Hemorrhagic Telangiectasia. Nature medicine *16*, 420-428.

Lee, J., Kim, H.K., Han, Y.M., and Kim, J. (2008). Pyruvate Kinase Isozyme Type M2 (Pkm2) Interacts and Cooperates with Oct-4 in Regulating Transcription. Int J Biochem Cell Biol *40*, 1043-1054.

Leveen, P., Pekny, M., Gebre-Medhin, S., Swolin, B., Larsson, E., and Betsholtz, C. (1994). Mice Deficient for Pdgf B Show Renal, Cardiovascular, and Hematological Abnormalities. Genes Dev *8*, 1875-1887.

Levy, D., Kenchaiah, S., Larson, M.G., Benjamin, E.J., Kupka, M.J., Ho, K.K.L., Murabito, J.M., and Vasan, R.S. (2002). Long-Term Trends in the Incidence of and Survival with Heart Failure. New England Journal of Medicine *347*, 1397-1402.

Li, D.Y., Sorensen, L.K., Brooke, B.S., Urness, L.D., Davis, E.C., Taylor, D.G., Boak, B.B., and Wendel, D.P. (1999). Defective Angiogenesis in Mice Lacking Endoglin. Science *284*, 1534-1537.

Li, X., Ponten, A., Aase, K., Karlsson, L., Abramsson, A., Uutela, M., Backstrom, G., Hellstrom, M., Bostrom, H., Li, H., Soriano, P., Betsholtz, C., Heldin, C.H., Alitalo, K., Ostman, A., and Eriksson, U. (2000). Pdgf-C Is a New Protease-Activated Ligand for the Pdgf Alpha-Receptor. Nat Cell Biol *2*, 302-309.

Liao, R., Jain, M., Cui, L., D'agostino, J., Aiello, F., Luptak, I., Ngoy, S., Mortensen, R.M., and Tian, R. (2002). Cardiac-Specific Overexpression of Glut1 Prevents the Development of Heart Failure Attributable to Pressure Overload in Mice. Circulation *106*, 2125-2131.

Lilly, L.S., and School, H.M. (1998). Pathophysiology of Heart Disease: A Collaborative Project of Medical Students and Faculty. (Williams & Wilkins).

Limaye, N., Wouters, V., Uebelhoer, M., Tuominen, M., Wirkkala, R., Mulliken, J.B., Eklund, L., Boon, L.M., and Vikkula, M. (2009). Somatic Mutations in Angiopoietin Receptor Gene Tek Cause Solitary and Multiple Sporadic Venous Malformations. Nature genetics *41*, 118-124.

Lindahl, P., Johansson, B.R., Leveen, P., and Betsholtz, C. (1997). Pericyte Loss and Microaneurysm Formation in Pdgf-B-Deficient Mice. Science *277*, 242-245.

Lindblom, P., Gerhardt, H., Liebner, S., Abramsson, A., Enge, M., Hellström, M., Bäckström, G., Fredriksson, S., Landegren, U., and Nyström, H.C. (2003). Endothelial Pdgf-B Retention Is Required for Proper Investment of Pericytes in the Microvessel Wall. Genes Dev *17*, 1835-1840.

Lipshultz, S.E., Lipsitz, S.R., Sallan, S.E., Simbre, V.C., Shaikh, S.L., Mone, S.M., Gelber, R.D., and Colan, S.D. (2002). Long-Term Enalapril Therapy for Left Ventricular Dysfunction in Doxorubicin-Treated Survivors of Childhood Cancer. Journal of Clinical Oncology *20*, 4517-4522.

Little, R.F., Wyvill, K.M., Pluda, J.M., Welles, L., Marshall, V., Figg, W.D., Newcomb, F.M., Tosato, G., Feigal, E., and Steinberg, S.M. (2000). Activity of Thalidomide in Aids-Related Kaposi's Sarcoma. Journal of Clinical Oncology *18*, 2593-2602.

Liu, J., Wu, N., Ma, L., Liu, M., Liu, G., Zhang, Y., and Lin, X. (2014). Oleanolic Acid Suppresses Aerobic Glycolysis in Cancer Cells by Switching Pyruvate Kinase Type M Isoforms. PloS one *9*, e91606.

Louvet, C., Szot, G.L., Lang, J., Lee, M.R., Martinier, N., Bollag, G., Zhu, S., Weiss, A., and Bluestone, J.A. (2008). Tyrosine Kinase Inhibitors Reverse Type 1 Diabetes in Nonobese Diabetic Mice. Proc Natl Acad Sci U S A *105*, 18895-18900.

Lu, L., Payvandi, F., Wu, L., Zhang, L.-H., Hariri, R.J., Man, H.-W., Chen, R.S., Muller, G.W., Hughes, C.C., and Stirling, D.I. (2009). The Anti-Cancer Drug Lenalidomide Inhibits Angiogenesis and Metastasis Via Multiple Inhibitory Effects on Endothelial Cell Function in Normoxic and Hypoxic Conditions. Microvasc Res *77*, 78-86.

Luo, W., Hu, H., Chang, R., Zhong, J., Knabel, M., O'meally, R., Cole, R.N., Pandey, A., and Semenza, G.L. (2011). Pyruvate Kinase M2 Is a Phd3-Stimulated Coactivator for Hypoxia-Inducible Factor 1. Cell *145*, 732-744.

Luo, W., and Semenza, G.L. (2012). Emerging Roles of Pkm2 in Cell Metabolism and Cancer Progression. Trends in Endocrinology & Metabolism *23*, 560-566.

Luptak, I., Yan, J., Cui, L., Jain, M., Liao, R., and Tian, R. (2007). Long-Term Effects of Increased Glucose Entry on Mouse Hearts During Normal Aging and Ischemic Stress. Circulation *116*, 901-909.

Mackey, J., Clemons, M., Côté, M., Delgado, D., Dent, S., Paterson, A., Provencher, L., Sawyer, M., and Verma, S. (2008). Cardiac Management During Adjuvant Trastuzumab Therapy: Recommendations of the Canadian Trastuzumab Working Group. Current Oncology *15*, 24.

Malkoff, J. (2005). Non-Invasive Blood Pressure, Rat and Mouse. In Animal Lab News (https://www.kentscientific.com).

Martin, S., Slot, J.W., and James, D.E. (1999). Glut4 Trafficking in Insulin-Sensitive Cells. Cell biochemistry and biophysics *30*, 89-113.

Mccarty, M.F., Somcio, R.J., Stoeltzing, O., Wey, J., Fan, F., Liu, W., Bucana, C., and Ellis, L.M. (2007). Overexpression of Pdgf-Bb Decreases Colorectal and Pancreatic Cancer Growth by Increasing Tumor Pericyte Content. J Clin Invest *117*, 2114-2122.

Mokhtari, D., and Welsh, N. (2010). Potential Utility of Small Tyrosine Kinase Inhibitors in the Treatment of Diabetes. Clinical Science *118*, 241-247.

Motzer, R.J., Hutson, T.E., Tomczak, P., Michaelson, M.D., Bukowski, R.M., Rixe, O., Oudard, S., Negrier, S., Szczylik, C., and Kim, S.T. (2007). Sunitinib Versus Interferon Alfa in Metastatic Renal-Cell Carcinoma. New England Journal of Medicine *356*, 115-124.

Mullen, A.R., Wheaton, W.W., Jin, E.S., Chen, P.-H., Sullivan, L.B., Cheng, T., Yang, Y., Linehan, W.M., Chandel, N.S., and Deberardinis, R.J. (2012). Reductive Carboxylation Supports Growth in Tumour Cells with Defective Mitochondria. Nature *481*, 385-388.

Muller, J.M., Davis, M.J., and Chilian, W.M. (1996). Integrated Regulation of Pressure and Flow in the Coronary Microcirculation. Cardiovasc Res *32*, 668-678.

Mulvagh, S.L., Roberts, R., and Schneider, M.D. (1988). Cellular Oncogenes in Cardiovascular Disease. Journal of Molecular and Cellular Cardiology *20*, 657-662.

Nees, S., Weiss, D.R., and Juchem, G. (2013). Focus on Cardiac Pericytes. Pflugers Arch *465*, 779-787.

Nees, S., Weiss, D.R., Senftl, A., Knott, M., Förch, S., Schnurr, M., Weyrich, P., and Juchem, G. (2012). Isolation, Bulk Cultivation, and Characterization of Coronary Microvascular Pericytes: The Second Most Frequent Myocardial Cell Type in Vitro. American Journal of Physiology-Heart and Circulatory Physiology *302*, H69-H84.

Nehls, V., and Drenckhahn, D. (1993). The Versatility of Microvascular Pericytes: From Mesenchyme to Smooth Muscle? Histochemistry *99*, 1-12.

Ngoh, G.A., Facundo, H.T., Zafir, A., and Jones, S.P. (2010). O-Glcnac Signaling in the Cardiovascular System. Circulation Research *107*, 171-185.

Nguyen, V., Mossberg, K.A., Tewson, T.J., Wong, W., Rowe, R.W., Coleman, G.M., and Taegtmeyer, H. (1990). Temporal Analysis of Myocardial Glucose Metabolism by 2-[18f] Fluoro-2-Deoxy-D-Glucose. American Journal of Physiology-Heart and Circulatory Physiology *259*, H1022-H1031.

O'connell, T.D., Rodrigo, M.C., and Simpson, P.C. (2007). Isolation and Culture of Adult Mouse Cardiac Myocytes. Methods Mol Biol *357*, 271-296.

Oakes, N.D., Kennedy, C.J., Jenkins, A.B., Laybutt, D.R., Chisholm, D.J., and Kraegen, E.W. (1994). A New Antidiabetic Agent, Brl 49653, Reduces Lipid Availability and Improves Insulin Action and Glucoregulation in the Rat. Diabetes *43*, 1203-1210.

Okere, I.C., Young, M.E., Mcelfresh, T.A., Chess, D.J., Sharov, V.G., Sabbah, H.N., Hoit, B.D., Ernsberger, P., Chandler, M.P., and Stanley, W.C. (2006). Low Carbohydrate/High-Fat Diet Attenuates Cardiac Hypertrophy, Remodeling, and Altered Gene Expression in Hypertension. Hypertension *48*, 1116-1123.

Opie, L.H. (2004). Heart Physiology: From Cell to Circulation. (Lippincott Williams & Wilkins).

Ozerdem, U., Grako, K.A., Dahlin-Huppe, K., Monosov, E., and Stallcup, W.B. (2001). Ng2 Proteoglycan Is Expressed Exclusively by Mural Cells During Vascular Morphogenesis. Developmental Dynamics *222*, 218-227.

Pal, S.K., Williams, S., Josephson, D.Y., Carmichael, C., Vogelzang, N.J., and Quinn, D.I. (2012). Novel Therapies for Metastatic Renal Cell Carcinoma: Efforts to Expand Beyond the Vegf/Mtor Signaling Paradigm. Mol Cancer Ther *11*, 526-537.

Parnell, K.M., Foulks, J.M., Nix, R.N., Clifford, A., Bullough, J., Luo, B., Senina, A., Vollmer, D., Liu, J., and Mccarthy, V. (2013). Pharmacologic Activation of Pkm2 Slows Lung Tumor Xenograft Growth. Mol Cancer Ther *12*, 1453-1460.

Patan, S. (1998). Tie1 and Tie2 Receptor Tyrosine Kinases Inversely Regulate Embryonic Angiogenesis by the Mechanism of Intussusceptive Microvascular Growth. Microvasc Res *56*, 1-21.

Poche, R.A., Larina, I.V., Scott, M.L., Saik, J.E., West, J.L., and Dickinson, M.E. (2009). The Flk1-Myr::Mcherry Mouse as a Useful Reporter to Characterize Multiple Aspects of Ocular Blood Vessel Development and Disease. Dev Dyn *238*, 2318-2326.

Raines, S.M., Richards, O.C., Schneider, L.R., Schueler, K.L., Rabaglia, M.E., Oler, A.T., Stapleton, D.S., Genové, G., Dawson, J.A., and Betsholtz, C. (2011). Loss of Pdgf-B Activity Increases Hepatic Vascular Permeability and Enhances Insulin Sensitivity. American Journal of Physiology-Endocrinology and Metabolism *301*, E517-E526.

Rajabi, M., Kassiotis, C., Razeghi, P., and Taegtmeyer, H. (2007). Return to the Fetal Gene Program Protects the Stressed Heart: A Strong Hypothesis. Heart failure reviews *12*, 331-343.

Rajendran, J.G., Mankoff, D.A., O'sullivan, F., Peterson, L.M., Schwartz, D.L., Conrad, E.U., Spence, A.M., Muzi, M., Farwell, D.G., and Krohn, K.A. (2004). Hypoxia and Glucose Metabolism in Malignant Tumors Evaluation by [18f] Fluoromisonidazole and [18f] Fluorodeoxyglucose Positron Emission Tomography Imaging. Clinical Cancer Research *10*, 2245-2252.

Ramani, R., Vela, D., Segura, A., Mcnamara, D., Lemster, B., Samarendra, V., Kormos, R., Toyoda, Y., Bermudez, C., and Frazier, O. (2011). A Micro-Ribonucleic Acid Signature Associated with Recovery from Assist Device Support in 2 Groups of Patients with Severe Heart Failure. Journal of the American College of Cardiology *58*, 2270-2278.

Ramaswamy, S., Ross, K.N., Lander, E.S., and Golub, T.R. (2003). A Molecular Signature of Metastasis in Primary Solid Tumors. Nature genetics *33*, 49-54.

Rapisarda, A., and Melillo, G. (2012). Overcoming Disappointing Results with Antiangiogenic Therapy by Targeting Hypoxia. Nature reviews Clinical oncology *9*, 378-390.

Rasey, J.S., Koh, W.-J., Evans, M.L., Peterson, L.M., Lewellen, T.K., Graham, M.M., and Krohn, K.A. (1996). Quantifying Regional Hypoxia in Human Tumors with Positron Emission Tomography of [18 F] Fluoromisonidazole: A Pretherapy Study of 37 Patients. International Journal of Radiation Oncology* Biology* Physics *36*, 417-428.

Razeghi, P., Sharma, S., Ying, J., Li, Y.-P., Stepkowski, S., Reid, M.B., and Taegtmeyer, H. (2003). Atrophic Remodeling of the Heart in Vivo Simultaneously Activates Pathways of Protein Synthesis and Degradation. Circulation *108*, 2536-2541.

Razeghi, P., Young, M.E., Alcorn, J.L., Moravec, C.S., Frazier, O., and Taegtmeyer, H. (2001). Metabolic Gene Expression in Fetal and Failing Human Heart. Circulation *104*, 2923-2931.

Rees, M.L., Subramaniam, J., Li, Y., Hamilton, D.J., Frazier, O.H., and Taegtmeyer, H. (2015). A Pkm2 Signature in the Failing Heart. Biochem Biophys Res Commun.

Richards, O.C., Raines, S.M., and Attie, A.D. (2010). The Role of Blood Vessels, Endothelial Cells, and Vascular Pericytes in Insulin Secretion and Peripheral Insulin Action. Endocrine reviews *31*, 343-363.

Rini, B.I. (2007). Vascular Endothelial Growth Factor–Targeted Therapy in Renal Cell Carcinoma: Current Status and Future Directions. Clinical Cancer Research *13*, 1098-1106.

Rini, B.I., Campbell, S.C., and Escudier, B. (2009). Renal Cell Carcinoma. The Lancet *373*, 1119-1132.

Rini, B.I., Cohen, D.P., Lu, D.R., Chen, I., Hariharan, S., Gore, M.E., Figlin, R.A., Baum, M.S., and Motzer, R.J. (2011). Hypertension as a Biomarker of Efficacy in Patients with Metastatic Renal Cell Carcinoma Treated with Sunitinib. Journal of the National Cancer Institute *103*, 763-773.

Roberts, W.G., Whalen, P.M., Soderstrom, E., Moraski, G., Lyssikatos, J.P., Wang, H.-F., Cooper, B., Baker, D.A., Savage, D., and Dalvie, D. (2005). Antiangiogenic and Antitumor Activity of a Selective Pdgfr Tyrosine Kinase Inhibitor, Cp-673,451. Cancer research *65*, 957-966.

Rock, E.P., Goodman, V., Jiang, J.X., Mahjoob, K., Verbois, S.L., Morse, D., Dagher, R., Justice, R., and Pazdur, R. (2007). Food and Drug Administration Drug Approval Summary: Sunitinib Malate for the Treatment of Gastrointestinal Stromal Tumor and Advanced Renal Cell Carcinoma. The Oncologist *12*, 107-113.

Rubio, R., and Berne, R.M. (1975). Regulation of Coronary Blood Flow. Progress in cardiovascular diseases *18*, 105-122.

Rushmer, R.F. (1976). Cardiovascular Dynamics. (Saunders).

Sambrook, J., and Russell, D.W. (2001). Inverse Pcr. Molecular Cloning; A Laboratory Manual, 8.81-88.85.

Sampaio, E.P., Sarno, E.N., Galilly, R., Cohn, Z.A., and Kaplan, G. (1991). Thalidomide Selectively Inhibits Tumor Necrosis Factor Alpha Production by Stimulated Human Monocytes. The Journal of experimental medicine *173*, 699-703.

Santos, D., Moreno, A., Leino, R., Froberg, M., and Wallace, K. (2002). Carvedilol Protects against Doxorubicin-Induced Mitochondrial Cardiomyopathy. Toxicology and applied pharmacology *185*, 218-227.

Sawyer, D.B., Zuppinger, C., Miller, T.A., Eppenberger, H.M., and Suter, T.M. (2002). Modulation of Anthracycline-Induced Myofibrillar Disarray in Rat Ventricular Myocytes by Neuregulin-1β and Anti-Erbb2 Potential Mechanism for Trastuzumab-Induced Cardiotoxicity. Circulation *105*, 1551-1554.

Schelbert, H.R. (2010). Anatomy and Physiology of Coronary Blood Flow. J Nucl Cardiol *17*, 545-554.

Schmierer, B., and Hill, C.S. (2007). Tgfβ–Smad Signal Transduction: Molecular Specificity and Functional Flexibility. Nature Reviews Molecular Cell Biology *8*, 970-982.

Scott, J.M., Khakoo, A., Mackey, J.R., Haykowsky, M.J., Douglas, P.S., and Jones, L.W. (2011). Modulation of Anthracycline-Induced Cardiotoxicity by Aerobic Exercise in Breast Cancer Current Evidence and Underlying Mechanisms. Circulation *124*, 642-650.

Sen, S., Kundu, B.K., Wu, H.C.J., Hashmi, S.S., Guthrie, P., Locke, L.W., Roy, R.J., Matherne, G.P., Berr, S.S., and Terwelp, M. (2013). Glucose Regulation of Load-Induced Mtor Signaling and Er Stress in Mammalian Heart. Journal of the American Heart Association *2*, e004796.

Sennino, B., Falcón, B.L., Mccauley, D., Le, T., Mccauley, T., Kurz, J.C., Haskell, A., Epstein, D.M., and Mcdonald, D.M. (2007). Sequential Loss of Tumor Vessel Pericytes and Endothelial Cells after Inhibition of Platelet-Derived Growth Factor B by Selective Aptamer Ax102. Cancer research *67*, 7358-7367.

Sheskin, J. (1964). Thalidomide in the Treatment of Lepra Reactions. Clinical pharmacology and therapeutics *6*, 303-306.

Simpson, P. (1983). Norepinephrine-Stimulated Hypertrophy of Cultured Rat Myocardial Cells Is an Alpha 1 Adrenergic Response. Journal of clinical investigation *72*, 732.

Simpson, P. (1985). Stimulation of Hypertrophy of Cultured Neonatal Rat Heart Cells through an Alpha 1-Adrenergic Receptor and Induction of Beating through an Alpha 1-and Beta 1-Adrenergic Receptor Interaction. Evidence for Independent Regulation of Growth and Beating. Circulation Research *56*, 884-894.

Singhal, S., Mehta, J., Desikan, R., Ayers, D., Roberson, P., Eddlemon, P., Munshi, N., Anaissie, E., Wilson, C., and Dhodapkar, M. (1999). Antitumor Activity of Thalidomide in Refractory Multiple Myeloma. New England Journal of Medicine *341*, 1565-1571.

Smith, P.K., Krohn, R.I., Hermanson, G.T., Mallia, A.K., Gartner, F.H., Provenzano, M.D., Fujimoto, E.K., Goeke, N.M., Olson, B.J., and Klenk, D.C. (1985). Measurement of Protein Using Bicinchoninic Acid. Anal Biochem *150*, 76-85.

Song, S., Ewald, A.J., Stallcup, W., Werb, Z., and Bergers, G. (2005). Pdgfrβ+ Perivascular Progenitor Cells in Tumours Regulate Pericyte Differentiation and Vascular Survival. Nat Cell Biol *7*, 870-879.

Soriano, P. (1994). Abnormal Kidney Development and Hematological Disorders in Pdgf Beta-Receptor Mutant Mice. Genes Dev *8*, 1888-1896.

Spiegelman, B. (1998). Ppar-Gamma: Adipogenic Regulator and Thiazolidinedione Receptor. Diabetes *47*, 507-514.

Stumvoll, M., Nurjhan, N., Perriello, G., Dailey, G., and Gerich, J.E. (1995). Metabolic Effects of Metformin in Non-Insulin-Dependent Diabetes Mellitus. New England Journal of Medicine *333*, 550-554.

Sun, Q., Chen, X., Ma, J., Peng, H., Wang, F., Zha, X., Wang, Y., Jing, Y., Yang, H., and Chen, R. (2011). Mammalian Target of Rapamycin up-Regulation of Pyruvate Kinase Isoenzyme

Type M2 Is Critical for Aerobic Glycolysis and Tumor Growth. Proceedings of the National Academy of Sciences *108*, 4129-4134.

Swain, S.M., Whaley, F.S., Gerber, M.C., Weisberg, S., York, M., Spicer, D., Jones, S.E., Wadler, S., Desai, A., Vogel, C., Speyer, J., Mittelman, A., Reddy, S., Pendergrass, K., Velez-Garcia, E., Ewer, M.S., Bianchine, J.R., and Gams, R.A. (1997). Cardioprotection with Dexrazoxane for Doxorubicin-Containing Therapy in Advanced Breast Cancer. Journal of Clinical Oncology *15*, 1318-1332.

Taegtmeyer, H. (1994). Energy Metabolism of the Heart: From Basic Concepts to Clinical Applications Applications. Current problems in cardiology *19*, 61-113.

Taegtmeyer, H. (2000). Metabolism—the Lost Child of Cardiology∗. Journal of the American College of Cardiology *36*, 1386-1388.

Taegtmeyer, H., Roberts, A.F., and Raine, A.E. (1985). Energy Metabolism in Reperfused Heart Muscle: Metabolic Correlates to Return of Function. Journal of the American College of Cardiology *6*, 864-870.

Tam, C.S., Xie, W., Johnson, W.D., Cefalu, W.T., Redman, L.M., and Ravussin, E. (2012). Defining Insulin Resistance from Hyperinsulinemic-Euglycemic Clamps. Diabetes care *35*, 1605-1610.

Telli, M., Witteles, R., Fisher, G., and Srinivas, S. (2008). Cardiotoxicity Associated with the Cancer Therapeutic Agent Sunitinib Malate. Annals of oncology *19*, 1613-1618.

Templeton, A., Brandle, M., Cerny, T., and Gillessen, S. (2008). Remission of Diabetes While on Sunitinib Treatment for Renal Cell Carcinoma. Ann Oncol *19*, 824-825.

Thomas, W.E. (1999). Brain Macrophages: On the Role of Pericytes and Perivascular Cells. Brain Res Brain Res Rev *31*, 42-57.

Thurston, G., Suri, C., Smith, K., Mcclain, J., Sato, T.N., Yancopoulos, G.D., and Mcdonald, D.M. (1999). Leakage-Resistant Blood Vessels in Mice Transgenically Overexpressing Angiopoietin-1. Science *286*, 2511-2514.

Tigges, U., Boroujerdi, A., Welser-Alves, J.V., and Milner, R. (2013). Tnf-Alpha Promotes Cerebral Pericyte Remodeling in Vitro, Via a Switch from Alpha1 to Alpha2 Integrins. J Neuroinflammation *10*, 33.

Tsapas, A., Vlachaki, E., Sarigianni, M., Klonizakis, F., and Paletas, K. (2008). Restoration of Insulin Sensitivity Following Treatment with Imatinib Mesylate (Gleevec) in Non-Diabetic Patients with Chronic Myelogenic Leukemia (Cml). Leuk Res *32*, 674-675.

Uraizee, I., Cheng, S., and Moslehi, J. (2011). Reversible Cardiomyopathy Associated with Sunitinib and Sorafenib. N Engl J Med *365*, 1649-1650.

Uray, I.P., Connelly, J.H., Thomázy, V., Shipley, G.L., Vaughn, W.K., Frazier, O.H., Taegtmeyer, H., and Davies, P.J.A. (2002). Left Ventricular Unloading Alters Receptor Tyrosine Kinase Expression in the Failing Human Heart. The Journal of Heart and Lung Transplantation *21*, 771-782.

Vander Heiden, M.G., Cantley, L.C., and Thompson, C.B. (2009). Understanding the Warburg Effect: The Metabolic Requirements of Cell Proliferation. Science *324*, 1029-1033.

Veneri, D., Franchini, M., and Bonora, E. (2005). Imatinib and Regression of Type 2 Diabetes. N Engl J Med *352*, 1049-1050.

Vikkula, M., Boon, L.M., Iii, K.L.C., Calvert, J.T., Diamonti, A.J., Goumnerov, B., Pasyk, K.A., Marchuk, D.A., Warman, M.L., and Cantley, L.C. (1996). Vascular Dysmorphogenesis Caused by an Activating Mutation in the Receptor Tyrosine Kinase Tie2. Cell *87*, 1181-1190.

Warburg, O. (1956). On Respiratory Impairment in Cancer Cells. Science (New York, NY) *124*, 269-270.

Watson, L.J., Facundo, H.T., Ngoh, G.A., Ameen, M., Brainard, R.E., Lemma, K.M., Long, B.W., Prabhu, S.D., Xuan, Y.-T., and Jones, S.P. (2010). O-Linked B-N-Acetylglucosamine Transferase Is Indispensable in the Failing Heart. Proceedings of the National Academy of Sciences *107*, 17797-17802.

Wegrzyn, J., Potla, R., Chwae, Y.-J., Sepuri, N.B., Zhang, Q., Koeck, T., Derecka, M., Szczepanek, K., Szelag, M., and Gornicka, A. (2009). Function of Mitochondrial Stat3 in Cellular Respiration. Science *323*, 793-797.

Wilkinson-Berka, J.L., Babic, S., De Gooyer, T., Stitt, A.W., Jaworski, K., Ong, L.G., Kelly, D.J., and Gilbert, R.E. (2004). Inhibition of Platelet-Derived Growth Factor Promotes Pericyte Loss and Angiogenesis in Ischemic Retinopathy. The American journal of pathology *164*, 1263-1273.

Will, Y., Dykens, J.A., Nadanaciva, S., Hirakawa, B., Jamieson, J., Marroquin, L.D., Hynes, J., Patyna, S., and Jessen, B.A. (2008). Effect of the Multitargeted Tyrosine Kinase Inhibitors Imatinib, Dasatinib, Sunitinib, and Sorafenib on Mitochondrial Function in Isolated Rat Heart Mitochondria and H9c2 Cells. Toxicological sciences *106*, 153-161.

Winkler, E.A., Bell, R.D., and Zlokovic, B.V. (2011). Central Nervous System Pericytes in Health and Disease. Nat Neurosci *14*, 1398-1405.

Winkler, F., Kozin, S.V., Tong, R.T., Chae, S.-S., Booth, M.F., Garkavtsev, I., Xu, L., Hicklin, D.J., Fukumura, D., and Di Tomaso, E. (2004). Kinetics of Vascular Normalization by Vegfr2 Blockade Governs Brain Tumor Response to Radiation: Role of Oxygenation, Angiopoietin-1, and Matrix Metalloproteinases. Cancer cell *6*, 553-563.

Wollenberger, A., Ristau, O., and Schoffa, G. (1960). Eine Einfache Technik Der Extrem Schnellen Abkühlung Größerer Gewebestücke. Pflüger's Archiv für die gesamte Physiologie des Menschen und der Tiere *270*, 399-412.

Wong, N., De Melo, J., and Tang, D. (2013). Pkm2, a Central Point of Regulation in Cancer Metabolism. International journal of cell biology *2013*.

Yang, W., Xia, Y., Ji, H., Zheng, Y., Liang, J., Huang, W., Gao, X., Aldape, K., and Lu, Z. (2011). Nuclear Pkm2 Regulates [Bgr]-Catenin Transactivation Upon Egfr Activation. Nature *480*, 118-122.

Yokoyama, T., Nakano, M., Bednarczyk, J.L., Mcintyre, B.W., Entman, M., and Mann, D.L. (1997). Tumor Necrosis Factor-A Provokes a Hypertrophic Growth Response in Adult Cardiac Myocytes. Circulation *95*, 1247-1252.

Young, M.E., Laws, F.A., Goodwin, G.W., and Taegtmeyer, H. (2001). Reactivation of Peroxisome Proliferator-Activated Receptor A Is Associated with Contractile Dysfunction in Hypertrophied Rat Heart. Journal of Biological Chemistry *276*, 44390-44395.

Zhang, S., Liu, X., Bawa-Khalfe, T., Lu, L.-S., Lyu, Y.L., Liu, L.F., and Yeh, E.T.H. (2012). Identification of the Molecular Basis of Doxorubicin-Induced Cardiotoxicity. Nat Med *18*, 1639-1642.

Zhao, Y.-Y., Sawyer, D.R., Baliga, R.R., Opel, D.J., Han, X., Marchionni, M.A., and Kelly, R.A. (1998). Neuregulins Promote Survival and Growth of Cardiac Myocytes Persistence of

Erbb2 and Erbb4 Expression in Neonatal and Adult Ventricular Myocytes. Journal of Biological Chemistry *273*, 10261-10269.

Zhao, Y., Xue, T., Yang, X., Zhu, H., Ding, X., Lou, L., Lu, W., Yang, B., and He, Q. (2010). Autophagy Plays an Important Role in Sunitinib-Mediated Cell Death in H9c2 Cardiac Muscle Cells. Toxicology and applied pharmacology *248*, 20-27.

Zhou, G., Myers, R., Li, Y., Chen, Y., Shen, X., Fenyk-Melody, J., Wu, M., Ventre, J., Doebber, T., and Fujii, N. (2001a). Role of Amp-Activated Protein Kinase in Mechanism of Metformin Action. Journal of clinical investigation *108*, 1167.

Zhou, S., Palmeira, C.M., and Wallace, K.B. (2001b). Doxorubicin-Induced Persistent Oxidative Stress to Cardiac Myocytes. Toxicology Letters *121*, 151-157.

Zhu, X., Stergiopoulos, K., and Wu, S. (2009). Risk of Hypertension and Renal Dysfunction with an Angiogenesis Inhibitor Sunitinib: Systematic Review and Meta-Analysis. Acta Oncol *48*, 9-17.

VITA

Meredith Rees Rodriguez was born in Colorado Springs, Colorado to James and Tina Rees. After graduating from Air Academy High School in 2005, Meredith attended The University of Colorado at Boulder where she earned a Bachelor's of Arts in Molecular, Cellular and Developmental Biology. After graduating in May 2009, she moved to Texas where she began her dissertation work at The University of Texas Health Science Center at Houston's Graduate School of Biomedical Sciences.

Permanent address:

2038 Nina Lee Lane
Houston, Texas 77018